MEASURING CONCENTRATION OF ICE NUCLEATING PARTICLES IN THE ATMOSPHERE, PARTICULATE MATTERS AND GASEOUS POLLUTANTS IN MUSEUMS: INSIGHT FROM MODELS AND ELEMENTAL ANALYSIS.

By

Dereje Abera

SUBMITTED IN PARTIAL FULFILLMENT OF THE
REQUIREMENTS FOR THE DEGREE OF
DOCTOR OF PHILOSOPHY
AT
ADDIS ABABA UNIVERSITY
ADDIS ABABA, ETHIOPIA
OCTOBER 2017

ADDIS ABABA UNIVERSITY
DEPARTMENT OF
PHYSICS

The undersigned hereby certify that they have read and recommend to the Faculty of Graduate Studies for acceptance a thesis entitled "**Measuring Concentration of Ice Nucleating Particles in the Atmosphere, Particulate Matters and Gaseous Pollutants in Museums: Insight from Models and Elemental Analysis.**" by **Dereje Abera** in partial fulfillment of the requirements for the degree of **Doctor of Philosophy**.

Dated: October 2017

Research Supervisor: _____
Prof. Ashok V. Gholap

External Examiner: _____
Prof. Nnenesi A. Kgabi

Internal Examiner: _____
Dr. Kassahun Ture

Chair Person: _____
Dr. Teshome Senbeta

ADDIS ABABA UNIVERSITY

Date: **October 2017**

Author: **Dereje Abera**

Title: **Measuring Concentration of Ice Nucleating Particles in the Atmosphere, Particulate Matters and Gaseous Pollutants in Museums: Insight from Models and Elemental Analysis.**

Department: **Physics**

Degree: **Ph.D.** Convocation: **October** Year: **2017**

Permission is herewith granted to Addis Ababa University to circulate and to have copied for non-commercial purposes, at its discretion, the above title upon the request of individuals or institutions.

Signature of Author

For those who have unlimited potential but can't attend the school.

Table of Contents

List of Tables

List of Figures

Abstract

Ice nucleation in clouds affects the optical thickness and lifetime of mixed-phase clouds and is responsible for a significant proportion of precipitation formed globally and ultimately indirectly affect climate. In mixed-phase clouds, where temperatures range from -37^0C and 0^0C, ice crystals can only form on certain aerosol particles. Ice nucleating particles (INPs) constitute such aerosols with reduce energy barrier of ice nucleation. Despite significant advancement in the fundamental understanding of different ice formation processes in the last decades, the ice phase in clouds still contributes major uncertainties in climate model prediction of radiative forcing. This is partly due to a limited understanding of the behaviour of aerosol particles to act as INPs and paucity of observational data in the atmosphere quantifying INP distributions. Therefore, the first part of this employed Micro-liter Nucleation by Immersed Particle Instrument (μ-NIPI) to cool down droplets containing ice-nucleating material at a controlled rate and to monitor their freezing temperatures. The experiments reveal that aerosol droplets started to freeze at -14^0C down to -25^0C;while, the concentration evolved from 0.1 to 10^{-3} cm^{-3}. The average temperature in which 50% of the droplets froze occurred at -20^0C with a concentration of 10^{-3} cm^{-3}. The experimnets have shown that the type of aerosol species that make INPs in Leeds, UK, were dominantly feldspar from mineral dust. Moreover, meteorological factors such as wind speed, temperature and relative humidity affected INPs' concentrations. In addition to the aforementioned aerosol radiative forcing (climate forcing), aerosol has significant impact on the environment (e.g., air and water pollution). In fact, pollution is not a phenomenon just of modern time; it is intimately connected with the

dawn of the industrial age in which the effects of particulate matter and gaseous pollutants on precious cultural assets become obvious. The high atmospheric load caused strong soiling as well as corrosion outdoors and indoors. The increasing attraction on indoor pollutants in the museums environment and associated investigation contribute to the understanding of basic mechanisms. Particulate matter and gaseous pollutants are involved in deterioration processes and aging mechanism was not realized until macroscopic observable damages occurred which gave the starting point for scientific investigation. Therefore, in the second part of this work, particulate matter samples were collected on Teflon membrane filters using Harvard-type Impactor collector, Aethalometry and diffusive sampler are to measure black carbon and gaseous pollutants respectively. It was observed that the daily PM_{10} average mass concentrations inside and outside the Magritte and Reserve OB museums-varied between 2.71 and 5.25 $\mu g/m^3$ with an average concentration of 4.10 $\mu g/m^3$ and 0.36 and 7.75 $\mu g/m^3$ with an average concentration of 2.20 $\mu g/m^3$ respectively. The concentrations were usually lower when the museum was closed and there were no tourist activities around. Inside the museums, mass concentrations were much less than outside with daily variations, which were due to wind speed, wind direction, human activity and traffic activities outside of the museums. The average mass concentrations of indoor PMs were always lower than that of the outdoor ones that as reflected in low indoor/outdoor ratios indicating that the sources of pollutants were from outside the museums. Particle number concentrations in all sizes (i.e., PM_1, $PM_{2.5}$ and PM_{10}) remained at high levels during morning time which are correlated directly with temperature and inversely with relative humidity. Furthermore, the concentrations of gaseous pollutants (NO_2, SO_2 and O_3) were lower inside the museums than the outside with some of them at undetectable levels; in addition, the levels of these gases inside the two museums were lower and below the recommended level when compared to that of other museums. Bulk aerosol samples of different sizes were analyzed by means of energy-dispersive X-ray fluorescence analysis (EDXRF) to determine their composition. The analysis led to identification of 11 elements (Al, Si, P, S, Cl, K, Ca,

Mn, Fe, Cu and Zn). The levels of concentrations of these elements were found to be 27.45 and 281.85 ng/m^3 at Magritte and 16.16 and 154.26 ng/m^3 at Reserve OB inside and outside of the museums on average respectively; their sources were predominantly anthropogenic from traffic activities and industries. It was observed that air mass with trajectories emanating from maritime and continental sources severely affected the concentrations pollutants in the museums.

Acknowledgements

Words are not enough to express my appreciation to everyone helped me to make this work to come in shape. Addis Ababa University, Department of Physics, University of Leeds, School of Earth and Environment, Ice nucleation research group and University of Antwerp, Antwrp X-ray analysis, Electrochemistry and Speciation (AXES) research group have provided me with all the possible help and facilities in order to formulate my thoughts and bring them into your hands as a part of this scientific work. first of all, I wish to express my warmest gratitude to my advisor Professor A.V.Gholap for his positive and constructive guidance, advice, comments and useful suggestions throughout my study. I am also thankful to Prof. Gizaw Mengistu and Dr. Kassahun Ture for their fruitful suggestion and comments during my Ph.D. study.

Besides my advisor, I would like to thank the former Physics department head at Addis Ababa University, Dr. Belayneh Mesfin, current head Dr. Teshome Senbeta, Dr. Derbie Hirpo and secretary W/ro Tslat Adnew who helped me a lot in facilitation of administrative affairs. My thank extended to Prof. Solomon Bililign commenting final copy of the thesis.

My sincere thanks also go to Prof. Ben Murray, Dr. Theo Wilson, Prof. Edward Murray, Dr. Tom Whale, Dr. Danny O'Sullivan, Dr. Hannah Price, Dr. Nsikanabasi Silas Umo and Sandy James University of Leeds who provided me an opportunity to join their Ice nucleation research group as intern and who gave access to the laboratory and research facilities. Without their precious support it would not be possible to conduct this research. I also extend my heartfelt gratitude to Louis Bruyns S.J Scholarship, University of Antwerp, Belgium for the financial support and generous cooperation for the fulfillment of this research, AXES research group especially Prof. Dr. Karolien De Wael and Prof. Dr. Piet Van Espen constructive guidance and advice regarding my work at University of Antwerp. I am grateful to my friend Dr.

Yoseph Alresawum whose help and cooperation made the implementation of this thesis possible.
Last but not the least, I would like to thank my wife Nolawit Tefera and my families, my brothers, uncle and sisters especially my dear brothers Dr. Salle Workneh , Bahiru Abera and Wubetu Workneh for supporting me throughout my study and my life. I could not go a single step without them.

Dereje Abera
Addis Ababa, Ethiopia
August 15, 2017

Introduction

An aerosol is a collection of solid or liquid particles in suspension in the air. It includes both particles and suspending gas. Aerosols are always present in the atmosphere in variable concentrations ranging from 10^2 to 10^8 cm^{-3}. The concentration of aerosols depends on factors such as location, weather conditions, and level of industrial and urban activities [1, 2]. With such high concentrations, both natural and anthropogenic aerosols have wide-reaching impacts on the environment. Aerosols have an impact on air quality, visibility, cloud formation and atmospheric chemistry. Beside, they have significant impact on human health. This is due to the very large heterogeneity in aerosol sources, physical and chemical properties and their relatively short residence time in the atmosphere. Since the particle diameter is related to many other properties such as the deposition behavior, it is an important aerosol feature [1, 2]. Most of the liquid atmospheric particles are spherical in shape, thus their diameter can be determined easily. However, solid atmospheric particles usually have irregular shapes and sizes, thus it is difficult to describe them using a single parameter [3]. Different aerosol diameter descriptors in use are directly based on visual or microscopic measurements using the particle length and width. However, these measurements are often dependent on particle orientation. In that case, values which are obtained from individual measurement are not robust results thus average values over many

orientations have to be calculated [4]. The chemical composition of the aerosol is another important parameter that controls the hygroscopicity (its ability to take up water and grow in size as ambient relative humidity increases) of the aerosol. While the hygroscopic type of aerosols serve as cloud condensation nucleus (CCN) which initiates cloud droplet formation, the hydrophobic aerosols serve as ice nucleating particles (INPs) which trigger the formation of ice crystals in the atmosphere.

The process of formation of aerosols and their composition coupled with physical and chemical atmospheric properties, results in a large variability in aerosol composition. These are mineral based aerosols (inorganic), sea spray (mostly inorganic with some organic additions), biological, industrial aerosols (a mix of inorganic and organic material, with volatile and non-volatile components) and biomass burning aerosols (mostly organic material, with again volatile and nonvolatile components). Therefore, we have measured the concentration of ice nucleating particles in the atmosphere, which is presented in the first part of this thesis.

Understanding the role of INPs in cloud formation in the troposphere is an essential feature for predicting future climate. In mixed-phase clouds, ice crystals may be formed on certain aerosol particles which are known as ice nucleating particles, which reduce the energy barrier of ice nucleation where temperature between -37 ^{0}C and 0^0C. This is causes freezing at warmer temperatures, i.e., lower super saturations with respect to ice as compared to homogeneous nucleation. Only a subset of these aerosol particles can also serve as INPs with typical INPs concentrations ranging from 10^{-4} to 10^{-1} cm^{-3}. The presence of INPs in the atmosphere can lead to changes in the microphysical properties and lifetime of clouds. As a result, a change in INP concentrations can indirectly modify climate by changing cloud optical properties (for

example extinction coefficient, scattering coefficient, scattering phase function, scattering coefficient, single scattering albedo etc.), lifetime and cloud extent [5, 6, 7, 8]. Clouds and their radiative properties are very sensitive to the presence of rare particles (i.e., the INPs), which are capable of triggering the formation of an ice crystal. However, the abundances, identities and distributions of the INPs in the atmosphere are very poorly constrained. Typically, only one in a million aerosol particles are capable of nucleating ice. This makes their measurement in the atmosphere challenging. Currently, the role of INPs in climate change is highly uncertain [9]. To predict the role of INPs in climate change and precipitation, information on their types and sources in the atmosphere is needed. Possible candidates for INPs in the atmosphere include mineral dust, biological particles, carbonaceous combustion aerosol and volcanic ash [10]. Although immense progress has been made in the fundamental understanding of different ice formation processes, yet the ice phase in clouds still contributes to major uncertainties in climate model prediction of radiative forcing. This is partly due to inadequate knowledge on the requirements of aerosol particles to act as INPs and limited observational data in the atmosphere in quantifying the INPs distributions [9]. In this study, a major effort is made in understanding of the atmospheric INPs and also in highlighting that there is a real lack of data on concentration of INPs in the atmosphere. It is hoped that this work will (i) provide some input for the global aerosol modeling process and (ii) identify important types of INPs with which to work in the laboratory.

Atmospheric aerosols affect both air quality, which endanger human ecosystems well being [11, 12] and have an important role to play in the Earth's climate system [9]. Quite numerous efforts were made on the aerosol research are on both air quality and

climate, although the aerosol effect on climate is certainly the subject most widely studied. Over the last decade, specific subjects within atmospheric aerosol science have received the largest attention some of these are studying, organic aerosols (OAs), new particle formation, aerosol sources and atmospheric budget, radiative forcing of aerosols and precipitation (see for example, the Web of Science in the institute for scientific information (ISI) for most cited papers).

The close connection between climate and air quality is mostly reported in the form of impacts of climate change on air pollution levels and to a lesser extent in the impacts of air pollution on climate change. Most air quality studies worldwide agree that, aerosols which are spread globally and have a strong regional imbalance, can change the global climate through their direct and indirect effects on radiative forcing [1, 3, 6, 9]. Changes in climate affect air quality by perturbing ventilation rates (wind speed, mixing depth, convection), precipitation scavenging, dry deposition, chemical production and loss rates, natural emissions and background concentrations [1, 2, 3, 8, 11]. Thus the complex interactions between emissions, atmospheric changes and chemistry be considered for a more comprehensive assessment of the influence of climate change on regional air quality [1, 8, 11, 12].

From an environmental standpoint, aerosols also constitute an important policy issue in air quality and climate sciences. In fact, Particulate Matter (PM) pollution is probably the most pressing issue in air quality regulation worldwide and at the same time it represents one of the biggest sources of uncertainty in current climate simulations. Therefore, in the second part of this work, certain aerosols affect the environment adversely, for example, causing acidic rain and damaging buildings, especially of cultural heritage importance while some may affect the artifacts and damage

preserved articles in museums. Realizing these facts, during the last two decades, efforts have been made to avoid adverse environmental influences at a very early stage by optimizing the surrounding conditions of museum collections. Steps are taken to prevent the occurrence of damages on artworks and efforts are made for restoration. This conservation approach which is termed as preventive conservation is defined as an effort to decelerate the deterioration of the cultural heritage to preserve its integrity and to reduce the necessity of the restoration treatment to a minimum [13]. In order to achieve a comprehensive control of the surrounding conditions, many museum institutions are using today progressive containment as an underlying strategy to preserve artifacts in an ideal way. In order to minimize environmental influences, climatic requirements within the museum building and inside of galleries, exhibition areas and storage rooms are closely defined. To prevent further mechanical damage and to ensure a microclimate inside, which is independent of the surrounding room to suit the individual requirements of the specific artefact, mobile cultural assets are stored and displayed in the showcases, cabinets and envelopes; painting are glazed. This kind of nested prevention strategy is referred to as box in a box-model [14]. In order to meet these conditions, cases are predominantly constructed as airtight as possible at the request of conservators and exhibition technicians which imply that the air exchange rate should be minimum.

Environmental control in museums is usually limited to temperature and relative humidity. In some cases, this is supplemented with light and UV measurements. However, it is known that many other airborne substances such as particulate matter, on one hand and reactive gases such as nitrogen dioxide (NO_2), sulphur dioxide (SO_2), and ozone (O_3) on the other hand, play a crucial role in the deterioration of

materials. Currently, environment control in museums is done by monitoring temperature, relative humidity and Vis-UV radiation. reactive gases and PM.

Pollutants are present in museums and even indoor pollutant sources may exist. For example, the off-gassing of wood in showcases, release of products generated by the slow degradation of the building [15]. It is also known that acceptable target concentrations for collection caretakers (for example the annual limit for NO_2 is 10 $\mu g/m^3$) are even lower than the allowed annual limits for health and vegetation as prescribed by the European Union (EU) Directive 2008/50/EC (eg.: annual limit for NO_2 is 40 $\mu g/m^3$) [16]. Unfortunately, collection caretakers are not usually able to reach the mentioned thresholds. An additional problem with historical monuments is that such buildings were never built with the idea to achieve the suitable storage conditions as described in recent guidelines [17]. As a result, climatic conditions are difficult to control and outdoor pollutants have easy access to the interior. However, in such buildings there is also a need to reach the prescribed conditions. As far as we know, there is no complete tool or method that supports collection caretakers in their ever quest for improving the indoor air quality. This is reflected in the survey performed during the Seventh Framework Programme (FP7)-project Musecorr at 80 institutions in Europe and United States of America (USA): most of these institutions considered air quality and degradation monitoring as important but most of them are not satisfied with the current measuring tools. Preventive conservation methods are based upon the principle that deterioration and damage to works of art can be controlled or slowed down by managing the environmental conditions under which collections are housed and safeguarded. Therefore, it is possible to prolong the lifespan of objects by improving the indoor air quality (IAQ) of museums.

The effects of gaseous pollutants such as nitrogen oxides (NO_x), sulphur dioxide (SO_2) and ozone (O_3) are thoroughly investigated. The harmful effects of PM were only recently taken into account. Heritage related PM research is still quite new and mostly restricted to the study of the chemical composition and source of PM, rather than its effects on materials [18, 19, 20]. Thus, so far the PM research focuses on the environment. On the other hand, extensive research exists on the identification of historical materials. Among heritage artifacts, paintings and other pictorial representations take a special position, either because they represent windows into the past or because they are considered to be one of the most important remnants of human artistic creativity and innovation. Museums and heritage sites started to monitor temperature, relative humidity and to a lesser extent light irradiation. In addition, air quality became the subject of extensive research topics, both indoors and outdoors. In this study, we have tried to address overview of the current state of art regarding indoor concentrations of particulate matter and gaseous pollutants in Magritte and Reserve OB museums. In order to obtain information about the emission potential and spectrum of released substances, fundamental emission analysis was carried out to give a clue to develop an indoor air quality monitoring system. Thus, the main objectives of this thesis are to measure concentrations of ice nucleating particles (INPs) in the atmosphere, Characterization of particulate matters and gaseous pollutants in museums.

The specific objectives of the thesis are:

1. to investigate the concentration of the INPs in the atmosphere.

2. to compare INPs data that we have taken from the specific sampling site with the global distribution of INPs.

3. to understand the relationship between INPs and meteorological parameters as well as the origin of air mass that contain INPs at the measurement site.

4. to determine the concentrations of PMs that are present inside and outside of museums.

5. to characterize chemical composition of PMs.

6. to investigate the concentrations of gaseous pollutants such as O_3, NO_2 and SO_2 and to identify the sources of such pollutants in museums.

To achieve these objectives, the thesis is organized into two parts. Part I discusses measuring concentrations of the ice nucleating particles in the atmosphere under three chapters. Chapter 1 deals with the basic science of nucleation, models related with ice nucleation, ways of measuring INP activities and types of INPs components. Chapter 2 is about the methodology used in the measurement techniques and analysis of INP. Results and discussions are presented in Chapter 3. Part II deals with particulate matter and contains three chapters. Chapter 4 covers particulate matter, sources, formation and effect on cultural heritage. Chapter 5 presents materials and methods used in this research including sampling of gaseous and particulate matters and analysis techniques. Chapter 6 deals with results and discussions of characterization of particulate matter in museums. Chapter 7 addresses summary of the findings, conclusion and recommendation.

Chapter 1

Physical and chemical characteristics of aerosols and ice nucleating particles and their environmental impacts

The relevance of atmospheric components and how these components, specifically aerosols, affect the weather and climate systems is highlighted in this chapter. Ice nucleation is one of the principal cloud microphysical processes that influences cloud properties. This chapter introduces the theory of ice nucleation, some proposed mechanisms and its relevance in understanding aerosol-cloud interactions. Types of ice nucleating particles, experimental techniques measuring INPs and model related to ice nucleation with specific focus on the immersion mode ice nucleation by aerosols are presented.

1.1 Introduction

Earth's atmosphere comprises layers of gases that encapsulate the planet in a protective blanket. These are restrained from dispersing into space by Earth's gravitational

hold. The atmosphere absorbs ultraviolet radiation from the sun, thereby protecting life and warms the surface by retaining heat - the greenhouse effect. The troposphere, the lowest layer of the atmosphere, contains around 99% of the atmosphere's water vapour and aerosols (the dispersed fine particles in air) and these dictate cloud formation and can influence local and regional weather conditions. Clouds dictate the prevalence of precipitation in the form of water, snow or hail; they are fundamental to the hydrological cycle. Consequently, besides having a major impact on Earth's climate, cloud physics has important implications for ecosystems and human health. The frequency, duration and intensity of precipitation events along with infiltration, evaporation, transpiration and run-off at the Earth's surface dictate the influence on land, plants and life. Lack of precipitation leads to drought, desiccation of the ground and dust storms that erode the surface soils and result crop failures and famine. Heavy precipitation leads to rivers breaking their banks, flooding of land, washing away of productive soils, and collapse of settlement of sensitive soils and destruction of infrastructure, food shortages and pollution of drinking water. The ground interacts with the atmosphere and the atmosphere influences the ground in continuous, irregular phases that influence our everyday lives and wellbeing.

1.2 Impact of aerosols on climate

Regardless of their short atmospheric lifetimes on the order of days to weeks, aerosols play an important role in climate by modifying the radiative balance of the Earth atmosphere system [21]. The magnitude of this effect is quantified using radiative forcing defined as the extent by which an atmospheric constituent changes the balance between incoming solar radiation and outgoing terrestrial radiation over the Industrial

Era, typically specified as beginning in the year 1750 as indicated in Fig. 1.2. Values of radiative forcing are defined at the tropopause, which is the boundary between the troposphere (the lowest atmospheric layer) and the stratosphere (the second, overlying atmospheric layer). A positive radiative forcing denotes a net warming effect and a negative radiative forcing signifies a net cooling effect [9]. The direct effect occurs when aerosols either scatter incoming radiation (e.g. sulfate particles) to have a negative forcing or absorb radiation (e.g. black carbon particles) to have a positive forcing [9, 21, 22]. Aerosols can also influence climate indirectly by altering the number and size of water droplets or ice crystals within cloud systems, which can modify the optical properties of clouds in what is termed the first indirect effect or cloud albedo effect [23]. A change in water droplet or ice crystal number and size may also lead to a change in the precipitation rates of clouds in what is termed the second indirect effect or cloud lifetime effect [24]. The magnitude of radiative forcing of atmospheric aerosols as well as that of other relevant atmospheric constituents is shown in Fig. 1.2. Moreover, anthropogenic aerosols alter the planetary energy balance through a variety of mechanisms operating across a wide range of spatial scales: direct effects [25, 26], indirect effects [27] and semi direct effects [28, 29]. The term aerosol direct effects refers to the direct impact of anthropogenic aerosol particles on the planetary energy balance through scattering, absorption, and emission of radiation in the atmosphere, without consideration of the aerosol effects of the radiative heating on clouds. The indirect effects of aerosols refers to the impact through the influence of anthropogenic aerosol on the optical properties of clouds by serving as the nuclei for droplets and ice crystals and thereby changing droplet and ice crystal number concentration, which changes cloud particle surface area, influences

droplet collisions and changes the accumulation of liquid water and ice in clouds, all of which affect the reflectivity and emissivity of clouds. Semi-direct effects are changes in the planetary energy balance, hydrological and dynamical fields of the climate to the radiative influences of aerosols [30, 31]. Some of the semi-direct effects of aerosols are (i) changes in surface heat and moisture fluxes, (ii) modification in the vertical temperature profile, (iii) cloud formation, (iv) life time of cloud, (v) precipitation and (vi) the dynamics of the atmosphere [32, 33, 34, 35, 36, 37, 38]. Tesfaye et al. [38] reported that the radiative feedback of the desert dust particles results in positive response on net atmospheric radiative heating rate, cloud cover, cloud liquid water path and decrease surface temperature. The semi-direct effect could maximize the positive radiative forcing when the absorbing aerosols are located within the boundary layer [39]. However, Lohmann and Feichter [40] concluded that the absorption of solar radiation by absorbing aerosols (black carbon) can decrease cloud cover and liquid water path. Even though aerosols are thought to have a net cooling effect on climate, the large uncertainties coupled with a low level of scientific understanding indicate that there is still much to learn regarding aerosol-climate interactions.

1.3 Aerosols and cloud

Cloud droplets are formed within a supersaturated atmosphere with respect to liquid water. This means that relative humidity (RH) must exceed 100% to activate an aerosol particle and thus form a cloud droplet. The most common way to produce supersaturated air is by ascending air. In this case, air expands and cools adiabatically so that water vapour condenses on surrounding particles (heterogeneous activation)

or spontaneous formation of liquid droplets without any nuclei (homogeneous activation). The process of homogeneous activation of cloud droplets is the nucleation of vapour on embryos comprised vapour molecules only, i.e. water vapour is surrounded by perfectly clean air [1, 41, 42]. The process of cloud droplet activation was first described by the Köhler theory [43]. It describes the equilibrium vapour pressure (Seq) over a curved surface of an aqueous solution droplet which is given as:

$$S_{eq} = \frac{e}{e_s}, \tag{1.3.1}$$

while e and e_s are the partial vapour pressure and saturation vapour pressure respectively. The Köhler theory combines two competing mechanisms which describe the processes during the formation of a cloud droplet, namely the Raoult and the Kelvin effect. The Raoult effect describes the process of decreasing saturation vapour pressure when dissolving a solute in water. When solute molecules are added to an aqueous solution they act as a barrier and decrease the evaporation rate of water molecules. Thus, the surface is partly covered by solute ions such that water molecules cannot evaporate on the full surface. With decreasing concentration of water molecules, vapour pressure is decreased over the solution resulting in a lower evaporation rate. This effect in which water associates with various non-aqueous constituents is called water activity a_w and is defined as the vapour pressure of an aqueous solution over at surface (p_{sol}) divided by that of pure water (pH_2O) at the same temperature which is given by:

$$a_w = \frac{p_{sol}}{p_{H_2O}}, \tag{1.3.2}$$

For ideal solutions, the water activity is equal to its mole fraction of the water in the solution and can be calculated as [44]:

$$a_w = \exp\left(\frac{n_w}{n_w + \sum n_i}\right), \tag{1.3.3}$$

where, n_w and n_i indicate the amount of water molecules and the amount of each component in the solution expressed in moles, respectively. The summation in the denominator goes over the solution. n_w can be expressed as the ratio of the volume of water (V_w) to the partial molar volume of water in the solution (v_w):

$$n_w = \frac{V_w}{v_w}, \tag{1.3.4}$$

V_w depends on the dry particle diameter (D_{dry}) and the droplet diameter (D):

$$V_w = \frac{\pi}{6}(D^3 - D_{dry}^3). \tag{1.3.5}$$

By substitution of Eq. (1.3.5) in Eq. (1.3.4) and Eq. (1.3.3) the following relationship for a_w can be obtained:

$$a_w = \exp\left(-\frac{6v_w \sum n_i}{\pi(D^3 - D_{dry}^3)}\right), \tag{1.3.6}$$

The Kelvin formula describes the curvature effect which describes the enhancement of the equilibrium vapour pressure over a curved surface compared to a liquid surface. In a smaller droplet, the molecules are more exposed to the surface of the droplet and more likely to evaporate [45]. However, for larger droplets, the transfer of molecules from a liquid droplet to the surrounding gas is decreased. The equilibrium saturation ratio over a curved pure water surface (S_{Kelvin}) is given as:

$$S_{Kelvin} = \exp\left(\frac{4M_w\sigma_w}{RTD\rho_w}\right), \tag{1.3.7}$$

where M_w depicts the molecular weight of water and ρ_w its density. σ_w is the surface tension of water. R is the ideal gas constant, T is the temperature and D is the droplet diameter. Eq. (1.3.7) is not only applicable for pure water or for any other pure substance but also for solutions. In this case, the surface tension and density of the solution have to be used. The Köhler equation combines both the Raoult and Kelvin effect. It gives the relationship between equilibrium saturation ratio (S_{eq} or S) and the size of a solution droplet. In general, the equation can be used as follows:

$$S_{eq} = a_w S_{Kelvin}. \tag{1.3.8}$$

The assumption of ideal solutions is a common way to approximate the Raoult's law. Then, the Köhler equation takes the form:

$$S_{eq} = S = \exp\left(\frac{4M_w\sigma_w}{RTD\rho_w} - \frac{6v_w\sum n_i}{\pi(D^3 - D_{dry}^3)}\right), \tag{1.3.9}$$

The first term on the right is related to the Kelvin (curvature) effect; whereas, the second one accounts for the Raoult (solute) effect. Eq. (1.3.9) shows that both terms corresponding to Raoult's law and Kelvin effect increase with decreasing droplet size but Raoult's law (for solutes) increases much faster compared to the Kelvin effect. For Raoult's law S_{eq} is proportional to $1/D^3$; while, for the Kelvin effect $S_{eq} \propto 1/D$. Fig. 1.1 shows an example of the Köhler curve (calculated using Eq. (1.3.9) for a sodium chloride particle with a dry particle diameter (D_{dry}) of 50 nm (and taking $\delta_\omega = 0.072 Jm^{-2}$ and $T = 298\ K$ from Seinfeld, J. H. and Pandis, S. N [1]). The maximum of this Köhler equation is called the critical saturation ratio (S_{crit}) as shown in Fig.1.1. The diameter that belongs to S_{crit} is called the critical wet diameter (D_{crit}). For diameter $D < D_{crit}$, the droplet is in a stable equilibrium.

A stable droplet of this kind is called a haze droplet [46]. The condition is called stable as the addition of water in vapor phase to the droplet would increase its size but in order to keep this increased droplet size, a higher ambient saturation would be needed. On the other side, for diameter $D > D_{crit}$, the droplet is unstable because a slight increase in droplet radius D will lead to condensation and therefore lead to a further increase in radius [46]. The process where an aerosol particle is growing to larger diameters than D_{crit} is called the cloud droplet activation. A single aerosol particle which is in an air parcel where the supersaturation with respect to water already reached its S_{crit}, will act as cloud condensation nuclei (CCN). This means, when a CCN is activated, it takes up as much water as available.

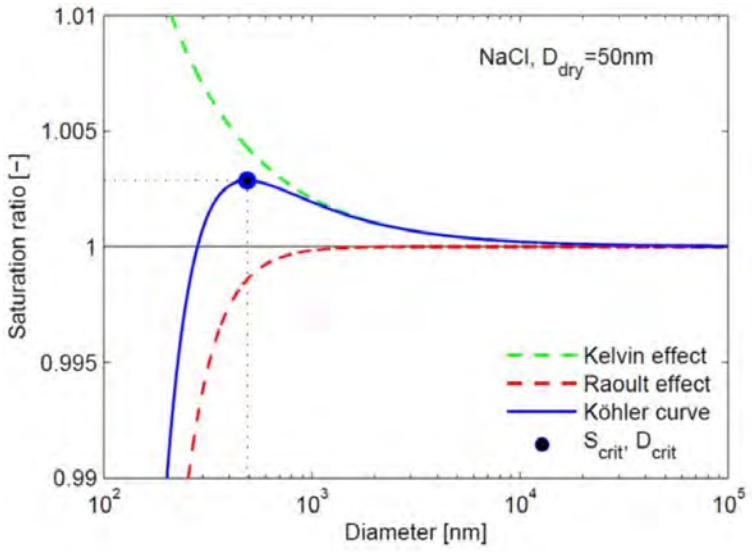

Figure 1.1: Köhler curve of NaCl particles with a dry particle diameter (D_{dry}) of 50 nm (and taking $\delta_\omega = 0.072 Jm^{-2}$ and $T = 298\ K$)[1].

Clouds are formed in various forms, extents and attitudes. They can be grouped into many categories based on their altitudes, level and temperatures [47]. The temperature regime and conditions from which clouds form are crucial, which give rise to various cloud types and classification which are grouped mainly into three families such as high clouds, medium clouds and low level clouds. There are also clouds with vertical development and special types of clouds such as the lenticulars [10, 48, 49]. In relation to the cloud composition, clouds can have its water content mainly in an ice phase, liquid state, or in both liquid phase and ice particles. The latter cloud type is referred to as mixed-phase cloud [49]. Mixed-phase clouds have been observed over a temperature range of 0^0C to $\sim -38^0C$ and it has been established that they can trigger precipitation when the ice particles grow to a critical size big enough to fall out from the clouds [10, 47, 50]. The growth of these ice crystals take place at the expense of the supercooled water droplets in the clouds that is referred to as Bergeron-Findeisen process [47]. With the occurrence of this phenomenon, this makes mixed-phase cloud an important cloud type in modifying weather and consequently climate.

Cloud formation and cloud cover greatly influence our environment and modify the climate [9, 47]. Integral to this is the abundance of not only water droplets but ice crystals in the clouds, which strongly affect cloud properties and impact on climate [47]. Murray et al. [10] reported that mixed phase clouds, one of which exists at temperatures between 0^0C and -37^0C in the low and middle troposphere, play a particularly important role in Earth's climate. However, other cloud formations, such as cirrus clouds in the upper troposphere, which are entirely composed of ice, also

have a part to play [47]. In the atmosphere, water droplets can persist in a supercooled state to below -37^0C in the absence of particles that catalyze ice formation at higher temperatures [47, 51, 52, 53]. This is where aerosols come into play; they greatly influence cloud formation. Homogeneous nucleation of water droplets and ice crystals directly from water vapour, without the catalyst of fine aerosol particles, is not possible in the troposphere. Instead, nucleation is largely controlled by heterogeneous nucleation involving the aerosol particles that act as 'cloud condensation nuclei' (CCNs) to form liquid cloud droplets, or as 'ice nucleating particles' (INPs) to form ice crystal. Aerosol particles strongly affect the properties of clouds, their size, abundance and rate of production and thus they influence cloud cover, cloud albedo and cloud lifetime [10, 54]. It is well known that ice melts at 0^0C, but it is less well understood that cloud water droplets can supercool to temperatures approaching -36^0C unless a special particle type is present. This special particle type known as an ice nucleating particle (INP), can trigger or seed droplet freezing at much higher temperatures but only about 1 in a million aerosol particles in the atmosphere is capable of serving as an INP. It is this inherent rarity that makes INP's and ice formation such an exciting and challenging field [55]. Therefore, currently much climate projection due to formation of ice through heterogeneous ice nucleation plays a great role in climate change [56, 57]. The recent Intergovernmental Panel on Climate Change (IPCC) report showed that there is still a significant uncertainty associated with cloud adjustments due to aerosols as presented in Fig. 1.2. Because of this, the level of scientific understanding and confidence in estimating the radiative forcing due to cloud adjustments by aerosols is poor [9, 58].

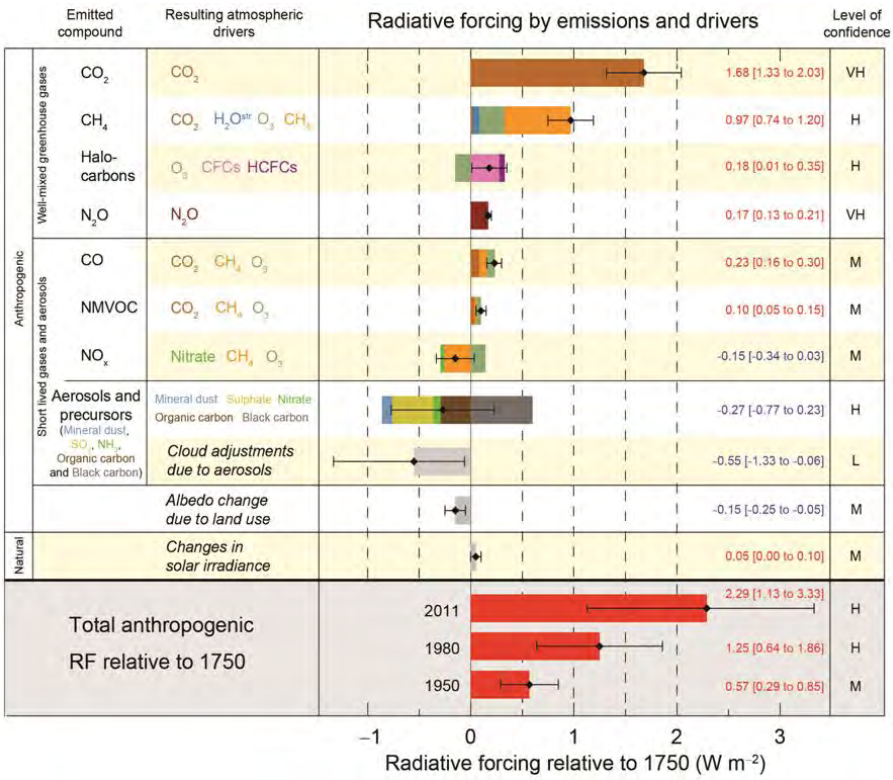

Figure 1.2: A chart showing the radiative forcing (Wm^{-2}) estimates for different atmospheric components between 1750 and 2011.There is a low confidence label on the radiative forcing estimate by cloud adjustments due to aerosols probably because of the level of uncertainty associated with the contribution of aerosols to the cloud adjustments. This high level of uncertainty is tied to the low level of scientific understanding of aerosol-cloud interactions. The chart was adapted from IPCC [9].

Human activities contribute to climate change by causing changes in Earth's atmosphere in the amounts of greenhouse gases, aerosols (small particles) and cloudiness. The largest known contribution comes from the burning of fossil fuels, which releases carbon dioxide gas to the atmosphere. Greenhouse gases and aerosols affect climate by altering incoming solar radiation and out-going infrared (thermal) radiation that are part of Earth's energy balance. Changing the atmospheric abundance or properties of these gases and particles can lead to a warming or cooling of the climate

system. Since the start of the industrial era (about 1750), the overall effect of human activities on climate has been a warming influence. The human impact on climate during this era greatly exceeds that are perceived due to known changes in natural processes. Furthermore, as human activities have increased, the total aerosol loading in the atmosphere throughout the industrial age has increased as shown in Fig. 1.3 (pre and after industrial age). INP concentrations may also be increasing [10, 58, 59]. It is therefore important to identify the types of aerosols that exhibit ice nucleation activity and quantify their atmospheric abundance to accurately predict the role of INPs in climate and precipitation is important.

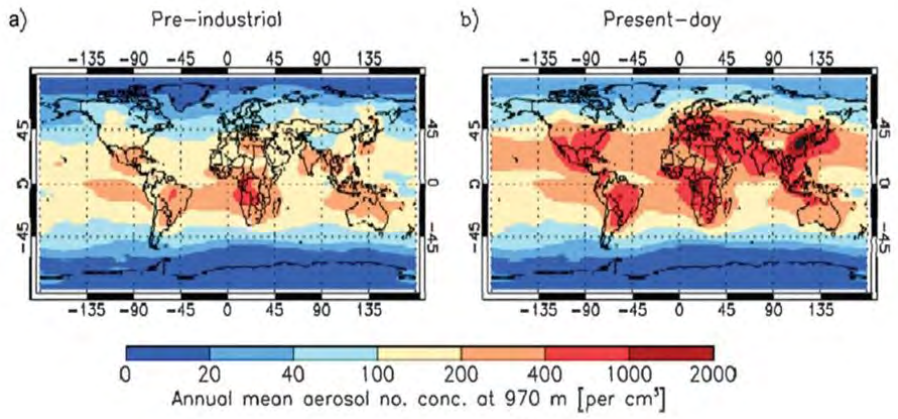

Figure 1.3: Modeled global distribution of annual mean aerosol particle concentrations in the pre-industrial and present day. Adapted from Murray et al. [10].

1.4 Effect of ice nucleating particles on climate

Ice formation in clouds is important to life on Earth since it is a key process in the formation of precipitation and strongly influences the radiative properties of clouds [10]. Following its formation in the atmosphere, the lower saturation vapor pressure

over ice compared to liquid water may result in the growth of ice crystals at the expense of cloud droplets [60]. This mechanism is known as the Wegener-Bergeron-Findeisen process. Vapor transfer, along with the growth of ice crystals by accretion and aggregation, may result in the formation of precipitation. For example, Lau and Wu [61] determined that most precipitation over tropical oceans originates from ice-phase processes and in some cases even low concentrations of INPs are sufficient to be the cause of precipitation [62]. Through modifying cloud properties, INPs can also indirectly influence Earth's radiation budget as shown in Fig. 1.4. Due to their cold temperatures, upper level cirrus clouds trap a greater amount of outgoing long wave radiation emitted from the Earth than the amount of incoming solar radiation that reflect, resulting in a net warming effect on climate [63, 64, 65]. Lynch et al. [66] suggested at altitudes, approximately $7 - 18\ km$ conditions are such that ice nucleation can occur both homogeneously and heterogeneously [66, 67, 68, 69, 7, 71]. In the presence of INPs, ice crystal formation may occur before the beginning of substantial homogeneous freezing, depleting available water vapor and thereby suppressing homogeneous freezing. The net result is a decrease in the surface area of ice (assuming constant water content) and a corresponding decrease in their net warming effect. At lower altitudes, where temperatures are too warm for homogeneous nucleation and mixed-phase clouds dominate, ice formation is initiated by the presence of INPs via a heterogeneous mechanism. This is sometimes referred to as the glaciation indirect effect [27, 72]. Mixed-phase clouds contain both liquid water and ice crystals and are believed to have a net cooling effect on climate [63, 64]. Increasing the concentration of INPs may lead to increased precipitation as a result of the Wegener-Bergeron-Findeisen process causing a decrease in the cloud albedo [56]. While a decrease in ice

crystal size caused by increasing INP concentrations may partially offset the cloud lifetime effect by increasing cloud albedo. Many modeling studies indicate that the increased precipitation and decreased cloud lifetime resulting from an increase in atmospheric INPs will reduce the net cooling effect of mixed-phase [27, 72, 73].

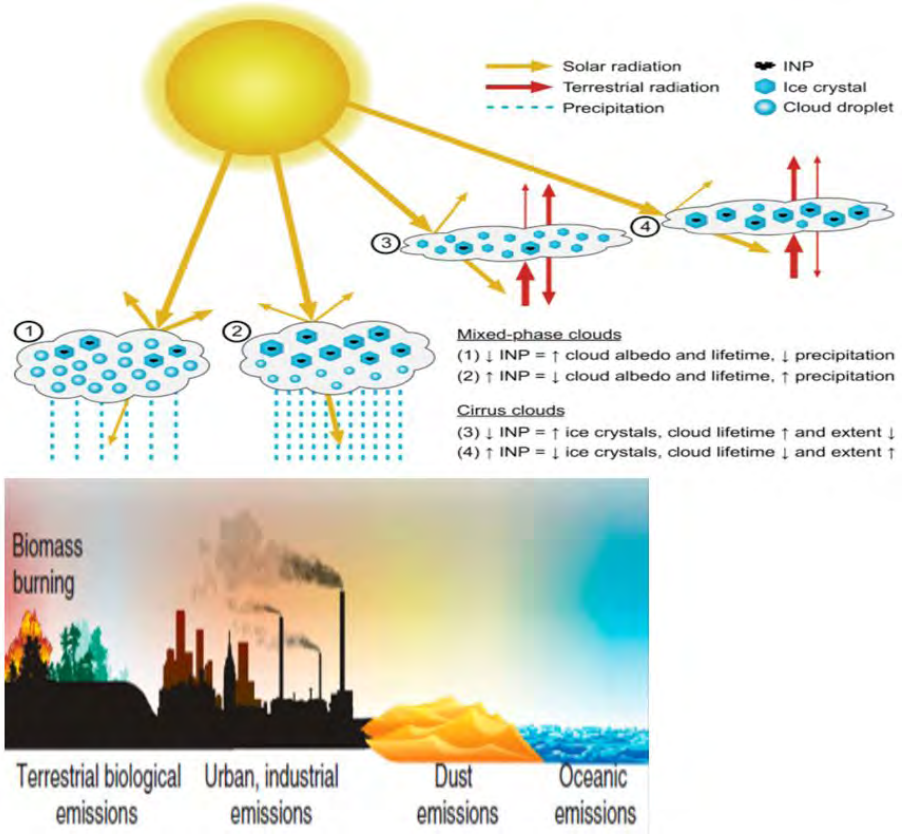

Figure 1.4: Effect of INPs on climate by ice nucleation in mixed phase clouds and cirrus clouds. Where elements (1) and (3) denote low INP number concentrations and elements (2) and (4) denote increased INP number concentrations. Arrow thickness indicates the relative intensity of radiation. Adapted from DeMott et al. [56].

1.5 The basic science of nucleation

Aerosol particles in the atmosphere generally range from 0.001 to 100 μm in size, with ground derived mineral particles generally at the coarser end of the spectrum forming the largest component. Huge quantities of mineral dust are lifted into the atmosphere by wind and turbulence from a range of sources but notably from the arid, desert regions in Africa, the Middle East and Asia, the so called Dust Belt [74]. Thousands of tonnes of mineral dust are lifted into the atmosphere each year with a part of this is a result of anthropogenic activity including desertification and deforestation. Atmospheric dust is composed to a large part of a variety of clay minerals but with significant quantities of quartz and feldspar [10]. Minerals are naturally occurring crystalline solid substances with a specific chemical composition and specific crystal structure. It was recently shown that the feldspar component nucleates ice much more effectively than the other minerals [75]. But particulate dust can also include important contributions from biologically derived species such as pollen, bacteria, fungal spores and plankton [76]; carbonaceous combustion products from burning fossil fuels or forest clearing and volcanic ash from eruptions [77, 78]. The evidence suggests that ice nucleation below about -15^0C is dominated by soot and mineral dust; the only materials above this temperature known to nucleate ice are biological [10]. Both direct and indirect influences on Earth's atmosphere have been attributed to aerosols in the troposphere in complex interaction mechanisms notably with other elements of the climate system. This leads to uncertainties in future climate projections [9]. More precise evaluation of the direct and indirect effects of tropospheric aerosols on climate requires global information on aerosol properties such as optical thickness, size distribution, refractive index, phase and chemical composition. Valuable global

information on these factors can be acquired using satellite passive and/or active remote sensing in conjunction with direct sampling and measurement techniques. The indirect effect is the mechanism where aerosols indirectly influence the radiative forcing by altering the microphysical properties of the clouds. Through the uptake of water at high relative humidity (RH), aerosol particles are able to act as cloud condensation nuclei (CCN) or ice nuclei (IN) and thus are responsible for formation of cloud droplets.

Ice formation in the atmosphere takes place via two major processes - homogeneous and heterogeneous ice formation [80]. While homogeneous process involves the formation of ice particles without any foreign material, heterogeneous ice formation requires a particle for ice to nucleate which leads to freezing as illustrated in Fig. 1.5. The latter process can occur via different nucleation or freezing mechanisms referred to as modes of heterogeneous ice formation such as deposition nucleation, contact, condensation and immersion freezing [47, 54, 80, 81, 82]. Deposition nucleation mechanism entails a direct formation of ice from the water vapour phase on a dry particle; this process usually requires high super saturated water vapour with respect to ice. Contact freezing mechanism is generally described as an ice formation mechanism that occurs when a particle comes in contact with a super-cooled water droplet. The contact by a particle can either be from the outside or the inside of the droplet. However, the extent to which the particle must make contact with the interface of the super-cooled water droplet before ice formation takes place is not clearly understood [83, 84]. On the other hand, condensation freezing is defined to be a mechanism whereby water condenses on a particle followed by ice formation. In immersion, ice nucleation occurs when a particle is completely immersed in a water

droplet and cooled before ice nucleation takes place [10, 82]. Looking at the interaction of aerosol particles and water in the atmosphere, it is unclear how the last two mechanisms - condensation and immersion freezing, can be distinguished in the atmosphere. If the specific definition of condensation freezing involves the condensation of super-cooled water on the particle, then, a clear distinction can be made between the two processes. Also, the timescale between the condensation process and freezing of water needs to be clearly defined. The model shown in Fig. 1.5 summarized the different heterogeneous freezing pathways.

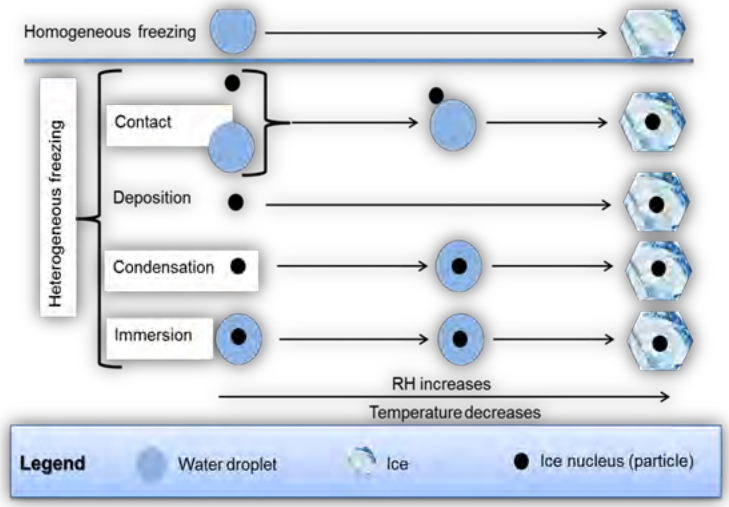

Figure 1.5: Homogeneous and heterogeneous freezing mechanisms according to Vali [82] and Pruppacher and Klett [47].

Phase changes of water are basic to cloud microphysics. These transitions do not occur at thermodynamic equilibrium, but in the presence of a strong free energy barrier. Water droplets, for example, are characterized by strong surface tension forces. For a droplet to form by condensation from the vapor, the surface tension must be overcome by a strong gradient of vapor pressure. It is a fact of cloud physics that

the phase transitions of most interest, the cloud forming processes, are those that do not occur at equilibrium. The Clausius-Clapeyron equation describes the equilibrium condition for a thermodynamic system consisting of bulk water and its vapor [46]. It describes how the saturated vapor pressure changes with changing temperature. As it determines the saturation vapour pressure for water, it provides the physical basis of the hydrological cycle and becomes a principal equation in hydrology, meteorology and climatology. Specifically, the saturation vapour pressure also known as equilibrium vapour pressure, is an upper limit of the quantity of vapour that the atmosphere can contain. When this limit is reached, no additional liquid water is evaporated, while below the limit more water evaporates. This limit is expressed in terms of the partial pressure of the vapour. At standard temperature and pressure (STP) conditions, i.e. at a temperature of 273.15 K (0^0C), the saturation vapour pressure is 6.11 hPa, i.e. 0.611% of the total pressure of 1000 hPa. When the saturation vapour pressure increases at higher temperatures, for example at 25^0C, it is over five times higher. Conversely, when moist air ascends and its temperature decreases, so does the saturation vapour pressure. Vapour in excess of the lower saturation pressure starts to condense, giving rise to the formation of clouds [1, 79]. The Clausius-Clapeyron equation derives from entropy maximization, determines the equilibrium between two phases of a substance. Mathematically it is expressed as the relationship between temperature, T and pressure, p at the equilibrium. Usually, it is expressed in differential form:

$$\frac{dp}{dT} = \frac{\partial S}{\partial V} = \frac{L}{T\partial V} \tag{1.5.1}$$

where ∂S is the entropy gained as units of mass for the transition of water from liquid to vapor, L is the latent heat of vaporization per unit mass for the transition from

liquid to vapor and ∂V is the increase of volume as unit mass as water changes from liquid to vapor. The specific volume V_v of the water vapor is much greater than that of the liquid; thus, $\partial S \approx 1/\rho_v = R_v T/p$, using the ideal gas law for water vapor. Here ρ_v is the vapor density and R_v is the specific gas constant for vapor. By using the ideal gas law, Clausius-Clapeyron equation can be written in the more convenient form:

$$\frac{dp}{dT} = \frac{Lp}{R_v T^2} \tag{1.5.2}$$

where p and T refer to the values at the phase transition. By these considerations pressure p and temperature T apply to water vapor on its own, but can also be applied to a volume of a mixing of vapor and surrounding air [46]. In addition to the vapor-liquid phase transition, there are solid-liquid and solid-vapor transitions. These transition regimes cross one another at the triple point (T), which is at temperature T = 273 K (0^0C) and pressure p = 6.11 hpa (mb) for pure water as shown in Fig. 1.6. The phase transition line solid-vapor shows a small difference in comparison to the line of liquid-vapor. This difference is depicted in Fig.1.6 with the two lines below 0^0C. The red line indicates the transition line between solid-vapor and the red line indicates the phase transition line in case the available water would still remain liquid below 0^0C. The difference between these slopes is due to the difference in their specific volume V and latent heat as shown in Eq. (1.5.2). Since $V_{vapour} >> V_{ice}$ and the two latent heat of ice-vapor and water-vapor are fairly similar, the two curves are quite close. However, the slope of the solid-liquid transition curve is very different. In this case, V_{liquid} is slightly smaller than V_{ice} and negative but the latent heat is strongly positive, hence the solid-liquid transition has a large negative slope [41, 46].

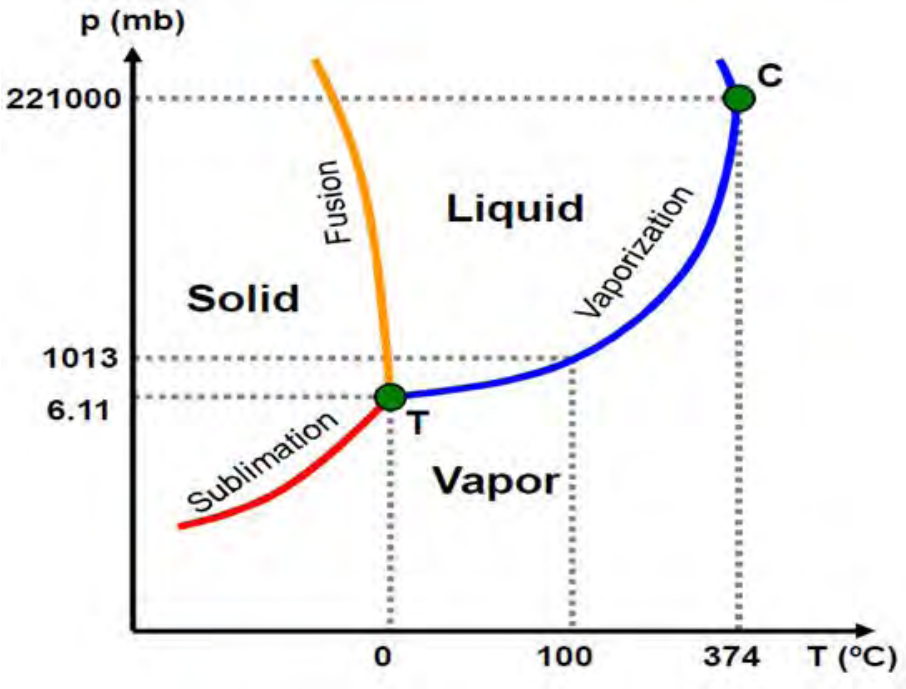

Figure 1.6: Clausius Clapeyron Curve with described phase transition between all three phases: solid (ice),liquid (water) and gas (vapor). Triple point (T) (p=6.1 hPa (mb), T=273K) is shown where all the transition lines come together.

1.6 Types of ice nucleating components

According to Pruppacher and Klett [47], list of general requirements for a particle to be effectively nucleate ice include: (i) insolubility, water absorption may cause the substrate to disintegrate (ii) size, a correlation between the number of larger aerosol particles, (iii) chemical bond requirement, water must be able to make chemical bonds with the INPs surface and (iv) crystallographic, a good INPs should template ice. These requirements might be met either on a particular crystallographic face of a nucleant or at specific active sites such as cracks or defects. These criteria were set out in part to help the atmospheric science community establish which atmospheric materials are likely to serve as INPs.

1.6.1 Dust and K-feldspar

Dust is considered the most important component for heterogeneous freezing due to its high frequency of appearance in cloud ice-crystals. Pratt et al. [85] found that about 50% of the aerosols inside high altitude cloud ice-crystals over Wyoming were dust particles and about 33% are biological components. It is important to remark that around 60% of the dust particles were found to be internally mixed with biological material, which presumably shows that part of its ice nucleating ability comes from small biological fragments with high ice nucleating ability [76]. However, not all dust can be considered to have the same ice nucleation ability. K-feldspar has been found to have bigger ice nucleation ability than most of the other kinds of dust particles. Its contribution to INP concentration in the atmosphere has been identified as a good first order approach for modeling the INP distribution [75]. Its effect can predict most of the INP observations below -15^0C within an order of magnitude.

However, above -15^0C, the observations cannot be explained just with feldspar, and so we have to focus on other kinds of aerosols in order to model the total INP spectra at all temperatures. Feldspar is primarily emitted in desserts such as the Saharan and then transported to other parts of the world; because of this transport, it can be of primary importance as cloud glaciation component in places very far away from the deserts. However, simulated values of the INP concentration tend to overestimate the amount of INPs at low temperatures, which could be explained by the effect of surface coatings by sulfates in the ice nucleating activity of feldspar [75].

1.6.2 Marine organic aerosols

In order to explain the amounts of INP present in remote oceans where transport of aerosols from other regions is small, we have to look at the aerosol emissions of the ocean. It has been found that organic components present in the sea-surface microlayer as well as some kinds of phytoplankton have ice nucleating ability [86]. This fact, together with the low amount of aerosols from other sources present in the remote oceans, could make this kind of particles the dominant INP.

1.6.3 Primary biogenic organic aerosols (PBOA)

The role of bacteria such as Pseudomonas syringae has a minor importance on global scale despite their high temperature activity, which is in part due to their low concentration in the atmosphere [54]. However, Tobo et al. [87] found an increase in INP after rain events in mid-latitude pine forest ecosystems, which were correlated to an increase in fluorescent biological aerosol particles (FBAPs). This fact suggested that

PBOA can have important regional impacts in INP concentration in forest ecosystems. This kind of ecosystem such as the Amazon, biogenic INPs from plants could be important on the sustainability of the ecosystem and it helps to develop rain processes and hence creats feedback effect between rains and vegetation [88]. Other PBOAs such as fungus or pollen have been found to have a high ice nucleating ability but their low concentration in the atmosphere suggests that their importance might be small. On the other hand, recent biological aerosols (fungus and pollen) can break into smaller parts, usually nanometer scale particles, which have an important ice nucleating ability. This effect could increase the number concentration of INP due to this kind of sources considering that a pollen grain can break into 10^4 smaller pieces [76].

1.7 Experimental methods to measure INPs activities

Experiments are performed under a wide range of conditions in an effort to empirically understand ice nucleation and determine rates for use in predictions of freezing behaviour. Some of these instruments are designed to take real-time measurements of ambient air; whilst, others are designed for use in laboratories with known samples and quantities.

The Aerosol Interaction and Dynamics in the Atmosphere (AIDA) cloud chamber is distinctly different from the other methods. It is designed to reproduce the evolution of a cloud. The AIDA cloud chamber is an 84 m^3 insulated chamber that can be

cooled down to -90^0C [89]. A representative atmosphere is achieved through mechanical expansion of the chamber using a vacuum and a frost layer on the inside of the chamber. Cooling experiments at a range of rates can be performed where temperature is varied with time [90]. The scale of the AIDA cloud chamber permits the interaction of the hydrometeors and therefore a more realistic treatment of ice formation processes in the atmosphere. However, it is impossible to determine the individual freezing events and the precluding nucleation event. Cooling rates are typically limited to above $\sim 1^0C\ min^{-1}$, which in terms of a typical cloud up draught speed is relatively high.

Among the different methods of measuring ice nucleation ability of different types of aerosols, the most common method is the Continuous Flow Diffusion Chamber (CFDC) [91]. These instruments typically have an impactor upstream to prevent any larger aerosol particles from entering [92]. That is, nothing bigger than 2 microns gets in. In the instrument, these smaller particles < 2 microns are activated as cloud droplets and some as ice crystals. The cloud droplets are evaporated in the lower section because the relative humidity is reduced below water saturation (toward ice saturation). In the modified CFDC method Saito et al. [93], "Automated CFDC type Ice Nucleus Counter" states that Particle detector is optical particle counter OPC (Climet Model CI-7350A). (Size range: 0.5$\sim$8 μm) and "Nucleated ice crystals are determined by their sizes >3 μm". For example, instruments based on the continuous flow diffusion chamber (CFDC) design of Rogers et al. [94] limit the size of particles analyzed to those with an aerodynamic diameter $\leq$0.75 μm in some cases DeMott et al. [95] and $\leq$ 2.4 μm in others Garcia et al. [96]. There is no lower size cut for aerosols entering the CFDC except for very small sizes under about 30 nm for

which diffusional losses would be large within inlet parts and tubing. It may be mentioned that aerosol particles are exposed to an ice super saturation and a temperature (-10^0C$\sim$ -35^0C) and for a few seconds (usually 5sec to 20sec). These instruments have some advantages as it is possible to do real-time airborne measurements but also have some limitations as the biggest aerosol particles have to be removed before the measurements to avoid their detection as ice nucleating particles [56].

Cold-stage instruments consist of cooling aerosols suspended in water droplets of different sizes. With these methods, we can measure the INP activity of different types of aerosols in the immersion freezing mode [97]. Droplets containing a known concentration of INPs are applied to a substrate and cooled at a constant rate. Freezing events are measured using an optical microscope. Using this method, varying cooling rates can be used to investigate the temperature-dependence of an INP (ranging from $\sim$ 0.01 to $10^0 C\ min^{-1}$). Freeze-thaw cycles can be performed in order to understand the reproducibility and isothermal experiments, where the temperature is held constant for a duration of time (on the scale of minutes to days), can be used to examine the time-dependent behaviour of an INP [81, 98]. One of the common ways of measuring the INP concentration with these methods is defining a density of active sites dependent on a parameter of the aerosol population such as the surface area in some cases, the mass. In this approach we are using the singular description of INP in which we are considering the time dependence as an effect of secondary importance and so, not taking it into account for heterogeneous freezing. With this method we can calculate the density of active sites per unit of aerosol surface density of nucleation sites (n_s) as depend on the fraction of frozen droplets (f_{ice}) for a certain temperature, knowing the total surface of the aerosol population [10, 75].

By now, some materials have been identified to nucleate ice very efficiently, among those; k-feldspar has been discovered as one of the most important contributors to global INP distribution [75]. Other aerosols that have been identified as possible contributors to INP are bacteria (P. syringae), soot, birch pollen, fungal spores, mineral dust, volcanic ash, etc (Fig. 1.7).

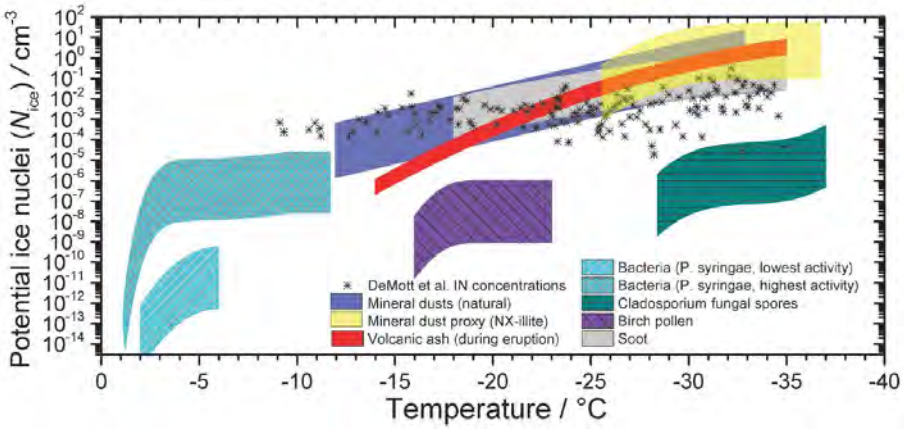

Figure 1.7: Contribution of different aerosols to INP distribution from Murray et al. [10].

1.8 Models related with ice nucleation

Understanding the process of ice nucleation is important not only in describing ice nucleation properties of aerosols in the atmosphere but also in predicting the ice nucleation behaviour of new materials. Classical nucleation theory (CNT) describes the formation of new phases from a parent phase which is usually a metastable phase [47, 80, 99]. In the process of homogeneous nucleation, the overall free energy (ΔG_v) is dependent on the free energy of the unit volume (ΔG_v) and free energy associated with the transformation in the interfacial surface tension (ΔG_s) that depends on the

surface tension [99]. ΔG_s is a positive quantity, the magnitude of which is proportional to r^2. In a supersaturated solution G_v is a negative quantity proportional to r^3. Thus, the change in the overall energy is given by

$$\Delta G = \Delta G_s + \Delta G_v. \tag{1.8.1}$$

The surface interface of free energy (ΔG_s) can be expressed as

$$\Delta G_s = 4\pi\sigma r^2, \tag{1.8.2}$$

where r is the radius and σ is the surface energy of the interface between the new and parent phase (sometimes surface forming energy) [100]. Similarly, the transition energy of the volume (ΔG_v) can be expressed as

$$\Delta G_v = -\frac{4\pi r^3}{3v} kT \ln S, \tag{1.8.3}$$

where v is the volume of water, S is the ratio of vapour pressures of liquid water and ice (P_l/P_{ice}), which can be obtained as previously defined by Murphy et al. [101]. k is the Boltzmann constant, T is the temperature. By combining Eqs. (1.8.1)-(1.8.3) we get,

$$\Delta G = 4\pi\sigma r^2 - \frac{4\pi kT \ln S}{3v} r^3 \tag{1.8.4}$$

The first term explains the energy of the interface between the new phase and the parent phase; while, the second term is the energy associated with the molecular volume of the new phase. The free energy of a subsaturated vapor ($S > 1$) is known to increase as the radius (r) increases. Hence, at a certain radius, the overall free energy (ΔG) will reach a maximum and this is equivalent to the amount of energy needed to overcome the barrier for a cluster of new phase to form. Setting the

derivative $d\Delta G/dr = 0$ in Eq. (1.8.4) and the CNT suggests that for a new phase to form, there is a critical radius (r^*) that a cluster of molecules must reach,

$$r^* = \frac{2\sigma v}{kT \ln S}, \tag{1.8.5}$$

The Gibb's critical energy of formation (ΔG^*) needed to overcome the barrier for a critical radius (r^*) and it can then be obtained by substituting Eq. (1.8.5) into Eq. (1.8.4):

$$\Delta G^* = \frac{16\pi\sigma^3 v^2}{3(kT \ln S)^2}, \tag{1.8.6}$$

From the expression above, the nucleation rate of the new phase (ice) can be obtained from an Arrhenius form equation:

$$J = A \exp\left(-\frac{\Delta G^*}{kT}\right), \tag{1.8.7}$$

where J is the nucleation rate usually reported as nucleation events per unit volume per unit time and A is the pre-exponential factor which depends on viscosity and other parameters [53, 102]. Substituting Eq. (1.8.6) in Eq. (1.8.7) will result in:

$$\ln J = \ln A - \frac{16\pi\sigma^3 v^2}{3k^3T^3(\ln S)^2}. \tag{1.8.8}$$

We can obtain the value of A from the graph of $\ln J$ versus $T^{-3}(\ln S)^{-2}$. For heterogeneous ice nucleation where a particle is involved, Eq. (1.8.7) can be modified to accommodate the particle properties that are responsible for the reduction in the Gibb's energy as adapted from Murray et al. [10].

$$J = A \exp\left(-\frac{\Delta G^* \delta}{kT}\right), \tag{1.8.9}$$

where δ represents the factor that accounts for the surface properties of the particle involved in the nucleation process (i.e. in the formation of the new phase). To describe

an atmospherically relevant ice nucleation mechanism by different particles, various models have been adopted [10, 103, 104, 105, 106, 107, 108, 109]. It is known that the behaviour of INPs in the immersion mode can depend on several factors such as the cooling rate, the temperature, the nature of particle, dispersion of the particles in droplets, etc [10, 54, 110]. The two main models are: (1) the time-dependent model or stochastic, and (2) the time-independent model that is called singular or deterministic model. The stochastic model describes the probability of a critical cluster forming as being time-dependent, that means the tendency of ice forming is higher for a longer timescale cooling. In a time-dependent freezing model, the freezing temperature is higher at a slower cooling rate and vice versa. In the homogeneous case, the rate at which droplets freeze is defined by the equation in Mullin [100]:

$$R = \frac{dN}{dt} = J_{hom} V N, \tag{1.8.10}$$

where J_{hom} is the homogeneous nucleation rate, V is the volume of the droplet which freezes at time t, and N is the number of liquid droplets [100]. When the above equation is integrated within the integral limits of N_1 to N_2 and a corresponding time change of t_1 to t_2, the resultant equation is given below:

$$N_2 = N_1 \exp\left(-J_{hom} V \triangle t\right), \tag{1.8.11}$$

where N_1 is the number of droplets at $t = 0$, and N_2 is the number of droplets at $t = t$. When $N_2 = N_1$, the maximum probability of all droplets being frozen is 1. However, when a particle is present in a droplet, the volume parameter is substituted with an approximate parameter (s), which describes the surface area of the particle immersed in the droplet; the modified equation is given by:

$$N_2 = N_1 \exp\left(-J_{het} s \triangle t\right), \tag{1.8.12}$$

here, J_{het} represents the heterogeneous nucleation rate defined as nucleation events per unit surface area (s) of the particle per droplet per unit time. There is also a corresponding change in the units from J_{hom} ($cm^{-3}s^{-1}$) to J_{het} ($cm^{-2}s^{-1}$). The assumption here is that there is a particle-to-particle uniformity for every droplets studied; and this model is described as the single-component stochastic model [10]. In a situation where there is particle-to-particle variability, the observed distribution of freezing temperatures is a product of both the stochastic nature of nucleation and the variability of individual nucleation sites present in the droplet. This can be described using a multiple-component stochastic model [10, 109]. However, for this study, time-dependent model will not be applied, because in an atmospheric timescale of cloud formation in the mixed-phase cloud, time-dependency is less important [73]. From laboratory experiments, it was shown that an order of magnitude difference in the cooling rate does not introduce any significant change [111]. In atmospheric modeling studies, the error from neglecting time dependence is negligible compared to the exact thermodynamics conditions of the cloud [90]. More so, Vali [104] and Ervens and Feingold [112] suggested that particle-to-particle variability is more important than the time-dependency of INP. The sensitivity of CNT for immersion freezing established that ice nucleation has by far the lowest sensitivity to time as compared to temperature, INP diameter and the contact angle. The adoption of a modified singular approximation is found valid for all range of times and temperatures encountered in mixed phase clouds [10]. For a singular or a deterministic model, ice nucleation is assumed to occur at a characteristic temperature irrespective of the cooling rate at which the particle is subjected to [81, 106]. Here, a particle is assumed to have sites

on its surface and each site has a predetermined temperature at which it can trigger freezing. Assuming a droplet contains only one particle with different sites, the overall freezing temperature of the droplet will depend on the site with the highest characteristic temperature. To estimate the active sites distribution on particles, the stochastic model shown in Eq. (1.8.12) given below:

$$N_2 = N_1 \exp\left[-n_s(T)s\right], \tag{1.8.13}$$

where $n_s(T)$ is the density of nucleation sites that become active at a particular temperature (T) per unit surface area and s is the surface area per unit volume (in this study, a unit volume is represented by a droplet). Usually, freezing occurs over a range of temperatures; therefore, it is useful to represent the fraction of frozen droplets at temperature (T) [113]:

$$f_{ice}(T) = \frac{n_{ice}(T)}{N_{tot}} = 1 - \exp\left[-n_s(T)s\right], \tag{1.8.14}$$

where $f_{ice}(T)$ is the cumulative number of frozen droplets at temperature T and $n_s(T)$ is the cumulative number of nucleation sites per unit surface area that are active between 0^0C and temperature T^0C.

Chapter 2

Methodology and instrumentation

In this chapter, we discuss the experimental methodology used in this study for measuring concentrations of the INPs. It provides a detailed description of the sampling site, sampling techniques, freezing experiments and the model associated with ice nucleation. The chapter concludes with a section on the data analysis approach used for the treatment of the data sets obtained during the experiments.

2.1 Sample site

The experimental site was located at a 3^{rd} floor balcony (12 m above the ground) in the School of Earth and Environment (SEE) building, University of Leeds, United Kingdom (53.78^0E, 1.55^0W, 63 m a.s.l.) shown in Fig. 2.1. The experiments were conducted in October 2014 and from February to March 2015. In order to measure the concentration of INPs, ambient aerosol particles were collected in a Biosampler impinger. The sampling was conducted by daily measurement of ambient aerosol sampling during at 10:30 A.M. to 02:00 P.M. The basic meteorological parameters such as temperature, relative humidity and wind speed were measured using an automatic weather station installed at the top of the building, School of Earth and

Environment, Leeds, UK.

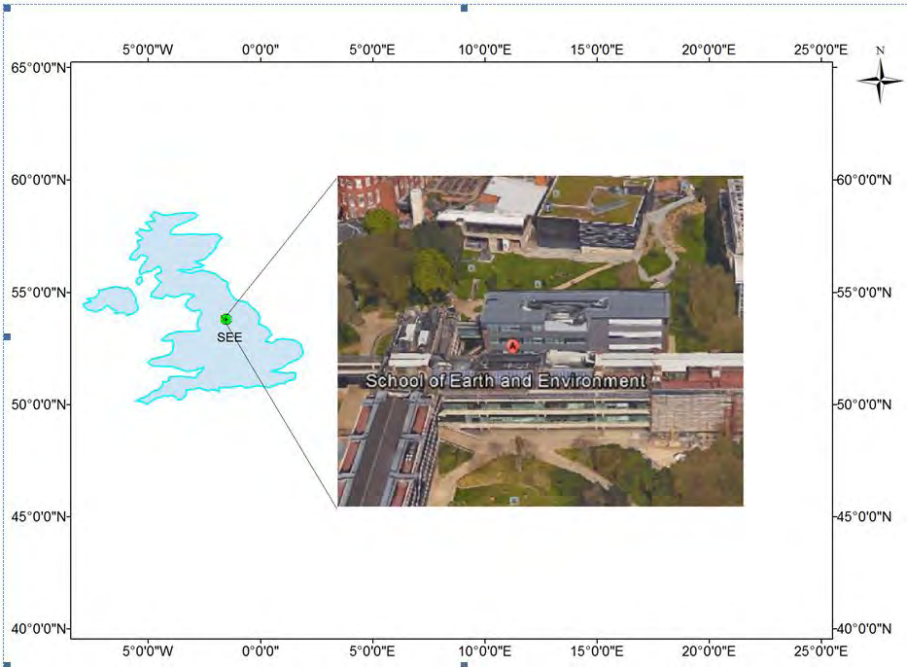

Figure 2.1: Sampling Location at the School of Earth and Environment, Leeds, UK.

2.2 Biosampler

SKC BioSampler (SKC Inc., Eighty Four, PA, USA) is a highly efficient bioaerosol and biologically inert airborne particle collection device that traps airborne microorganisms into swirling liquid for subsequent analysis [114]. The BioSampler is made of glass and consists of three parts: inlet, nozzle section (with three tangential sonic nozzles), and collection vessel (Fig. 2.2). The collection vessel can be filled with a liquid collection medium or coated with a sticky medium. The BioSampler can be used with water or non-evaporating liquids 1,000 times more viscous than water for sampling up to eight hours. The BioSampler requires a high-volume vacuum pump

such as the SKC Sampler. It has three 0.630-mm nozzles that are aligned such that flow passing through the nozzles causes a swirling motion in the collection liquid.

2.3 Working principles

The BioSampler is designed for sampling ambient particles in the atmosphere at the flow rate of 12.5 L/min. The device is composed of 3 parts: the inlet section, the nozzle section, and the collection vessel section. As shown in Fig. 2.2, the ambient aerosol is sampled horizontally into the inlet. The downward aerosol flow is then split into 3 nozzle flows. Each nozzle has a sonic orifice, which allows up to about 4.2 L/min of ambient air to pass through if the sampling pump establishes a downstream pressure of 0.5 atm or less. Each of the nozzle orifices is directed at an identical angle toward the curved inner surface. Thus, the aerosol particles are thrown at an angle toward the surface and are removed by the combined forces of impaction and centrifugal motion. The presence of three angular nozzles establishes swirling air motion in the collection vessel. The swirling air flow contains the liquid and swirls it upward into the region where the aerosol flows from the nozzles reach the inner vessel surface. Thus, the aerosol particles are flown down into the liquid reservoir. Ambient aerosol particle is pulled through an inlet where it is directed towards air water interface in a collection well by three tangential orifices. The sample well holds 20 mL of ultra-pure water in which particles were collected upon impact with an efficiency of $\sim$80% for particles D = 200 nm. The collection efficiency was $\sim$100% for particles 1 μm <D <6 μm. For D = 10 μm the collection efficiency was $\sim$50% [92]. Due to evaporation, the water level within the collection well decreased over time. To maintain high collection efficiency through the impinger was injected ultra-pure

water through the flow meter to the system through the collection inlet. The addition of the water was expected to wash off large particles that impacted and adhered to the glass of the inlet. After four hours of operation, a new collection vessel, filled with ultra-pure water, was placed on the impinger. Finally, we were weighing the volume of sample for the analysis. Volume of air passed through the BioSampler can be calculated using the formula V [Liter] = [L/min] x t [min]. Collecting sample was processed in a drop freezing assay to calculate the concentration of the INPs.

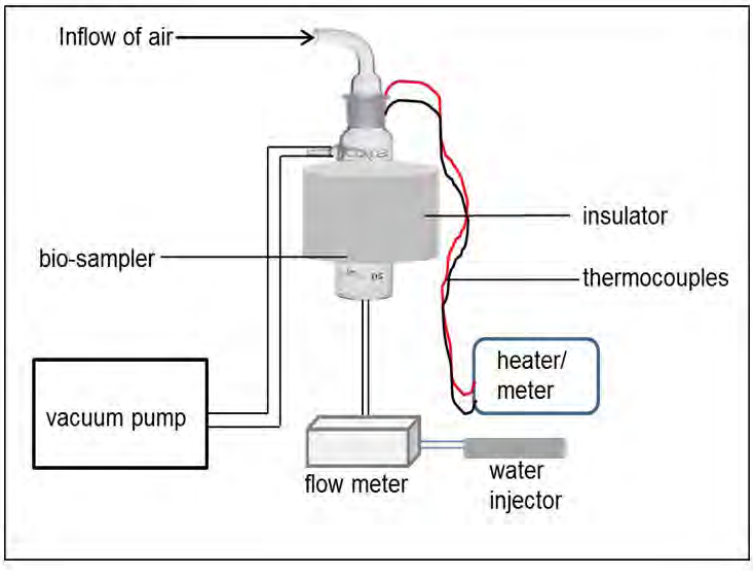

Figure 2.2: Schematic of the BioSampler.

2.4 Materials and samples preparation for the freezing experiments

2.4.1 Ultra-pure water and solvents

For the purpose of establishing a baseline and for validating the instrumental set-up used in this study, ultra-pure water was used. The ultra-pure water (Milli-Q water) was obtained from a Milli-Q Integral System (Millipore Water Purifier, USA) with the following properties: 18.2 MΩ at 25^0C resistivity, Total Organic Carbon (TOC) <10 ppb and filtered through a 0.22 μm. All ambient aerosol particles were sampled with this water source and the water was collected from the Milli-Q Integral System dispenser just before use. All pre-cleaning procedures were also carried out with the same water source. Chloroform (anhydrous ≥99%, containing 0.5 - 1.0% ethanol stabilizer), methanol (chromasolv for HPLC ≥99.9%) and silicon oil (CAS 63148-62-9) were all obtained from the Sigma-Aldrich Corporation for cleaning hydrophobic silanised glass slides.

2.4.2 Instrumental set-ups and freezing experiments

Drop freezing assay is a long established method and is widely applied in studying the ice nucleating abilities of particles in cloud conditions [81, 83, 102, 110, 115]. This technique involves a simultaneous cooling of droplets of equal volumes - here, in cloud-relevant conditions; while, the freezing temperatures are observed and recorded [113]. In this study, drop freezing assay experiments were used. The set-up is generically called Nucleation by Immersed Particles Instrument (NIPI) shown in Fig. 2.3.

2.4.3 The micro-liter Nucleation by Immersed Particle Instrument

The μl-NIPI forms part of a suite of instruments which are designed to make measurements of n_s over 10 orders of magnitude. Thus, covering the range relevant for the atmosphere. The micro-liter technique described in detail here has been used to study ice nucleation by mineral dusts (Atkinson et al. [75]), soil (O'Sullivan et al. [116]), nanoscale INPs (O'Sullivan et al. [76]), combustion ash (Umo et al. [117]) and time dependence of nucleation by kaolinite and K-feldspar [109]. This instrument was also included in an inter-comparison between 17 instruments [118]. The μl-NIPI also offers a number of advantages over some other instruments; experiments can be performed relatively quickly; freezing events are easy to detect and the continuous monitoring of freezing during a controlled temperature ramp allows the generation of a nucleation spectrum; in addition, there is no need for cooling fluids and the equipment is portable allowing it to be readily deployed in field settings. The general layout of the μl-NIPI is shown in Fig. 2.3.

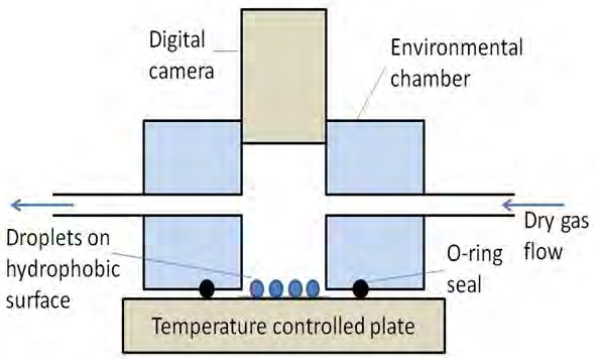

Figure 2.3: Diagram showing the main components of the droplet freezing instrument (μl-NIPI).

The μl-NIPI consists of a cold stage, a hydrophobic surface which supports the droplets, an enclosure in which the humidity experienced by the droplets can be controlled and a digital camera to monitor the state of the droplets. To provide cooling and temperature monitoring, a Grant-Asymptote EF600 cold stage was employed. The EF600 was developed for the purpose of cooling samples for biological cryopreservation and can control the temperature of a sample between 20 and -100^0C. For cryopreservation, a top plate capable of holding multiple cryovials is typically employed. However, a flat aluminum top plate is also available and was used for this experimental setup. To conduct a droplet-freezing experiment, a 22 mm diameter hydrophobic silanised glass slide of 0.22 mm thickness (Hampton Research HR3-231) was placed onto this flat top plate. Prior to the experiments, the slide was cleaned using water, methanol and chloroform. Around 40 droplets of 1 μL volume were pipetted onto the slide using a Picus Biohit electronic pipette; while, the slide was at room temperature as shown in Fig. 2.4. To ensure that individual droplets contained the same amount of material, the suspensions were stirred during the pipetting process. The uncertainty in volume quoted by the manufacturer is ± 0.025 μL. The droplets and slide were then covered within a Perspex chamber with ports for a camera (Microsoft Lifecam HD) and stainless steel pipes for delivering a gas flow to the cell. A recessed rubber O-ring was used to seal the chamber to the EF600 cold stage and an O-ring is also used to seal the camera opening. Both O-rings were coated with vacuum grease. A flow of dry zero-grade nitrogen ($0.2 L min^{-1}$) was passed through the cell in order to prevent frost growth. The EF600 was internally controlled by a Eurotherm 2416 PID controller, run via Eurotherm's iTools control software. This software was used to program and commence a $1^0C\ min^{-1}$ temperature ramp from 1

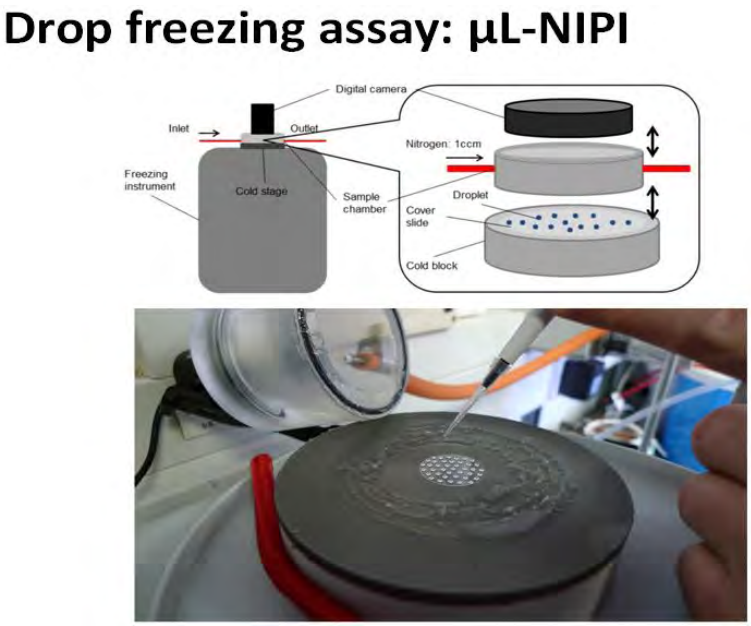

Figure 2.4: Schematic of the μl-NIPI cold stage used for immersion mode droplet freezing experiments and Pipetting 1 μl droplets onto a hydrophobic glass slide.

to -35^0C. Once the ramp was commenced, data logger software associated with the EF600 was started and used to produce a log of temperature against time. A LabView program was used to record an image series from the digital camera, typically at a rate of one frame per second, and to produce a time stamp for each frame. Hence, the temperature of the cold stage during each frame was known. Videos were reviewed frame by frame and the temperature of freezing of each droplet was recorded. Stills from the digital camera at several stages in the freezing experiment when the droplets frozen with temperature are shown in Fig. 2.5. The first change in droplet structure leading to droplet freezing was taken to be the nucleation event, and this information was used to establish the fraction of droplets frozen as a function of temperature. The EF600 has a quoted temperature uncertainty of $\pm 0.15^0C$ at -7^0C. To check the reliability of temperature measurement across a range of temperatures, a variety

of compounds with known melting points were frozen and then melted by heating at $0.1^0C\ min^{-1}$. The melting temperature range was determined visually. It is necessary to calibrate using melting points, rather than freezing points; crystallisation observed during cooling is always subject to nucleation, making them unsuitable for calibration of temperature unless the nucleation temperatures are very well defined [119]. By propagating the temperature error of the EF600 and the melting point range seen for water, a maximum temperature error of $\pm 0.4^0C$ has been estimated.

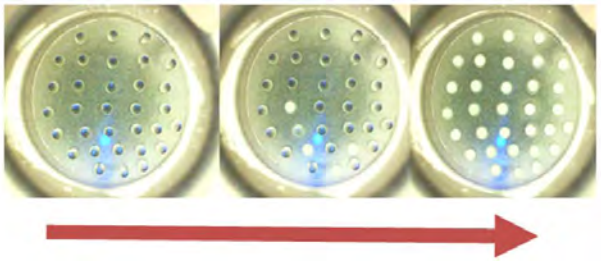

Figure 2.5: Some of the images captured during a typical freezing experiment. The temperature shown to decrease from left to right of as the individual droplets froze.

Before carrying out experiments with sampling droplets, it was necessary to establish a baseline for the instrument/experiment. The freezing of ultra-pure water was used to check the performance and sensitivity of the μL-NIPI set-up as well as to establish a baseline for the drop freezing experiment for this particular set-up. The baseline here is defined as the cut-off temperature that allows a distinction to be made between freezing caused by particles immersed in droplets and freezing that is due to ultra-pure water alone or the supporting surface (substrate). For each baseline test, ultra-pure water was obtained from a Milli-Q machine daily and used for the experiment. A summary of the fraction of droplets frozen for the ultra-pure water on the μL-NIPI is shown in Fig. 2.6. Droplets of ultra-pure water ($\sim$1.0 μL) froze within $\sim 18^0C$ range, which is unusual for the freezing of ultra-pure water. This wide range

of freezing temperatures could be due to a surface dependent nucleation mechanism. From the plot, it is shown that more than 90% of the droplets froze at temperatures below -23^0C. Following this observation, -23^0C was chosen as a reasonable baseline for the μL-NIPI set-up. The sporadic freezing events of droplets population observed above -23^0C could be due to impurities in the water or irregularities on the surface used for supporting the droplets. Further filtering of the water with a 0.02 μm did not improve the freezing curve which indicates that the sporadic freezing could be caused more by the irregularities on the surface. This could not be tested because of limited instrumentation.

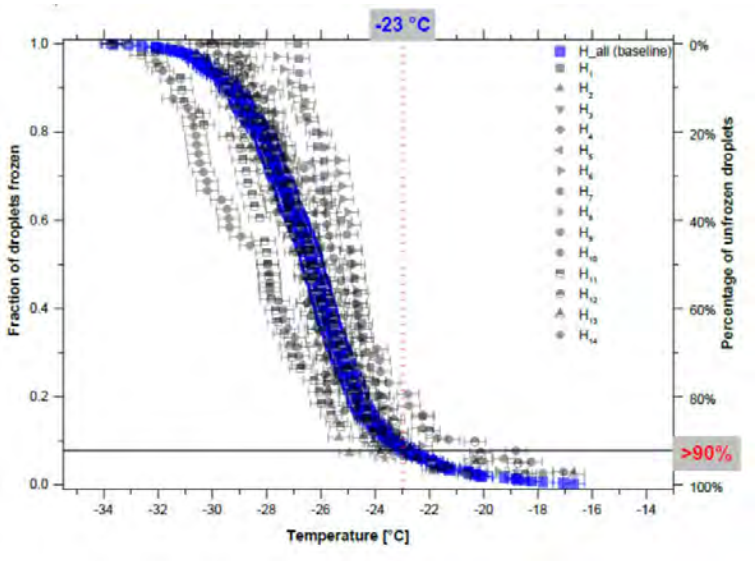

Figure 2.6: Fraction of frozen droplets of ultra-pure water (18.2 MΩcm resistivity @ 25^0C. The percentage of unfrozen droplets used in establishing a freezing baseline or a threshold for the μL-NIPI experiment. The uncertainty in the temperature is quoted as $\pm 0.4^0C$. The grey data points indicate fourteen (14) different experiments with ultra-pure water while the blue sigmodal fit is the cumulative fraction of all frozen droplets ($\sim$500 droplets). The vertical red dotted line indicates where the baseline is taken.

2.4.4 Artifacts associated with μL-NIPI experiments

Experimental artifacts and uncertainties are common problems in most laboratory measurements; an experimental procedure is always aimed at keeping the possible error sources as minimal as possible [120]. Some experimental artifacts were observed and the knowledge gained enabled the experimental methods to be optimized to ensure accurate results. During μL-NIPI experiment a humidity-controlled cell was used to limit the effect of mass transfer by the droplets (i.e. evaporation of droplets). In order to achieve, nitrogen gas was connstanly flushed through the cell during the experiment. The flow rate of nitrogen gas that was passed through the humidity-controlled cell was optimized to $\sim$ 1.8 x 10^{-3} lpm. This was measured with a Gilibrator 2 flow meter (Sensidyne, USA). A flow rate that is non-optimal could cause evaporation of the droplets around the area directly in the path of the flow. However, if the nitrogen flow is not sufficient to create and maintain the required balance in the humidity-controlled cell, it can result in a frost formation or condensation on or around the droplets. This frost formation could trigger the freezing of nearby droplets, thereby setting-off a freezing chain. This will ultimately lead to incorrect measurement of the actual freezing temperatures. The flow rate optimization can depend on some external factors such as the dew point of the experimental conditions as well as the general arrangement of the flow tubes to the humidity-controlled cell. Another effect observed was a frost formation on the cold plate. This happens as a result of deposition nucleation on the cold plate which may have formed from saturation vapour in the humidity-controlled cell.

2.5 Data processing

After the freezing experiments and acquisition of data, processing the acquired data was a priority. The steps taken in processing the data were: (i) all temperature, time and video data that were automatically logged in during the experiments were acquired and all necessary corrections were made to the computer time and temperatures (based on the temperature calibration). (ii) calculation of the droplets volume's used: For droplets used in the μL-NIPI experiment, the droplets volume were uniform (1.00 $\pm$0.03 μL); therefore, the same volume was used in the data analyses. To obtain the volume of the droplets, an indirect approach was used to calculate the volume of a spherical cap as illustrated in Fig. 2.7. This is not the exact volume but the best estimate for the volume assuming there is no further distortion. In Fig. 2.7, the part below the hydrophobic surface is to show how the height (h) is obtained by assuming '2r' is equivalent to 'h' or it is a bit less by 'a'. The illustrations show how the volume

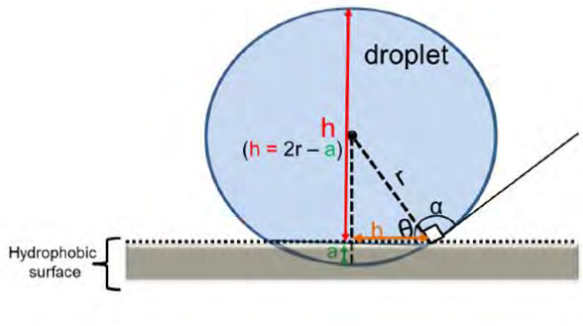

Figure 2.7: Schematic of droplets on hydrophobic surface onto a clean glass slide for μL-NIPI experiments.

of the spherical cap is used in calculating the volume of the droplets when the contact angle and the radius are known. The volume of the droplets was calculated from the

formula of a spherical cap as represented in Eq. (2.5.1) [121]:

$$V = \frac{\pi h^2}{3}(3r - h), \tag{2.5.1}$$

where V is the volume of the spherical cap (shaded blue), h is the height of the spherical cap and r is the radius of the sphere. Using the Pythagorean Theorem, the volume can be expressed as a function of a radius of the sphere and the contact angle with the normal of the sphere as given by Eq. (2.5.2):

$$V = \frac{\pi r^3}{3}(2 + 3\sin\theta - \sin^3\theta), \tag{2.5.2}$$

where V is the volume of the droplet, r is the radius of the droplets measured from the video analysis and θ is the contact angle of the droplets with the hydrophobic surface which in this case is the glass slide. The basic assumption here is that there is no evaporation of droplets sealed with the silicon oil. Due to the wide range sizes of the droplets used for the experiment, droplets were put in designated bins with less bias and treated together in order to obtain a symmetric value for further calculations. If droplets size distribution was highly skewed then 'rolling averaging' method was adopted. In rolling averaging method, the rolled-over average of the droplet volumes was used in lieu of the median volume used in the binning method. This approach prevented the bias that could have been introduced by median volume in the data analysis. (iii) Fraction of droplets frozen: From the video analysis, the total number of droplets at time t = 0 and also the freezing events with their corresponding temperatures were obtained. The fraction of droplets frozen (f_{ice}) per nucleation event was calculated by the Eq. (2.5.3) [81]:

$$f_{ice} = \frac{N(T)}{N_0}, \tag{2.5.3}$$

where N(T) is the number of droplets frozen at temperature T and N_0 is the initial number of liquid droplets at t = 0 of the experiment.

2.6 Data analysis

By assuming that ice nucleation by particles immersed in super-cooled droplets can be regarded as temperature-dependent and time-independent process, we determined the INPs concentration in the samples. The cumulative number of INPs per volume at a given temperature (T) is given by Eq. (2.6.1) [10, 113]:

$$K(T) = -\frac{\ln(1 - f_{ice})}{V}. \tag{2.6.1}$$

where K(T) is the cumulative number of INPs, f is the fraction frozen and V is the volume of the droplets. Applying Eq. (2.6.1) values the INPs concentration in the atmosphere was then determined in combination with the total volume of air passed through the sampler.

2.7 Air mass origin

To understand how concentrations of the INPs vary with air masses of different origin, we also used the National Oceanic and Atmospheric Administration (NOAA) Hybrid Single- Particle Lagrangian Integrated Trajectory (HYSPLIT) model to simulate the sources of air masses that influenced the sampling sites [122]. We then used the results to separate the types of 72-h back trajectories of the air masses during the INP sampling period at the third floor balcony of the School of Earth and Environment Building to study the effects of long-range transport and local air masses on INP

sampled at the experimental sites. The computation of the new position at a time step $(t+\triangle t)$ due to the mean advection by the wind determines the trajectory that a particle will follow. In other words, the change in the position vector P_{mean} with time is computed from the average of the three-dimensional velocity vectors V at their initial and first-guess positions [112].

$$P_{mean}(t+\triangle t) = P_{mean}(t)+\frac{1}{2}[V(P_{mean},t)+V(\{P_{mean}(t)+[V(P_{mean},t)\triangle t]\},t+\triangle t)]\triangle t \tag{2.7.1}$$

Eq. (2.7.1) is the basis for the calculation of trajectories in HYSPLIT and the advection component is considered when running trajectories. The outputs, showing the paths and time of the air parcels took, are shown on aerial maps. The map projection can be in any of the three map projections: Lambert, Polar or Mercator. The time intervals are defined by the user. A vertical view is also appended to show the air parcel through different altitudes. The model takes care of the diabatic and adiabatic processes in the vertical dimension. The boundary condition at the surface, where we assume no vertical motion, together with the consideration of atmospheric stability, permits trajectories to follow the terrain or go around obstacles when the trajectories approach the surface. Backward trajectories are useful in tracing aerosols and trace gases back in time and space to their source regions. Forward trajectories of air parcels provide a guide on the locations where pollutants are likely to be advected to. The HYSPLIT model can run interactively on the Web through the READY system on NOAA's site. The PC based version of HYSPLIT has also been used. Similar results are obtainable from both versions. Except that, the Web based version does not do the clustering. The model is based on the principle of Lagrangian advection with

the zonal (u), meridional (v) and the vertical (w) wind components at a time, atmospheric layer and grid used to compute a new upstream (or downstream) location of an air parcel at chosen time steps. This location is then iteratively re-determined using the components at the new position to calculate the next location. The procedure is then repeated for a specified starting time on a desired date for six days to produce a backward trajectory over five days. The following are some of the assumptions that are necessary to have the HYSPLIT model run according to Draxler and Hess [122]:

1. When the input data are given on pressure-sigma surfaces it is assumed that these surfaces, are the native grid of the meteorological model; hence, moisture is expected as specific humidity and temperature is assumed to be a dry temperature.

2. In a puff model, the source is assumed to be releasing pollutant puffs at regular intervals over the duration of the release. That each puff contains the appropriate fraction of the pollutant mass and the puff is advected according to the trajectory of its centre position while the size of the puff (both horizontally and vertically) expands in time to account for the dispersive nature of a turbulent atmosphere.

3. In a particle model, the source is assumed to be releasing many particles over the duration of the release. In addition to the advective motion of each particle, a random component to the motion is added at each step according to the atmospheric turbulence at that time.

4. Pollutant vertical mixing is assumed to follow the coefficients for heat. If the Turbulent Kinetic Energy (TKE) field is available, the mixed layer depth can

also be computed from the TKE profile instead of the temperature profile.

5. For puff dispersion, when the puff is larger than the meteorological model grid size, it is assumed that the meteorological model is capable of resolving turbulent motions on that scale. In the vertical direction, a puff distribution is always assumed to be a constant value inside the puff and zero outside.

6. For wet deposition one of the two assumptions taken is that the polluted air is continuously ingested into a cloud from a polluted boundary layer and those in which rain falls through a polluted layer.

7. At the grid points, where it is raining, the cloud bottom is defined at the level when the RH first reaches 80% and the cloud top is reached when the RH drops below 60%. All removal amounts are adjusted by the fraction of the pollutant mass that is within the cloud layer by defining the fraction of the pollutant layer that is below the cloud top and the fraction of the pollutant layer that is above the cloud bottom.

As summery, this chapter presented the ice nucleation experimental approach adopted in the study of the ice nucleating efficiencies of aerosols particles. Sampling site, working principles of Biosampler, materials and sample preparation for the freezing experiment were discussed. The baseline temperature for heterogeneous freezing for all μL-NIPI experiments was taken as -23^{0}C, below this temperature means that the freezing is influenced by the background freezing (freezing of pure water). This was determined following a series of experiments performed with ultra-pure water. Homogeneous freezing of pure water was observed, which their nucleation rates showed an agreement with earlier studies by Murray et al. [53] and Riechers et al. [102] within

the temperature uncertainties quoted. Most of the experiments performed were repeated to ensure reproducibility (precision). Finally, data processing, data analysis and calculating the origin of air masses were explained. All results obtained from the ice nucleation study of ice nucleating particles are presented in chapters three.

Chapter 3

Results and discussions

The methodology and data analysis techniques of this ice nucleating particles study as described in the chapter 2 of this thesis. This chapter describes the results obtained from the ice nucleation experiments of ice nucleating particles using the experimental set-ups (μL- NIPI) described in Chapter Two. All results are presented alongside the discussion.

In the course of this study, the total ambient aerosol data were collected in October 2014 and February to April 2015. The fractions of droplets frozen as droplets were cooled down at a rate of 1 $Kmin^{-1}$ were collected for a range of experiments for analysis. Fig. 3.1 shows the variation of fraction frozen with temperature. Droplets containing atmospheric aerosol always froze at higher temperatures than droplets of ultra-pure water. The analysis was performed between 0 and -37^0C at which all droplets facilitated heterogeneous freezing at temperatures well above the homogeneous freezing temperature. Most of the droplets froze at temperature lower than -17.5^0C. Moreover, the droplets in all samples froze between -18^0C and -23.5^0C. 50% of the droplets froze at a temperature of -20^0C, which is warmer than that reported by Barbara et al. [21] and Andreae and Rosenfeld [22]. We boiled some of

the samples at 100^0C which led to the loss of some of the INPs due to heat; these INPs might be biological in origin. Biological INPs are to be dominant above the freezing temperature -15^0C; while, below this temperature, non biological INPs may be of greater importance. It is dominated by soot and mineral dust [10]. Paul J. DeMott et al. [123] showed that the freezing temperature -20^0C of INPs are INPs of plant and soil biological origins. Biological particles have also been identified as a possible source of INPs [124, 125, 126, 127]. Oceans and continents are both potential sources of ice-active biological particles [10, 54]. Biological material found in the ocean that may be a source of INP in the atmosphere includes phytoplankton, bacteria and biological material in the sea surface microlayer (for examples Thalassiosira pseudonana, Nanochloris atomus and Emiliania huxleyi). Studies have indicated that bacteria and phytoplankton found in sea water and sea ices are a potential source of INPs in the atmosphere [128, 129, 130, 131, 132, 133, 134]. Material in the sea surface microlayer has also been found to exhibit ice activity [135] and previous work has indicated that biological material generated during phytoplankton blooms may be a source of INPs in the atmosphere [123, 136]. The modeling work of Burrows et al. [137] indicates that ice-active primary biological particles from the ocean may be particularly important in remote regions such as the Southern Ocean.

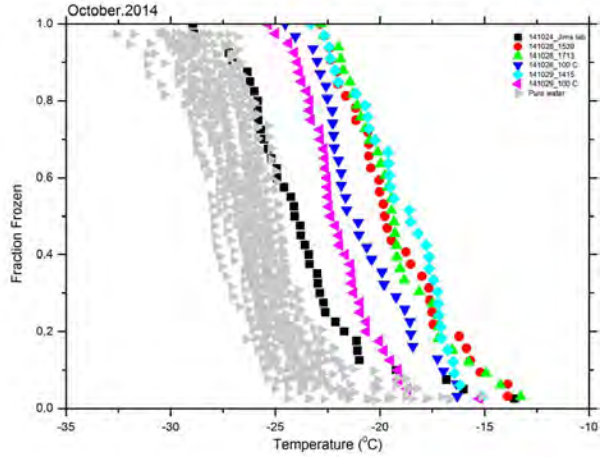
October.2014
Fraction Frozen
Temperature (°C)
1.0
0.8
0.6
0.4
0.2
0.0
-35
-30
-25
-20
-15
-10

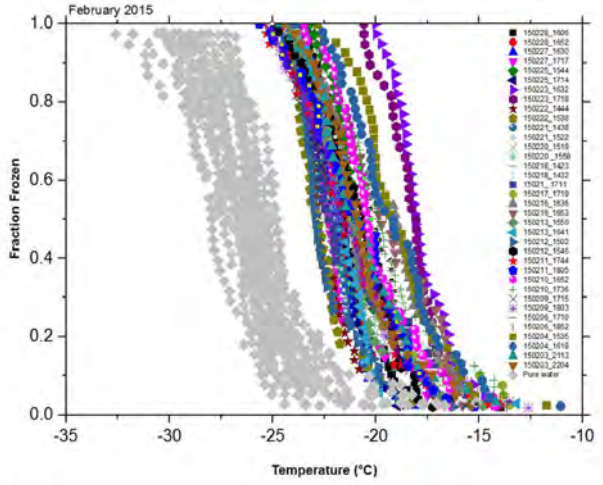
February 2015
Fraction Frozen
Temperature (°C)
1.0
0.8
0.6
0.4
0.2
0.0
-35
-30
-25
-20
-15
-10

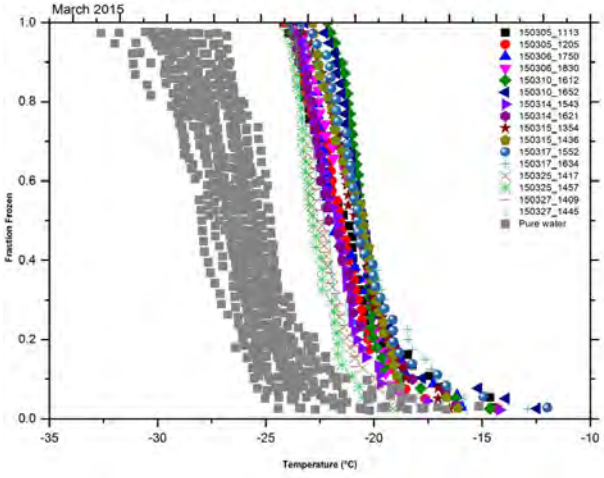
March 2015
Fraction Frozen
Temperature (°C)
1.0
0.8
0.6
0.4
0.2
0.0
-35
-30
-25
-20
-15
-10
150305_1113
150305_1205
150306_1750
150306_1830
150310_1612
150310_1652
150314_1543
150314_1621
150315_1354
150315_1436
150317_1552
150317_1634
150325_1417
150325_1457
150327_1409
150327_1445
Pure water

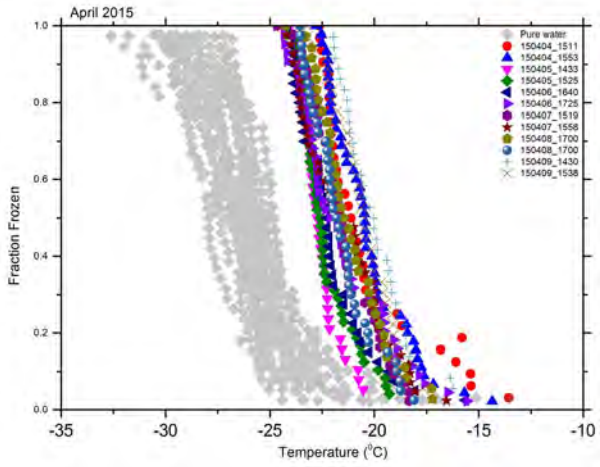

Figure 3.1: Fraction of droplets frozen for water samples from the particle into liquid sampler from October 2014, February 2015, March 2015 and April 2015.

In Fig. 3.1, the key is, the first six digits refer to the year, month and day and the second set of digits refers to the time at which the droplet freezing experiment was performed. Fig. 3.1 gives fraction of droplets frozen for water samples from the particle into liquid sampler from October 2014, February 2015, March 2015 and April 2015. The general trend of variation of the fraction of droplets of frozen droplets with temperature is identical. The background freezing curves for pure water are reported by O'Sullivan et al. [76] and Umo et al. [117]. Our results agree with their findings. They found that 90% ultra pure water froze at -23^{0}C. Using the fraction frozen graph in Fig. 3.1, we then determined the INPs concentration in the water samples using Eq. (2.6.1). The resulting atmospheric INPs concentrations are shown in Fig. 3.2 as a function of temperature for all sampling periods. These data demonstrate large variability in INP concentrations at a single temperature and emphasize the small subset of total atmospheric aerosol concentrations that INPs represents. In similar

study, total aerosol concentrations range from <100 cm^{-3} in some remote regions to tens of thousands cm^{-3} in urban locations and regions of new particle formation, in comparison with an upper limit of approximately 0.5 cm^{-3} for INPs [56].

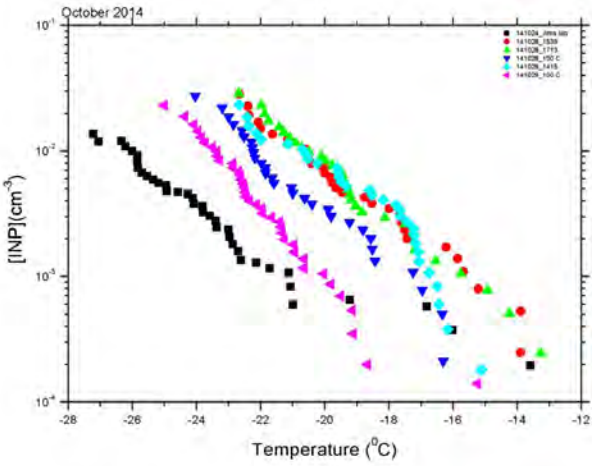

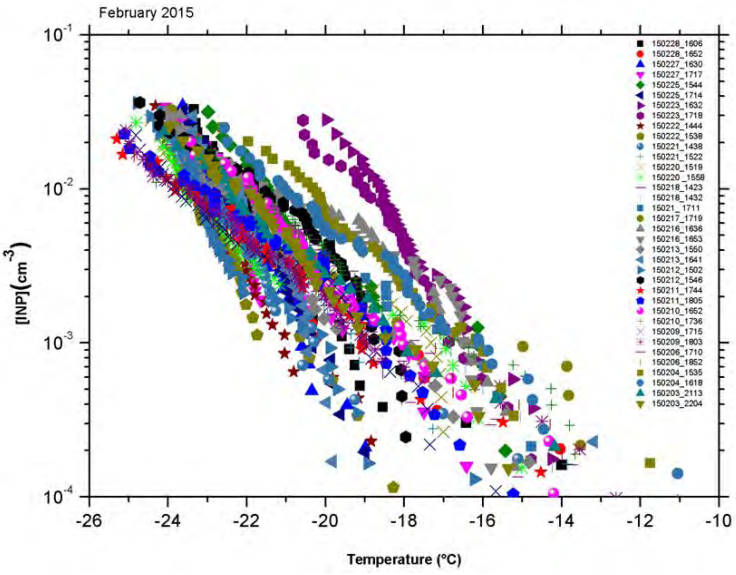

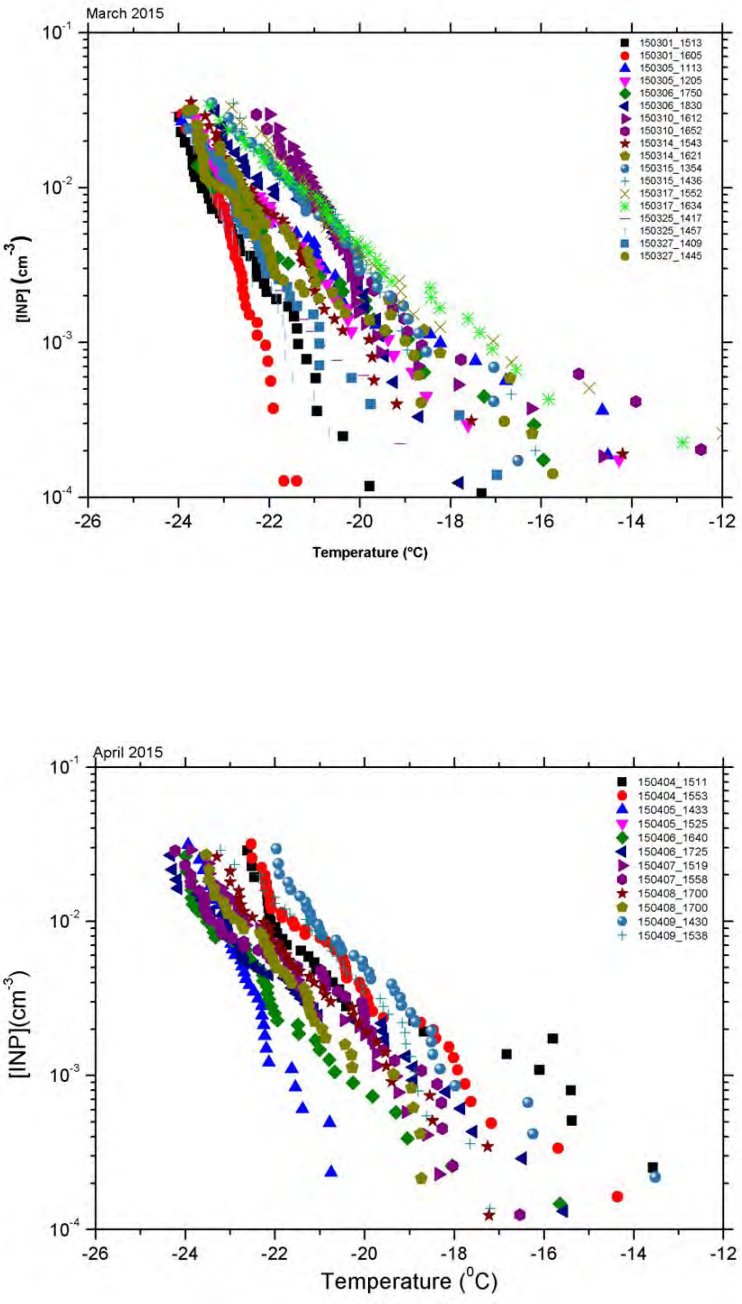

Figure 3.2: Cumulative number concentration of the INPs in October 2014, February 2015, March 2015 and April 2015 in Leeds, UK.

In addition, we compared our results with two commonly used parameterisations of INPs concentrations [138, 139] as shown in Fig. 3.3. Our results show that the droplets freeze in the range of temperatures -14 to -25^{0}C. This more likely agrees with Fletcher's observations which is more typical estimates of a few INP per standard liter at -20 ^{0}C but in Meyers et al. [138], the concentrations of INPs needed to explain observed precipitation rates range from as small as 10^{-3} per standard liter at -10 ^{0}C. Moreover, these parameterizations were based on observations available at the time, and the variability of INP relates to total ambient particle number concentrations [56].

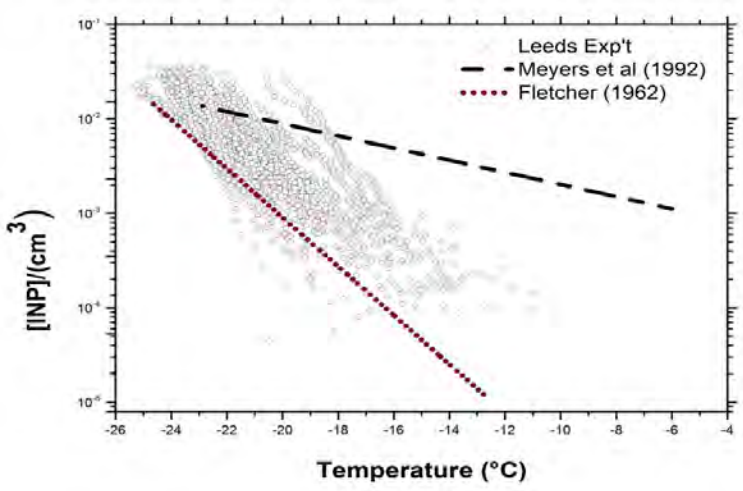

Figure 3.3: Comparison of our observed concentration of the INPs in Leeds, UK with two commonly used INPs parameterization: Meyers et al.[138]. and Fletcher [139].

As can be seen in Fig. 3.4, our observations showed a significant day-to-day variability in the INPs concentration. For example, at an activation temperature of

-20^0C, the INPs concentrations vary by nearly 2 orders of magnitude. We note that the days in February 2015, on which we measured the highest INP concentrations, was windy. Variability of INP at any temperature relate to spatiotemporal changes of INP sources, particle types and in different physicochemical categories of the overall atmospheric aerosol population.

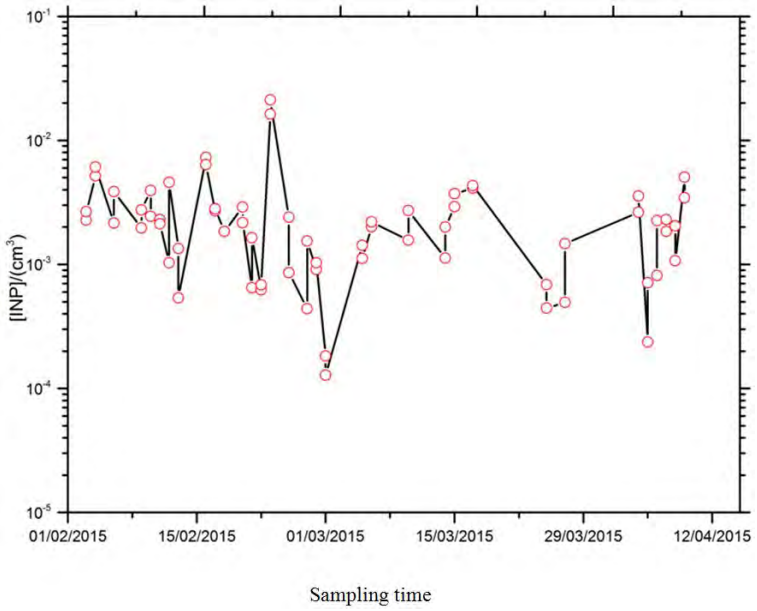

Figure 3.4: A typical fluctuations in concentration of the INPs measured in Feb.2015 to April 2015 at a temperature of T= -20^0C.

In addition, the INPs concentrations at temperature ranges between -14 to -25^0C were 10^{-4} to 10^{-2} cm^{-3}. The average concentration (10^{-3} cm^{-3}) of INPs was observed when the temperature was -20^0C (Fig. 3.5). DeMott et al [56] showed the role of the ice phase in climate and hydrological cycle; it is evident that an improved model description of IN number concentrations and of how these respond to anthropogenically and naturally induced changes in the ambient aerosol are important. Here, we

propose a remedy to the current lack of an observationally based, yet simple, parameterizations of INPs number concentrations. We combine our data and data from nine field studies occurring at a variety of locations over 14 years. We further show, using simultaneous measurements of total ambient aerosol size distributions, that a correlation exists between observed INP concentrations and the number concentrations of particles larger than 0.5 μm. Similarly, Murray et al. [10] reported INPs concentrations ranging from 10^{-4} to 10^{-1} cm^{-3}.

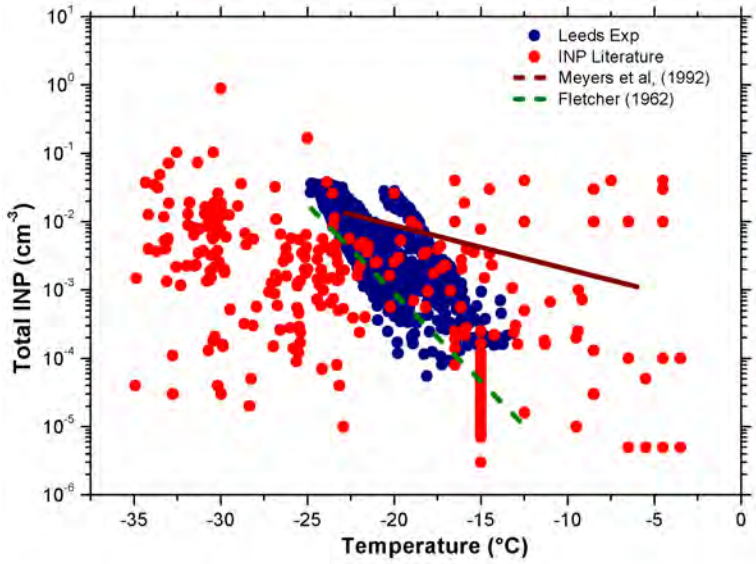

Figure 3.5: Concentration of the INPs as a function of temperature. The blue dots show the present observation and the red dots indicate the INPs concentrations by DeMott et al.[56].

Moreover, the types of aerosols in the INPs concentrations were measured and compared with other studies. The predominant type of aerosol species that forms INPs in Leeds was K-feldspar. Thus, our observation revealed that the INPs concentrations that were found in Leeds were in agreement with INPs concentrations that were measured in other locations [56].

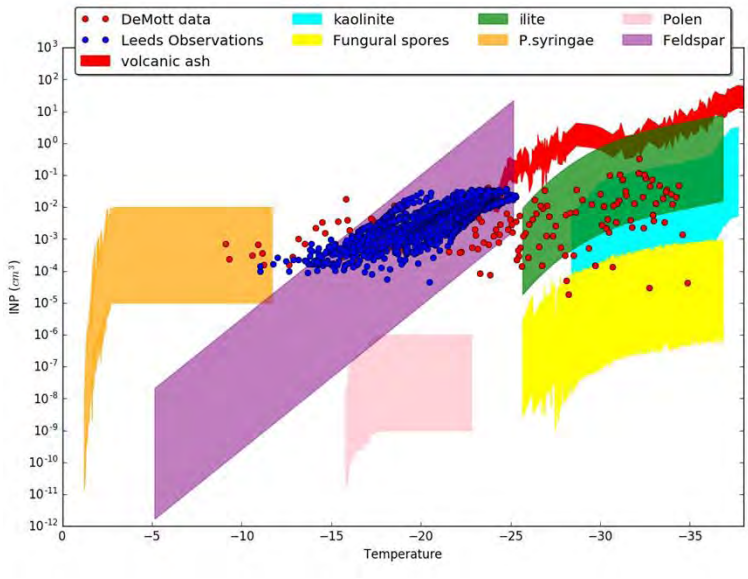

Figure 3.6: Comparison of our observed INPs concentration with INPs concentration species.

Fig. 3.6 shows immersion mode ice nucleating particles concentrations as a function of temperature for a range of different atmospheric aerosol species which are kaolinite, volcanic ashes, pseudomonas syringae, feldspar, pollen and ilite. The type of INPs concentration found in Leeds was feldspar for a range of temperature from -14 to -25^0C and their concentrations were 10^{-4} to 10^{-1} cm^{-3}. Calculations were performed using concentrations of different aerosol particle types in order to find ice crystal number concentrations. This was done through comparison of a range of aerosol types as INPs (including desert dusts, pollen grains, fungal spores, volcanic ash, bacteria and soot) based on DeMott et al. [56] and Murray et al. [10]. Recently, there is an oceanic source of INPs related to organic materials, which are emitted by phytoplankton as part of their natural life cycle [135] and another particular component of desert dust feldspar which is most important for its ice nucleating ability [75]. Through the global aerosol modelling process (GLOMAP), we were able to simulate

INP concentrations at the surface as shown in Fig. 3.7 for an activation temperature of -15^0C across the year 2015. The model result confirmed that the sources of INP in Leeds is K-feldspar. Feldspar dominates the INP concentration in environments influenced by terrestrial dust emission sources such as the Sahara and the Asian dust belt [75]. Feldspar and marine organics are the two main sources of INPs [75, 135].

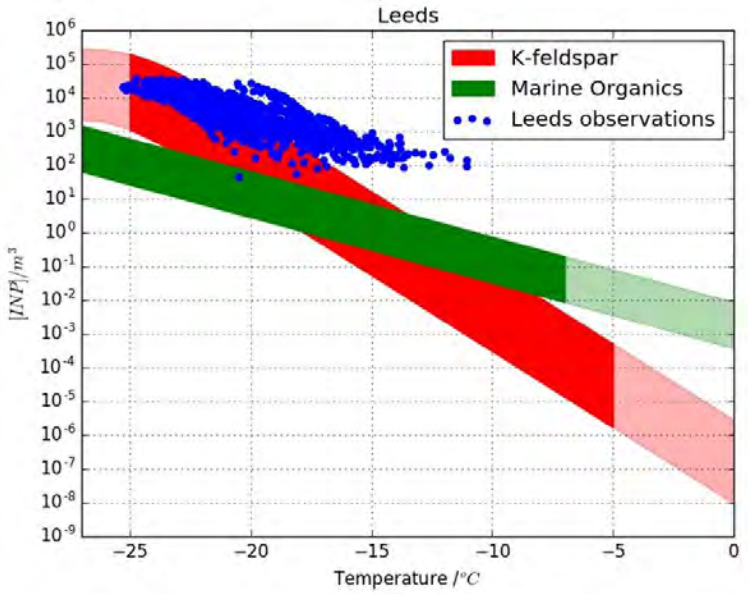

Figure 3.7: INPs simulated in Leeds across the year using GLOMAP model.

According to Wilson et al. [135], sea spray aerosol, which includes mostly marine organics, is one of the most important atmospheric INP types in the world's remote ocean regions,such as the Southern Ocean; whereas, feldspar is extremely important in many continental influenced regions where aerosols originated from mineral dusts [75].

Local meteorological parameters can affect the concentrations of INPs [140, 141]. Continuous observation of the concentrations of INP and the local meteorological parameters from February through March 2015 was made. Wind speed is one of the main factors that affects INPs concentrations. Each sample was therefore collected under different wind speeds. Thus, the highest peak of wind speed was observed on 23 February 2015. As can be seen from Fig. 3.8, the concentrations of INPs were highly correlated with wind speed. Therefore, high INPs concentrations were often observed on days with strong wind. In addition, it was observed that the concentration of immersion mode INPs also correlated with wind speed ($R^2 = 0.658$) (Fig. 3.8). This correlation points to a link between wind speed and the INPs population. Strong winds can increase the mixing of air near the surface and lead to higher concentrations of large particles and thus higher concentration of INPs [140].

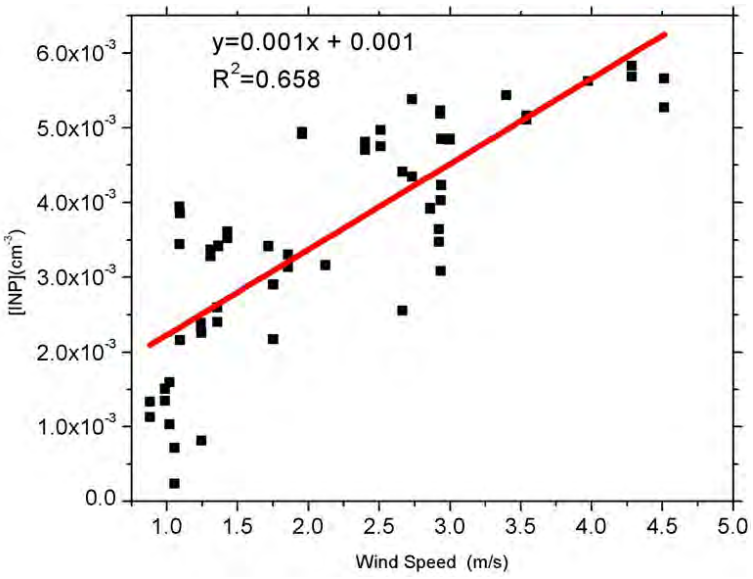

Figure 3.8: Concentration of the INPs at -20^0C as a function of wind speed.

Furthermore, the effect of relative humidity (RH) on INPs concentration was investigated. INPs concentrations were observed to increase with RH as shown in Fig. 3.9, which displays correlation between INPs concentration and RH ($R^2 = 0.909$). Thus, the result of this study is in agreement with previous findings reported by Timothy et al. [141].

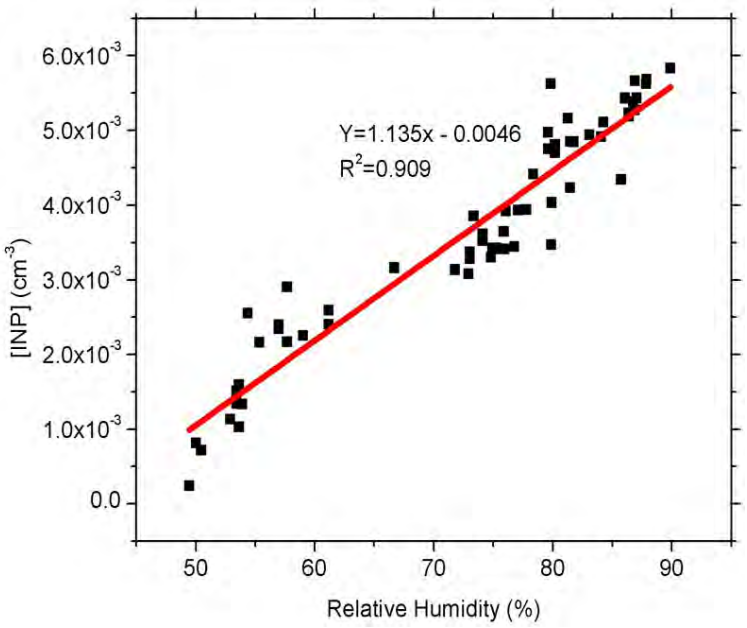

Figure 3.9: Concentration of the INPs at -20^0C as a function of relative humidity.

The Concentrations of INPs at -20^0C as a function of temperature ($R^2 = 0.610$) showed that when the temperature decreases the INPs concentration increased (Fig. 3.10). A small number of aerosol particles can serve as INPs at all temperatures although there is considerable seasonal and spatial variabilities [10]. Regarding the influence of temperature on INPs concentration and to relate temperature and INP concentrations, the number of particles capable of serving as INPs increases dramatically with decreasing temperature [139, 142, 143]. Thus, the concentration of INPs was found to exponentially increase with a decrease in temperature [10] and an increase in wind speed and relative humidity. It may be emphasized that our study shows that the concentrations of INPs are very much dependent on wind speed, relative humidity and temperature.

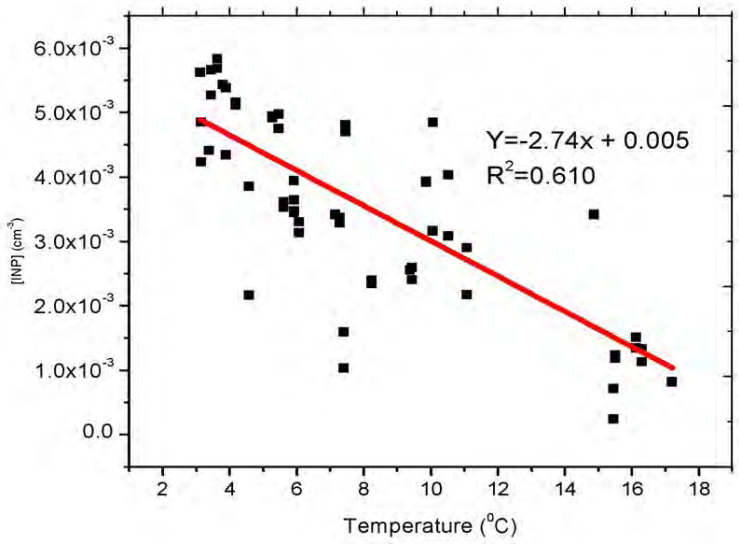

Figure 3.10: Concentration of the INPs at -20^0C as a function of temperature.

In addition to the effects of local meteorological conditions, air masses also had an influence on the concentration of INPs. The origin of the sampled air masses was investigated using Hybrid Single Particle Lagrangian Integrated Trajectory (HYSPLIT) model (http://www.arl.noaa.gov) in backwards mode. The variations of INPs concentration with air masses of different origins were investigated. Figure 3.11 shows examples of air masses back trajectories calculated using the HYSPLIT model during some sampling days. The sampling days on 28 and 29 Oct. 2014 showed that the air masses originated from the snow fields of Eastern Europe (Russia) and North Africa (Sahara)and moved to the UK (Fig. 3.11). During the Spring, the first two sampling days (10 and 11 February 2015) of the study area were characterized by maritime air mass. On the other day, 16^{th} Feb. 2015, the air mass had continental and maritime origins. In addition, on the other three days (18, 21 and 28 February 2015), the origins of the air masses moved from northern Canada and Greenland and reached the sampling site on a north-westerly air stream; moreover, the sources coming from tropical maritime air mass moved to was warm waters of the Atlantic Ocean (Fig. 3.11). The predominant wind direction across the UK in the course of the movements of tropical maritime air mass is south-westerly. It was also observed that in March 2015, the origins of the air masses were from tropical air mass, arctic maritime and polar continental (Fig. 3.11). The tropical air mass originates from North Africa and the Sahara (a warm source region). Moreover, 04, 06, 07 and 08 April 2015 were characterized by Tropical and returning maritime air mass sources. Isono et al. [144] used an ice nucleus counter and found that low INPs concentrations occurred in maritime air masses, and high concentrations in continental air masses. Particularly, higher concentrations were found in dust storms originating from arid

regions. Concentrations determined at -20^0C varied from $< 1 \times 10\ cm^{-3}$ (maritime) to $> 6\times\ 10\ cm^{-2}$ (dust storm) with typical daily concentrations of $\sim\ 1\ \times\ 10\ cm^{-3}$ to $1\ \times\ 10\ cm^{-4}$. This early work witnessed that mineral dusts made up a significant proportion of atmospheric INPs species and their concentrations varied depending on source region.

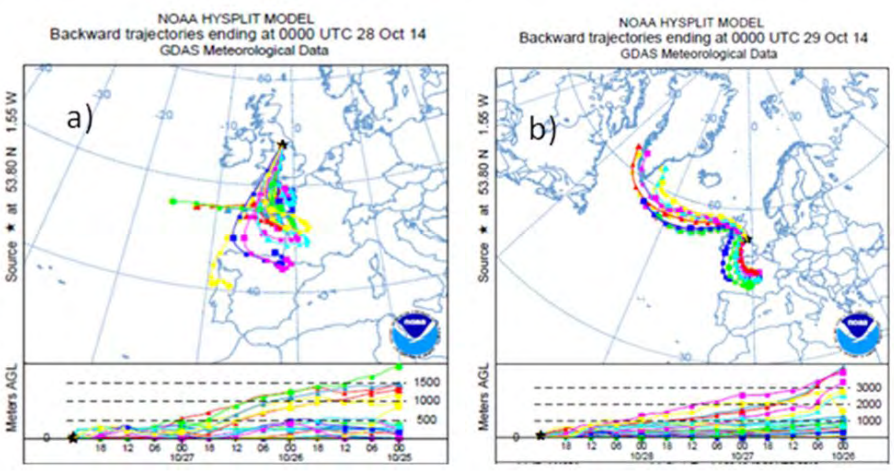

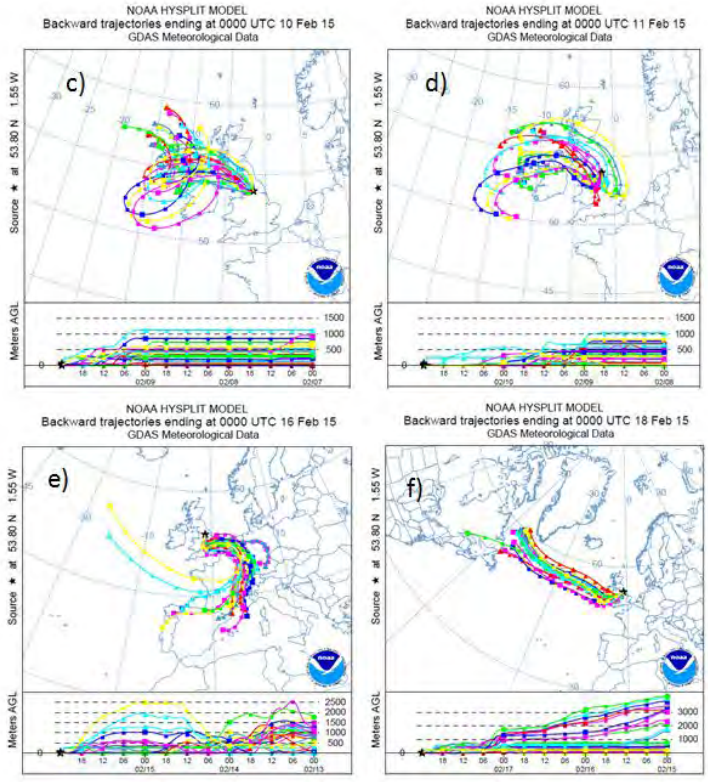
NOAA HYSPLIT MODEL
Backward trajectories ending at 0000 UTC 10 Feb 15
GDAS Meteorological Data
c)
Source ★ at 53.80 N 1.55 W
Meters AGL
1500
1000
500
NOAA HYSPLIT MODEL
Backward trajectories ending at 0000 UTC 11 Feb 15
GDAS Meteorological Data
d)
Source ★ at 53.80 N 1.55 W
Meters AGL
1500
1000
500
NOAA HYSPLIT MODEL
Backward trajectories ending at 0000 UTC 16 Feb 15
GDAS Meteorological Data
e)
Source ★ at 53.80 N 1.55 W
Meters AGL
2500
2000
1500
1000
500
NOAA HYSPLIT MODEL
Backward trajectories ending at 0000 UTC 18 Feb 15
GDAS Meteorological Data
f)
Source ★ at 53.80 N 1.55 W
Meters AGL
3000
2000
1000

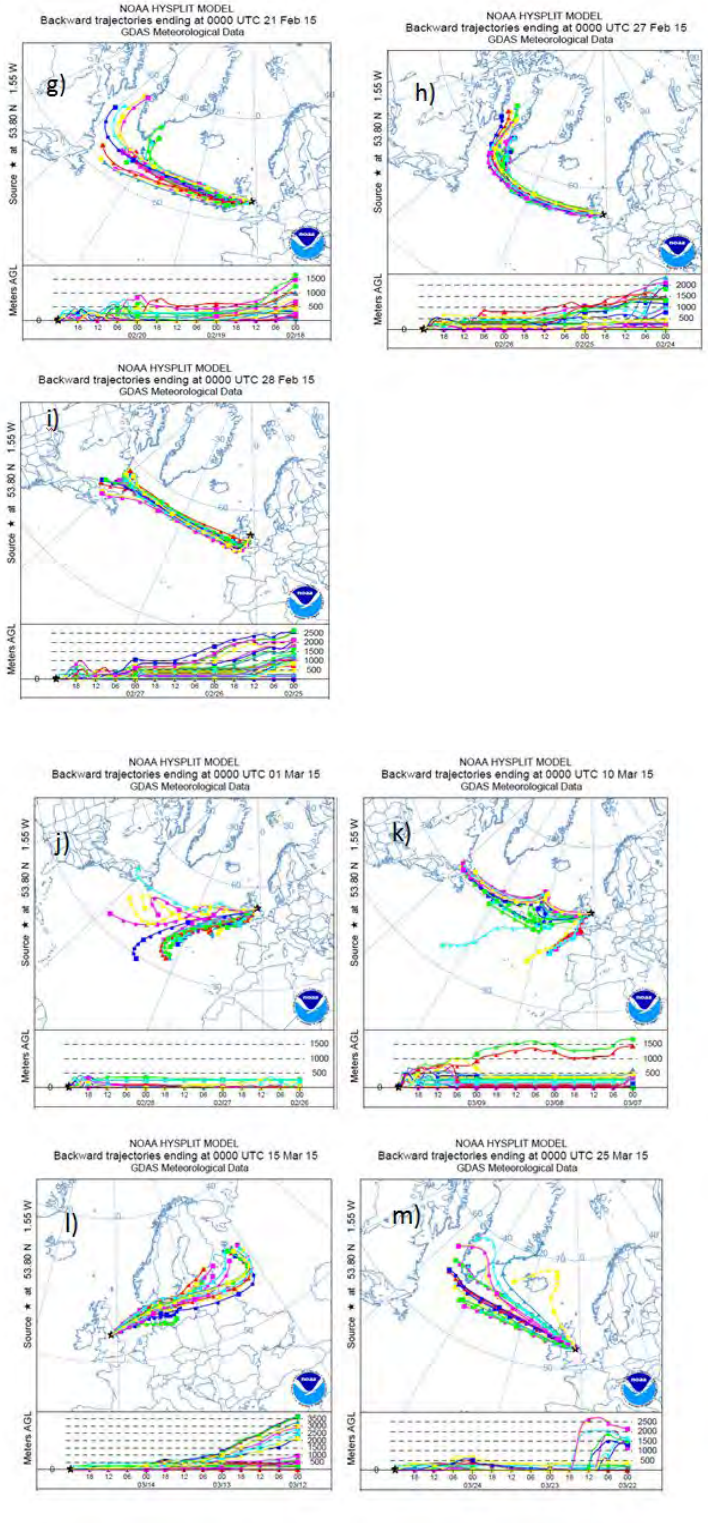
NOAA HYSPLIT MODEL
Backward trajectories ending at 0000 UTC 21 Feb 15
GDAS Meteorological Data
g)
NOAA HYSPLIT MODEL
Backward trajectories ending at 0000 UTC 27 Feb 15
GDAS Meteorological Data
h)
NOAA HYSPLIT MODEL
Backward trajectories ending at 0000 UTC 28 Feb 15
GDAS Meteorological Data
i)
NOAA HYSPLIT MODEL
Backward trajectories ending at 0000 UTC 01 Mar 15
GDAS Meteorological Data
j)
NOAA HYSPLIT MODEL
Backward trajectories ending at 0000 UTC 10 Mar 15
GDAS Meteorological Data
k)
NOAA HYSPLIT MODEL
Backward trajectories ending at 0000 UTC 15 Mar 15
GDAS Meteorological Data
l)
NOAA HYSPLIT MODEL
Backward trajectories ending at 0000 UTC 25 Mar 15
GDAS Meteorological Data
m)
Source ★ at 53.80 N 1.55 W
Meters AGL

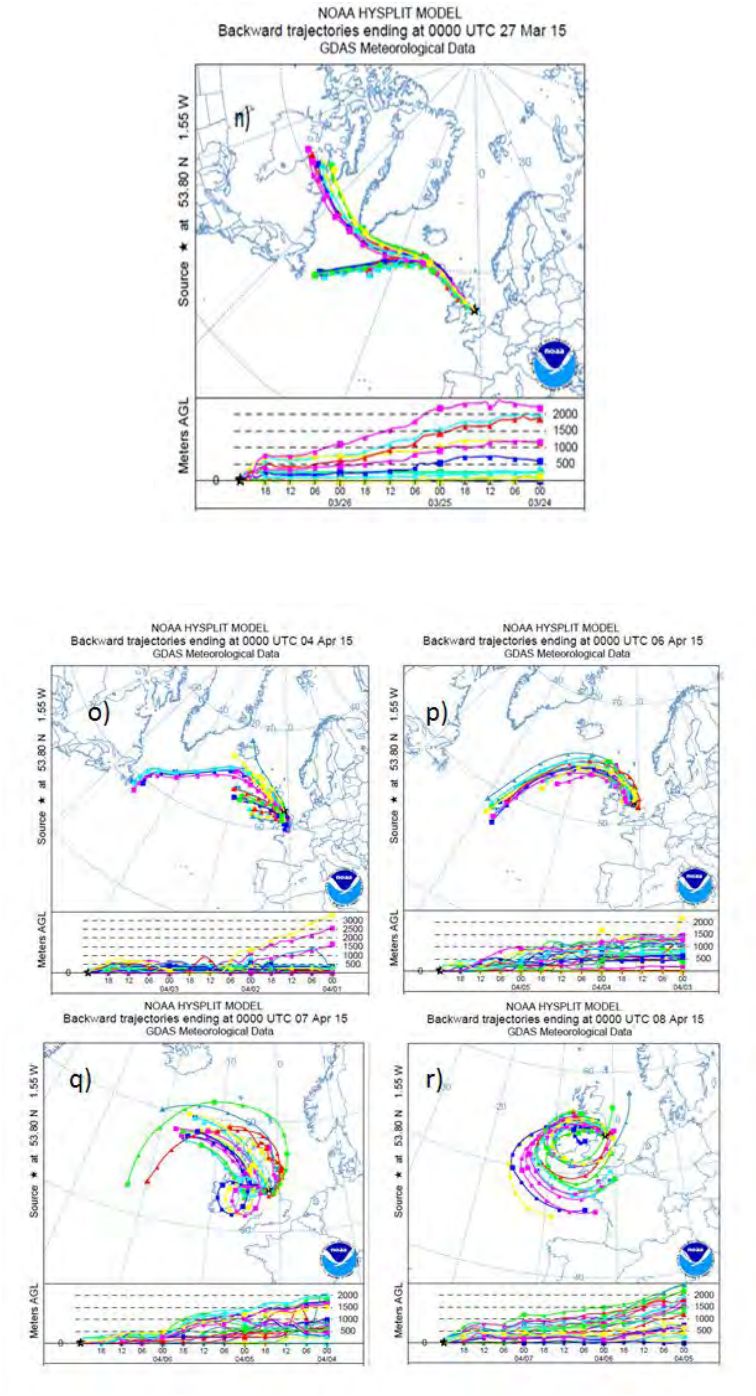

Figure 3.11: Backward trajectories for the different sampling days. Duration of 72 hours, 63 m above sea level and the color indicates the different trajectories.

3.1 Atmospheric relevance of this study

Atmospheric aerosols have an important influence on cloud properties through the direct and indirect aerosol effects, however there is significant uncertainty in quantifying both of these. Considering only the indirect effects, the ice phase has a particularly strong influence on cloud properties by affecting cloud lifetime and precipitation processes [9, 25]. The ice nucleating ability of many aerosols has been experimentally determined through both field (e.g. Cozic et al., 2008; Conen et al., 2012; Joly et al., 2014) and laboratory studies [10, 54]. Mineral dust has been identified as a major contributor to atmospheric ice nucleation at temperatures relevant for mixed phase [75, 95].

However, in this study, it is shown that measurements of ice nucleating concentration may be an important aerosol in assessing the total radiative budget of mixed-phase clouds due to its ice nucleating ability. Ice nucleation activity data is crucial in predicting and modelling these processes in aerosol-cloud microphysics models and global-climate models. The presence of more INPs will result in higher ice content in mixed-phase clouds; this reduces the cloud's lifetime by triggering precipitation via the Bergeron-Findeisen process [56].

Most precipitation in clouds initiates via the ice phase, which significantly influences the hydrological cycle and determines cloud lifetime [61, 94]. In mixed phase clouds, forecasting supercooled liquid is crucial because of its hazard in aircraft icing (Cober et al. 2001; Cober and Isaac 2012; Rasmussen et al. 2006; Siebesma et al. 2009). To predict the impact of the above processes and constrain estimates of the cloud radiation budget, it is imperative to understand the initiation and evolution of ice formation in the atmosphere.

3.2 Conclusion

The main findings in this study are:

1. From the experimental results, it is clearly shown that water droplets containing aerosols particles that form ice crystal froze heterogeneously.

2. It is also established that aggregation of aerosol particles in water droplets can influenced its ice nucleation efficiency. The agglomeration of aerosol particles increases with the concentration of INPs in the sample. However, at lower concentrations the effect of INPs aggregation is reduced to the minimum.

3. The potential INPs number concentration was estimated based on a parameterization from our experimental results, and compared with the atmospheric INPs distribution measured by DeMott et al. [56]. Feldspar may contribute to the INPs concentration from about -20^{0}C and may show competition with a more efficient INP such as mineral dust.

4. It can also be concluded from this study that the impact of INPs on mixed-phase clouds at a regional and global scale cannot be ignored due to its abundance in the atmosphere.

5. INPs concentrations were measured under varying weather parameters at the sampling site and were similar at droplet freezing temperatures of -14 and -25^{0}C and a strong linear correlation was found between INP concentrations and relative humidity.

To determine the impact of these ice-active particles on cloud properties and precipitation, additional measurements or calculations detailing their vertical convective

transport to altitudes relevant to mixed-phase cloud formation are needed. Furthermore, follow-up studies are necessary to determine if the close relationship between INPs and meteorological condition identified in this study is evident in other terrestrial regions.

Chapter 4

Characterization of particulate matters and gaseous pollutants in museums

4.1 Introduction

Cultural heritage is a unique witness of human civilization and is exposed to both natural disasters and anthropogenic pollution. Air quality in museums is critical to the preservation and conservation of rare antiquities with damage from air pollution being firstly reported in the middle of the 19^{th} century at the British Art Gallery [145, 146, 147, 149, 150, 151]. Since the 1990s, the microclimate in museums and airborne pollutants originating from indoor activities and/or penetration from outdoors have been of increasing concern in Europe [149, 151, 152, 153, 154, 155] and the United States [148, 156]. Cultural heritage plays an important role in our modern-day society. Therefore, its conservation and preservation have become a main concern in developed and developing countries during the last decades. As a result, research on cultural heritage objects has grown dramatically as scientific support and verification became imperative in the quest for preventive conservation. Preventive conservation is based

on the pioneering work of Garry Thompson, who established a set of environmental guidelines for the most optimal conditions in which heritage objects have to be stored and displayed. These recommendations can be consulted in the publication which is still a major inspirational source within the field of preventive conservation [157]. In general, all measures taken to delay the deterioration of cultural heritage belong to this domain. However, to reduce potential risks, the hazards first have to be identified. On a large scale, museums and heritage sites started to monitor temperature, relative humidity and to a lesser extent light irradiation. In addition, air quality became the subject of extensive research programs, both indoors and outdoors [147, 157].

4.2 Particulate matter

Particulate matter is an important class of atmospheric pollutants comprising a wide range of airborne objects with variable sizes and properties. According to Seinfeld [1], 'particulate matter' can be defined as 'any substance, except pure water, that exists as a liquid or solid in the atmosphere under normal conditions and is of microscopic or submicroscopic size but larger than molecular dimensions (about 2$\mathring{A}$). Apart from PM, different terminologies exist that can refer to atmospheric particles, such as 'environmental aerosol', 'aerosol', 'airborne particle' or 'suspended particles'. Due to the wide range of properties that has to be specified for the description of atmospheric particles, a unique classification does not exist. However, a common way to categorize PM is based on particle size. Airborne PM usually entails particles with sizes from 0.001 to over 100 μm [158]. Within this range, a coarse (> 2.5 μm) and fine (< 2.5 μm) fraction is generally discriminated. As indicated in Fig. 4.1, the coarse mode usually originates from mechanical processes such as wind-induced erosion. Particles

within the fine fraction, on the other hand, are dominantly generated by molecular processes. This fraction is subdivided into an accumulation and nucleation mode. The latter consists of particles formed from condensation of hot vapours (e.g., combustion processes) or nucleation of atmospheric compounds. The smallest particles approach the size of large gas molecules ($> 2\mathring{A}$), and also behave similarly. Particles in the nucleation mode are often subdivided in the ultrafine fraction ($<$ 100 nm). The accumulation mode arises from the coagulation of particles from the nucleation mode or by vapour condensation onto existing fine particles. Ideally, a trimodel size distribution exists. However, the distinction between nucleation and accumulation mode is not always clear, and often only a bimodal distribution is observed [1, 158].

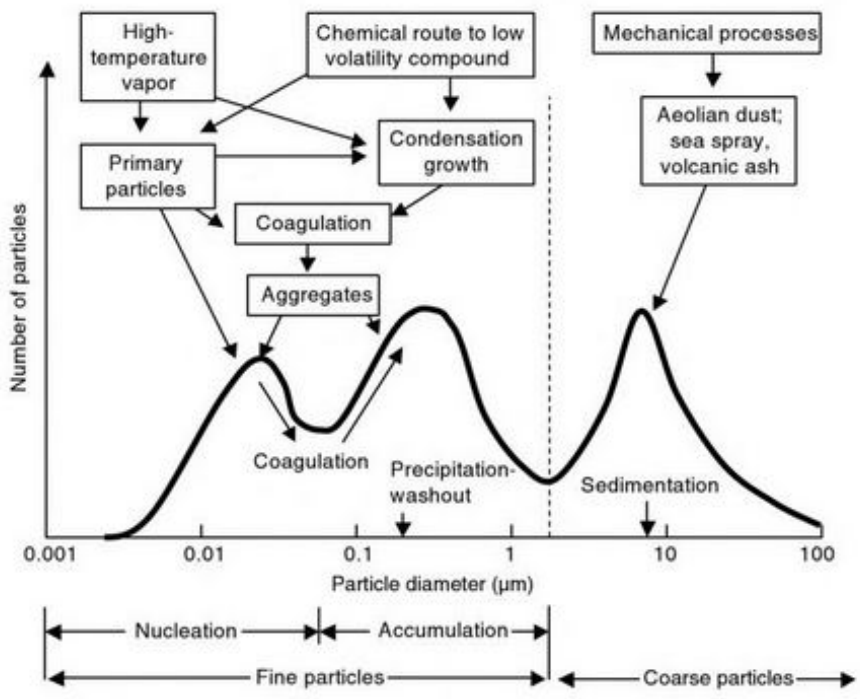

Figure 4.1: Prototypical size distribution of tropospheric particles with selected sources and pathways of how the particles are formed. Dashed line is approximately 2.5 μm diameter and adapted from UK Department of Environment, Food, and Rural Affairs, Expert Panel on Air Quality Standards [159].

4.3 Sources and formation of particulate matter

Nucleation involves the formation of very small particles [160, 161, 162]. Growth of nucleation mode particles occurs through coagulation and condensation [160, 163]. However, the rate of coagulation depends on particle number concentration and the rate of condensation depends on the surface area; therefore, particles do not normally grow above 1 μm because the condensation and coagulation rates decrease as the particle size approaches 1 μm. In that sense, aerosol particles in the size range between 0.1 - 1.0 μm are known as the accumulation mode particles. Coarse particles are formed by breaking up bigger particles into smaller particles; however, a lower limit of approximately 1 μm is established for coarse mode particles mainly because as particles become smaller and smaller, more energy is required to break them into smaller units. Other sources of coarse mode particles are windblown dust, dust restrained by turbulent air generated by traffic, destruction of buildings, evaporation of sea spray, pollen, mold, spores, and parts of plants and insects. The half-life of fine particles can be several days to few weeks, which corresponds to a spatial transport between hundreds to thousands of kilometers; whereas, the half-life of coarse mode particles is typically a few hours that corresponds to a spatial transport of approximately tens of kilometers [164]. Primary fine particles are directly emitted to the atmosphere or formed in the atmosphere by condensation or coagulation without chemical reactions. For example, primary fine particles are formed from metallic vapor during smelting or high temperature combustion. Primary fine particles are also formed from organic vapors during cooking or low temperature combustion. In the urban atmosphere, major sources of primary fine particles are combustion products from the burning of gasoline and diesel fuel. On the other hand, combustion of coal and heavy fuel

oil yields both fine primary particles, which are formed from the material vaporized during combustion, and coarse particles (i.e. fly ash), which are formed from non-combustible material.

Secondary fine particles are formed by the atmospheric conversion of gases into particles. One of the processes that form secondary fine particles is the conversion of a gas into the vapor of a material with a low saturation vapor pressure. For example, the oxidation of sulfur dioxide (SO_2) to sulfuric acid (H_2SO_4) that forms new fine particles by nucleation and then followed by coagulation forms secondary fine particles. Another process that forms secondary fine particles is the conversion of a gas into a different gas that can further react to form a substance with a low saturation vapor pressure. For example, the oxidations of nitrogen dioxide (NO_2) to nitric acid (HNO_3) can further react with ammonia to form secondary fine particles of ammonium nitrate.

4.4 Effect of particulate matter and gaseous pollutants on cultural heritage materials

Effects of indoor airborne particulate matter for the conservation of cultural heritage are well recognized [165]. Although the exact mechanisms are not yet fully understood, four different types of damage are generally identified: visual, mechanical, biological and chemical damage. Visual damage is probably the most obvious type of damage caused by PM. Particle accumulation on surfaces can change the aesthetic appearance of the object, thereby influencing the perception of the observer [165, 166, 167]. In general, dust accumulation is called 'soiling', which is defined as

'dirtying a surface'. When specifically intending the deposition of black particles, the term 'blackening' is commonly used. Soiling and blackening are related to the surface area covered by particles that scatter or absorb light that would otherwise be reflected [168, 169]. Visual damage is all about human perception, which is very hard to accurately measure. From which point soiling creates a visual nuisance. What are acceptable thresholds? For some people, soiling is perceived as a disturbance obscuring detail, while for others, soiling is appreciated as an aesthetic patina, evoking the feeling of an object to be old or antique [167, 170]. The second is mechanical damage such as enhanced abrasion which especially occurs with particles of high hardness (e.g., silicates) which are able to make micro-scratches or mechanically weaken the material. In general, cleaning is considered as a hazardous treatment [171, 172]. Nowadays, laser cleaning is possible and is widely used in various countries. Windblown particles are known to have potential abrasion capacities as well. Another specific example is the damage arising by walking on a carpet in which sharp edged particles are embedded, cutting the fabric fibers [173]. Depending on the material, the resulting micro-scratches can further influence the degradation process as a consequence of local humidity and pollutant accumulation. A third type of damage is bio-deterioration. Airborne PM can contain particles with biological origin, such as bacteria, bacterial and fungal spores, viruses and pollen. Once these particles settle on surfaces that are sensitive to biological attack, these particles give rise to fungal growth, provided favourable microclimatic conditions [173, 174, 175]. On the other hand, deposited dust can form a humid micro-environment on the surface, creating a nutritional resource for fungi which aids in their survival [176]. Additionally, microorganisms can metabolize adhesive exopolymers, which in their case induce a more

severe dust adhesion [177, 178, 179]. Chemical reactions between deposited PM and the underlying surfaces probably hasten the deterioration of many materials either by their chemical composition or their moisture absorption capacity. Moreover, particles can transport harmful substances to indoor surfaces. An example is soot particles that absorb reactive gases, bringing them in close proximity to the surface interface [180, 181].

In addition, inorganic compounds such as sulphur dioxide (SO_2), nitrogen oxide (NO_2) and ozone (O_3) are the most dangerous gaseous air pollutants. The main emission source is the combustion of sulphur-containing fuels (95% SO_2 and 5% SO_3) [182]. SO_2 is a colourless, water-soluble gas and forms (H_2SO_3) and (H_2SO_4), which are corrosive. SO_2 and O_3 are responsible for the degradation of dyes and damaging of photographic material [183] and leather [184]. This is the result of an oxidation reaction which causes conversion of the atmospheric SO_2 to (H_2SO_4) [185], which can damage the museum objects. These are mostly objects that are composed of calcium carbonate ($CaCO_3$) (marble, limestone and murals), but also cellulose (paper, cotton and linen), silk, iron (Fe) and steel [185]. Paper will be discolored and become brittle, textile and leather weaken and metals will become dull [184, 186, 187, 188, 189, 190, 191]. Iron acts as a catalyst for such oxidation reactions, as well as manganese (Mn) or copper (Cu) [192].

Tropospheric ozone causes a damage to the health, environment and material. Unlike in the case of most pollutants, there is no direct O_3 emission source. It is formed when sunlight is incident at different atmospheric polluting gases such as NO_x. O_3 is a highly reactive gas because of its strong oxidizing properties. It is capable to damage a variety of oxidation-sensitive materials, especially by ozonolysis reactions

with unsaturated organic compounds. Colour change and fading of pigments illustrate this phenomenon. Whitmore and co-workers [193, 194] have investigated the effect of O_3 on a range of pigments and textile dyes. They showed that the materials are at risk only if they are exposed to O_3 for a prolonged period. The discolouration or fading of dyes occurs when organic pigments are sensitive to specific oxidation reactions [195, 196, 197]. Additionally, O_3 causes damage to photographic material and paper [198] and reduces endurance of rubber [199].

NO_x-compounds are produced by combustion processes as a result of the oxidation of nitrogen (N_2) in the air. There are both anthropogenic and natural sources. NO_2 is a toxic, reddish brown gas and is similar to SO_2 regarding the damage to the exhibits. In humid air, it is oxidized to volatile nitric acid (HNO_3) by reaction with OH-radicals [185]. This acid can then induce fading of textile dyes and photographic film damage and weaken textile fibres [200].

Chapter 5

Sampling methodology and analysis techniques

In this chapter, sampling methodology and analysis techniques of particulate matter and gaseous pollutants were presented briefly. Including the sampling site, instrumental sampling of PM (Harvard type Impactor and lighthouse particle counter), black carbon (Aethalometry) and gaseous pollutants (Radiello diffusive sampler). Techniques of analysis were Gravimetry and XRFS for gaseous pollutants and elemental analysis of PM respectively.

5.1 Sampling site

The museums are situated in the capital Brussels in the downtown area on the Coudenberg. It is located in the city of Brussels (50.84^0N, 4.36^0E, 28 m a.s.l.) shown in Fig. 5.1 and it has a population of 1.187890 million. The collection of the Royal Museums of Fine Arts of Belgium covers a period extending from the 15^{th} to the 21^{st} centuries. It provides overview of western arts, with remarkable ensembles of works of artists from Belgium. In the museum, there is a collection of paintings,

sculptures, drawings and prints; it also includes, in particular through donations or deposits, items of decorative arts and furniture, along with a small number of non-European works. The online catalogue currently contains over 10,000 of the most representative works of the collection [201].

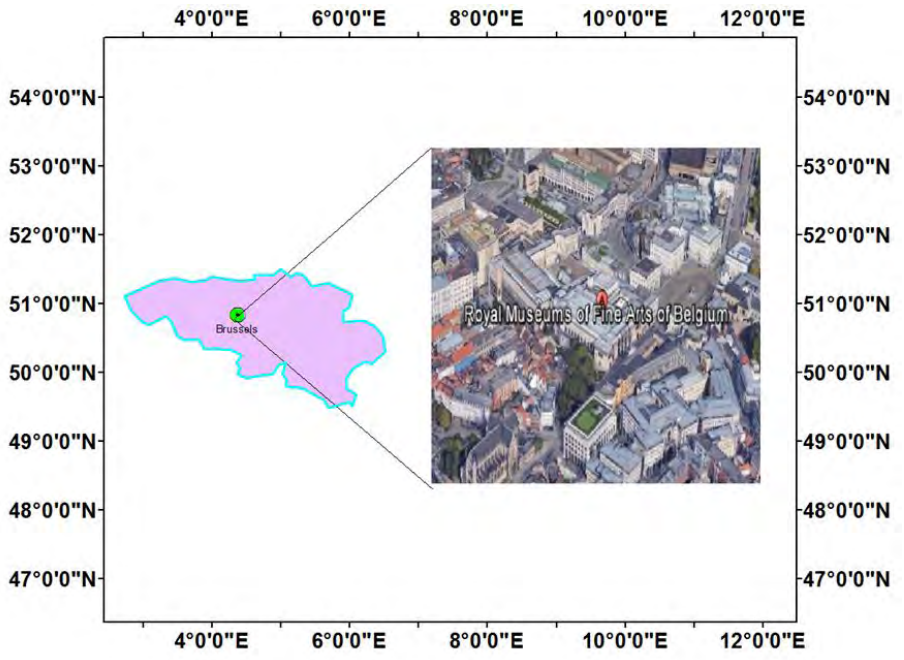

Figure 5.1: Sampling site.

5.2 Sampling of particulate matter

5.2.1 Harvard Type Impactor

For the determination of the airborne PM concentration, bulk composition (Harvard Impactor) and Particle number concentration (Lighthouse particle counters) were used. Both sampling methods filtrate PM out of the surrounding air based on the principle of inertial impaction [202]. Impaction occurs when a particle is not able to

follow its air streamline, hitting a surface. PM Impactor deliberately creates an air stream with the range of velocities 8.77 m/s to 297 m/s by sucking air with a pump. The air passes through the Impactor, where the present particles bend along certain obstacles, or impact on a substrate. An accurate Impactor design and a controllable flow rate gives the possibility to collect particles with a specific 'cut-off diameter', defined as the aerodynamic diameter for which the collection efficiency is 50%. Thus, sampling is directly based on the aerodynamic properties of the particle resulting in a size-segregation of the collected particles. Bulk particulate matter was sampled with a Harvard type Impactor (MS and T, Air Diagnostics and Engineering Inc., Harrison, ME, USA)[203]. A schematic illustration of this Impactor is shown in Fig. 5.2. The ambient air is sucked into the Impactor by a pumping unit that is connected to the Impactor base. The air enters the Impactor through the inlet of which the design prevents large objects such as insects and leaves coming in. The air is subsequently conducted via the nozzle, focusing the air towards the impaction plate where the flow is abruptly deflected. At this stage, size separation occurs. Particles with sufficient inertia are not able to follow the airstream and impact on the plate. The more the nozzle focuses the air stream, the lower the aerodynamic cut-off diameter. A drop of mineral oil is put on the Impactor plate to prevent particles from bouncing, or getting blown away after impaction. After the impaction unit, the air is transported along the Impactor body, where it finally reaches a filter on which the remaining airborne particles homogeneously deposit. The filter is supported by a drain disk preventing blowing out at high loading and high flow rates. For the performed sampling experiments, nozzles for PM_{10} and $PM_{2.5}$ were applied, connected to oil-less twin head

diaphragm pumps (Air Diagnostics and Engineering Inc.). Impactors consist of a series of stages each made up of a plate with specific nozzle arrangement, and collection surface (Fig. 5.2). Sample laden air is drawn into the impactor, flowing sequentially through the stages; nozzle size and total nozzle area decrease with stage number. As particles pass through the nozzles (see Fig. 5.2), they either remain entrained in the air stream, which is directed through a right angle at the exit of the nozzle or break through the lines of flow, impacting on the collection surface. Particles with sufficient inertia are collected; the rest pass onto the next stage. Each stage of the impactor is therefore associated with a cut-off diameter, a figure defining the size of particles that are retained on the collection surface of that stage [204] . Ideally, collection efficiency would be a step function - all of the particles above a certain size would be captured and those below it would pass through. As nozzle size decreases, velocity increases, allowing the collection of increasingly small particles, any residual material being captured in a final stage or filter. The sample is thereby separated into a series of size fractions, each of which is individually collected. The pumps control the air flow rate specified by the cut-off diameter of the nozzle, i.e., 10 L min^{-1} for both fractions. The noise level of the pumps is low, which makes them appropriate for indoor sampling in museum buildings (low annoyance). The volume of air sampled was monitored with a gas meter that was connected in between Impactor and pump. For the collection of bulk PM, polytetrafluoroethylene membrane filters (Teflon, TK15-G3M, 37 mm, Pall, East Hills, NY, USA) were used. All filters were handled with cleaned micro tweezers and transported in sealed Petri-dishes. Due to the instability of certain particulate at temperatures higher than the ambient sampling temperature, filters and substrates were kept in the fridge (4^0C) as soon as possible after particle collection. Sampling

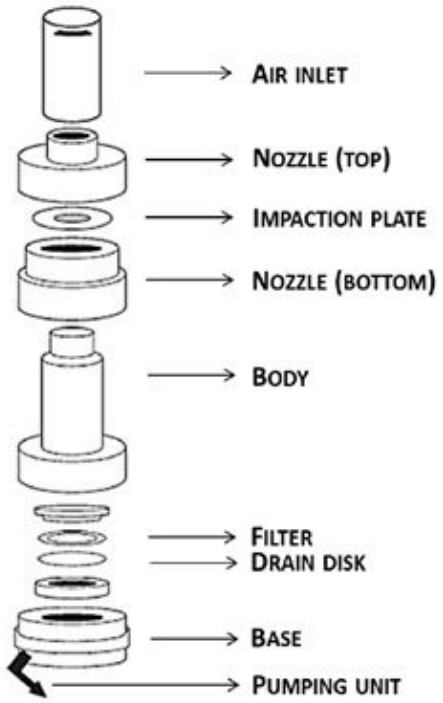

Figure 5.2: Schematic illustration of a Harvard Type Impactor.

of PM is based on the aerodynamic diameter (AD) behaviour of the air suspended particles. The particles are generally classified into three size fractions: PM_1 (AD <1 μm), $PM_{2.5}$ (AD < 2.5 μm) and PM_{10} (AD < 10 μm). For the purposes of this study, the following size fractions are also used: PM_1, $PM_{2.5-1}$ (particles with AD between 2.5 and 1 μm) and $PM_{10-2.5}$ (particles with AD between 10 and 2.5 μm).

5.2.2 Lighthouse particle counters

A Lighthouse Handheld 3016 indoor air quality (IAQ) (1221 Disk Drive Medford, OR 97501, USA) is the newest, most advanced handheld particle counter at this time, featuring mass concentration mode that approximates density in $\mu g/m^3$. It is ergonomically designed and lightweight. It is providing up to 6 particle size channels

of simultaneous counting, it can display cumulative and differential particle count data as well as temperature/relative humidity data on the fast and easy to read color touch screen. The model number signifies the minimum particle size measured by the instrument. The number "3016" indicates a 0.3 μm minimum channel size at 0.1 Volume of Air =Sample time (minutes) x Flow Rate (CFM) with up to 6 channels. Lighthouse Handheld 3016 IAQ can hold up to 3000 records of particle data and the configurable recipe database can store up to 50 recipes for sampling and reports. The Handheld 3016 IAQ (Fig. 5.3), monitors particulate levels accurately and reliably, even in hard to reach areas where two-handed operation is unsafe. The instrument uses a laser-diode light source and collection optics for particle detection. Particles scatter light from the laser diode. The collection optics collects and focuses the light onto a photo diode that converts bursts of light into electrical pulses. The pulse height is a measure of particle size. Pulses are counted and their amplitude is measured for particle sizing. Results are displayed as particle counts in the specified size channel. Lighthouse Particle counters allowed counting Particle Number concentrations. It provides particle concentration in six size channels (0.3, 0.5, 1.0, 2.5, 5 and 10 μm) and Particle counters count pulses of scattered light from particles. The amount of light a particle scatters has two factors such as the shape of the particle and the albedo (reflectivity) of the particle. Real time variations in PM levels were registered for 24 hours on every sampling day.

Figure 5.3: Lighthouse handheld 3016-IAQ particle counter adapted from the manual of a Lighthouse Handheld 3016 IAQ [205].

5.2.3 Aethalometry

Aethalometry is an instrument for the real-time measurement of optically-absorbing 'Black' or 'Elemental' carbon aerosol particles. It is a self contained instrument that measures the rate of change of optical transmission through a spot on a filter where aerosol is being continuously collected and uses the information to calculate the concentration of optically absorbing material in the sampled air stream. The instrument measures the transmitted light intensities through the sensing portion of the filter, on which the aerosol spot is being collected, and a reference portion of the filter as a check on the stability of the optical source. A mass flow meter monitors

the sample air flow rate. In Aethalometry, the aerosol absorption coefficient (α_λ) is defined by the intensities of two light beams which pass through a particle loaded spot (I) and a clean piece of a quartz fiber filter (I_0):

$$\alpha_\lambda = \sigma . \ln(\frac{I_0}{I}) \tag{5.2.1}$$

Where σ is the optical depth of the sampled air column (m^{-1}), it is the ratio of the area of the stained spot (m^2) divided by the sampled volume of air (m^3). Since black carbon (BC) is the only aerosol component which significantly absorbs light with $\lambda = 880nm$ (near-infrared), its concentration in air (μg m^{-3}) results from:

$$BC = (\frac{\alpha_{880}}{\sigma_{880}}) X 10^6, \tag{5.2.2}$$

where the specific attenuation of BC for an 880 nm light beam (σ_{880}) is empirically determined by Magee Scientific to be 16.6 m^2 g^{-1}. When measuring the reflection of an aerosol loaded filter, the absorption coefficient could be calculated in a similar way as for Aethalometry Eq. 5.2.1:

$$\alpha_\lambda = n.(\frac{\sigma}{2}). \ln(\frac{R_0}{R}) \tag{5.2.3}$$

where R_0/R is the ratio of the beams' reflectance on a blank filter to that of a sampled filter and the 2 arises since the reflectance is treated as a double transmission. The factor n depends on the wavelength of the used light as well as the penetration of particles into filter [206]. By convention, n = 2 when using white light and Whatman No. 1 filter papers [207]. Thus, a dual channel portable Aethalometer (AE42, Magee Scientific, Berkeley, CA, USA) was used for monitoring the BC concentration. The determination of BC is based on the optical attenuation of an 880 nm infra-red beam.

An additional 370 nm ultra-violet beam was used to estimate the Ultraviolet (UV)-absorbing aromatic content of the sampled PM, which can indicate the presence of Polycyclic aromatic hydrocarbons (PAH) found for example in cigarette smoke. At a time resolution of 1 min and a flow rate of 3 L min^{-1}, the AE42 is sensitive to BC concentrations down to 0.1 μg m^{-3}. Before taking them to the sampling site, two Aethalometers were inter-compared during a lab test for 98 hours with an optical measurement every 5 min.

$$BC_1 = 0.9031 \times BC_2 + 0.1310 (r = 0.965, p < 0.0001), \tag{5.2.4}$$

$$UV_1 = 0.7723 \times UV_2 + 0.4530 (r = 0.832, p < 0.0001), \tag{5.2.5}$$

The BC and UV readings of both instruments (μg m^{-3}) were highly correlated and reflection measurements were performed on PM_1 and PM_{10} filters by using an environmental exposure limit (EEL) 043 smoke stain reflectometer (Diffusion Systems Ltd., London, UK) with a white light source. Since no reports of reflection measurements on similar Teflon filter media were found in literature, the factor n was determined experimentally. The absorption coefficients were calculated from the reflection measurement when n = 2 (Eq. 5.2.3) and transformed to BC concentrations (Eq. 5.2.2) [208].

5.3 Gaseous sampling: Radiello diffusive sampler

The diffusive sampler (Fondazione Salvatore Maugeri, Padova, Italy) is a closed box, usually cylindrical. It has two opposite sides; one is transparent to gaseous molecules

which cross it, and are adsorbed onto the second side. The former side is named diffusive surface (S), the latter is the adsorbing surface (A) (marked with S and A in the figure). The diffusive body has a cylindrical symmetry in which the adsorbing cartridge is positioned coaxially (Fig. 5.4). The chemiadsorbing cartridges are positioned in the diffusive bodies and the whole is subsequently attached to a supporting plate, which also acts as a closure. When measuring outdoors, the samplers are protected from rain by a small shelter. Sampling periods ideally range from 3 to 7 days. Since the uptake rate of the gas molecules depends on temperature, the ambient temperature is measured simultaneously to obtain more accurate concentration values applying a temperature dependent correction factor. After sampling, the chemiadsorbing cartridges are well sealed from ambient air and transported to the lab for analysis. For the sampling of O_3, SO_2 and NO_2, the same diffusive body was used (code 120-1). It consists of microporous polyethylene with an average porosity of 25 $\pm$ 5 μm, opaque to light. The chemiadsorbing cartridges are compound specific. For ozone, the cartridge (code 172) is composed of silica gel coated with 4, 4'-dipyridylethylene. Upon exposure to ozone and water, both trapped in the silica gel, 4-pyridaldehyde is formed (Fig. 5.4). The analysis is based on colorimetry. The 4-pyridaldehyde is condensed with 3-methyl-2-benzothiazolinone hydrazone (MTBH) to obtain the corresponding aside which is yellow colored. The absorbance of the solutions is subsequently measured with UV-Visble spectrometry at a wavelength of 430 nm. By means of a calibration curve, the ozone mass is deduced (1 μg of 4-pyridylaldehyde = 0.224 μg of ozone). Finally, the average ozone concentration over the whole exposure time is calculated applying the appropriate temperature correction. The active compound of the chemiadsorbing cartridge for NO_2 and SO_2 (code

166) is triethanolamine (TEA). NO_2 and SO_2 are adsorbed as nitrite and sulphite or sulphate ions. The diffusive body ensures that the sampling is selective for gaseous molecules.

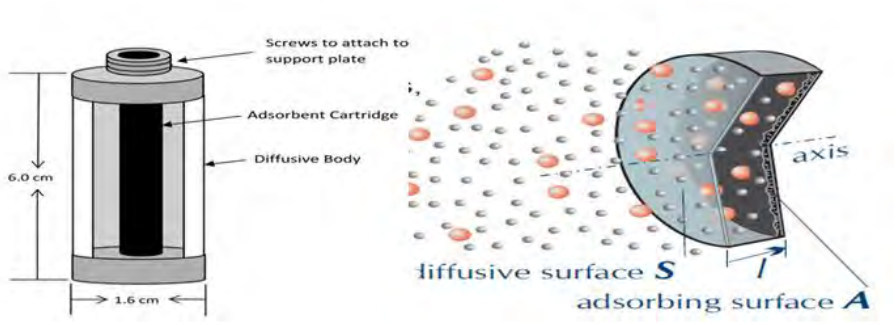

Figure 5.4: The Radiello passive samplers and its Schematic of the radial sampler and Diffusion principle. Adapted from Hitzenberger et al. [209].

5.4 Techniques of analysis: Gravimetry and X-ray fluorescence spectrometry

5.4.1 Gravimetry

Gravimetry analysis is used to determine the amount of particle deposited on filters. This method is based on measuring the mass difference of a filter before and after sampling. Filter samples and blanks are conditioned for a minimum of 48 hours at an air temperature (Tair) of 20 ± 1^0C and a relative humidity (RH) of $50 \pm 5\%$, just before static electricity is removed from the filters with an ionizer after which the mass is measured precisely ($\pm$ μg) with an electronic micro balance (Mettler-Toledo GmbH, Laboratory and Weighing Technologies, CH-8606 Greifensee, Switzerland).

Fig. 5.5 shows the filter before and after the sampling and the Gravimetry. When the sampled air volume is known, the airborne PM concentration was determined as:

$$PM_x(\mu g m^{-3}) = \frac{\triangle m}{V_{air}} \frac{(\mu g)}{m^3} \tag{5.4.1}$$

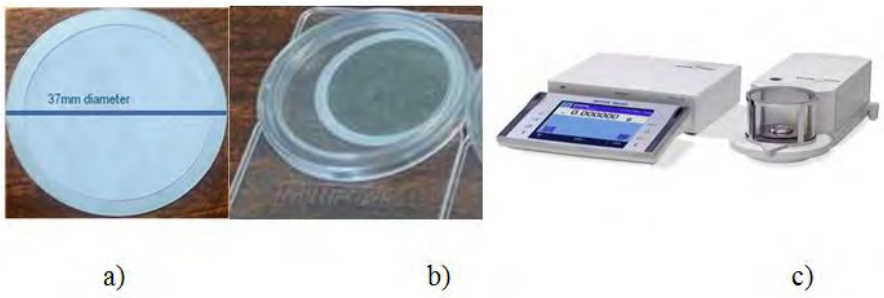

Figure 5.5: Filters before and after sampling (a and b) and the METTLER TOLEDO XP6 Microbalance (c).

5.4.2 X-ray fluorescence spectrometry (XRFS): Epsilon-5 spectrometer

X-ray fluorescence spectrometry (XRFS) can be used for quantitative elemental analysis. In general, XRS can be divided in two categories, depending on the way of X-ray detection. In wavelength dispersive (WD) spectrometry, a polychrome X-ray bundle is focused on a crystal which diffracts X-rays under different angles, depending on the wavelength of the photons. In this way, the polychrome X-ray bundle is stretched into separate monochromatic bundles which could be focused one by one on a sample by simply rotating the crystal. In energy dispersive (ED) spectrometry, the X-rays are collected directly on a semiconductor detector. An X-ray photon which impacts on such a detector initiates a propagation event which is proportional to the energy

of the photon. In this way, ED spectrometers register the whole energy spectrum at once. This is immediately the main advantage of such spectrometers since it enables the analyst to routinely analyze for a large range of elements in a relative short period. Disadvantages are the lower resolution compared to WD X-ray detection and the impossibility of analyzing low-Z elements (Na and below) [210]. Currently, X-ray fluorescence spectrometry is a very well established analytical technique for qualitative and quantitative elemental analysis of a wide variety of samples. In particular, It has a truly a multielement identification capability, fast, non destructive and easy of automation, together with the possibility to directly analyze solid samples are among the most important features of the spectroscopic techniques that have made it a very mature analytical tool for routine quality controls in many industries and research laboratories. Elemental analysis was performed on an Epsilon-5 spectrometer (PANalytical, Almelo, which is high-energy polarizing-beam energy-dispersive X-ray fluorescence spectrometer(ED-XRFS). (Fig.5.6(a)). The main feature of this instrument is that it uses targets which enable to create a 3-dimensional optical system with source, target, sample, and detector arranged in a Cartesian geometry (Fig. 5.6(b)) [211, 212]. This arrangement eliminates the spectrum from the X-ray tube by polarizing the beam, thereby reducing the spectral background and limit of detection (LOD) significantly. Also, use of some targets produces intense and almost monochromatic X-rays, making it possible to optimize the source according to the elements of interest. The primary beam (yellow), generated in a 600 W Gd-anode X-ray tube, is conducted towards a secondary target. This results in a polarized and almost monochromatic X-ray beam that irradiates the sample (purple). The instrument can switch between 15 different secondary targets (13 fluorescent and 2 Barkla targets), optimizing the

source according to the elements of interest. The X-rays emitted from the sample (blue) are subsequently collected by an energy dispersive high purity Ge-detector (PAN 32), simultaneously determining a wide range of elements [213] and is cooled down to liquid N_2 temperature. Finally, sampling filter deposits are directly loaded to the spectrometer in shown in Fig. 5.6(c) The aerosol filters did not require any specific sample preparation. The filters were mounted in a special holder and loaded into the instruments auto sampler. In case of many loose particles, X-ray transparent mylar foil was placed in between the filter and the incident beam. Optimized settings for the qualitative analysis of aerosol filters were explored by Spolnik et al. [214].

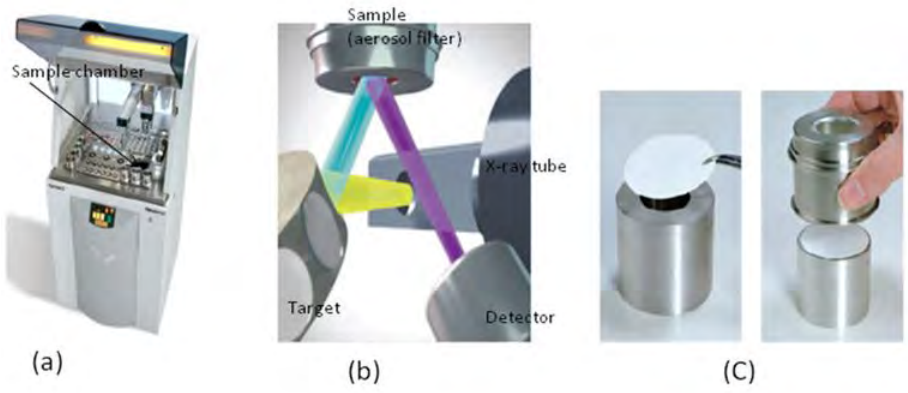

Figure 5.6: Epsilon-5 X-ray fluorescence spectrometer. The auto sampler can accommodate up to 130 samples (a) Optical path: source (yellow), target (blue) and sample (purple) (b). Aerosol filter deposits are directly loaded to the spectrometer (c).

Elemental analysis by means of energy dispersive X-ray fluorescence

Particulate matter was collected on the filters. Each filter was measured with 3 secondary targets: Ti, Ge and Mo. The element range and the optimal excitation conditions are given in table 5.1. The tube current was always set to the maximal

value possible given that the maximum power of the tube is 600 W. The X-ray spectra

Sec. Target	Voltage [kV]	Current [mA]	time[s]	Elements
Ti	25	24	500	Na, Mg, Al, Si, P, S, Cl, K, Ca
Ge	75	8	1000	V, Cr, Mn, Fe, Co, Ni, Cu, Zn
Mo	100	6	1000	As, Se, Br, Rb, Sr, Y, $Pb(L\alpha)$

Table 5.1: Experimental conditions used to determine the elements.

were fitted using the bAxil software package to obtain net Kα or Lα peak areas of the elements [215]. The element sensitivity in cps/mA/(ng/cm^2) was determined using commercial available Micromatter standards (MicroMatter, Vancouver, Canada). These are metals or simple compounds deposited onto a thin Mylar foil using vacuum deposition with known concentration of the order of 50 μg/cm^2. For each secondary target, the experimental sensitivity (S) was fitted as function of the atomic number of the element by Eq. (5.4.2):

$$S_i = aZ_i^b \tag{5.4.2}$$

where Z_i is the atomic number of element i and a, b are parameters for a particular excitation condition. The sensitivity was calculated for these elements. Table 5.2 shows the sensitivity S in cps/mA/ (g/cm^2) for Cr, Mn, Ni, Cu and Zn under various excitation conditions. Elements are better sensitivity by using Ge that of Co secondary target under similar conditions (Table 5.2).

Table 5.3 gives the count rate of the continuum under the peak in cps/mA for the same excitation conditions. As can be seen from Table 5.3, the sensitivity is higher for those elements that have their absorption edge close to the excitation energy (E); e.g. Mn is more sensitivity with Co than with the Ge secondary target under similar conditions of operating voltage of 50 kV. Moreover, the sensitivity of Ge targets was

Element	Co_{50}	Co_{75}	Co_{100}	Ge_{50}	Ge_{75}	Ge_{100}
Cr	5.82	7.99	9.31	2.68	4.26	5.51
Mn	6.95	9.53	11.1	3.21	5.90	6.62
Ni	-	-	-	6.11	9.81	12.7
Cu	-	-	-	6.78	10.9	14.1
Zn	-	-	-	8.65	13.67	17.26

Table 5.2: Sensitivity (S) using the Co and Ge secondary target at 50,75 and 100 kV.

Element	E(keV)	Co_{50}	Ge_{50}	Ge_{75}	Ge_{100}
Cr	5.41	0.120	0.104	0.345	0.907
Mn	5.90	0.295	0.109	0.359	0.916
Ni	7.47	-	0.153	0.398	0.933
Cu	8.08	-	0.238	0.523	1.10
Zn	8.63	-	0.458	0.893	1.56

Table 5.3: Under continuum, the peak (R_B) in counts per second per mA for the same excitation conditions.

found to increase for secondary targets (Cr, MN, Ni, Cu and Zn) with higher voltages applied to the X-ray tube. It is obvious from Table 5.3 that the sensitivity of Zn using the Ge secondary target at 100 kV is two times higher than 50 kV. Moreover, the continuum under the peak increases rapidly with the increase of the tube high voltage. The detection limit (DL) in counts is given by Eq. (5.4.3):

$$DL_{counts} = \sqrt[3]{N_B}, \tag{5.4.3}$$

where N_B is the number of counts in the continuum under the peak. The detection limit of g/cm^2 is then given by:

$$DL_{\mu g/cm^2} = \frac{DL_{counts}}{t \times c}\frac{1}{S} = \sqrt[3]{\frac{R_B}{t \times c}}\frac{1}{S}, \tag{5.4.4}$$

with t the measuring time in s, c the tube current in mA and S the sensitivity in cps/mA/(g/cm^2) and R_B the count rate per mA, $R_B = N_B/(t\ c)$. Fig. 5.7 shows

the sensitivity of elements from Al to Cu excited by the Ge secondary target between 25 and 100 kV. The sensitivity changes smoothly as a function of atomic number. The final concentrations of the elements under investigations in the Teflon membrane

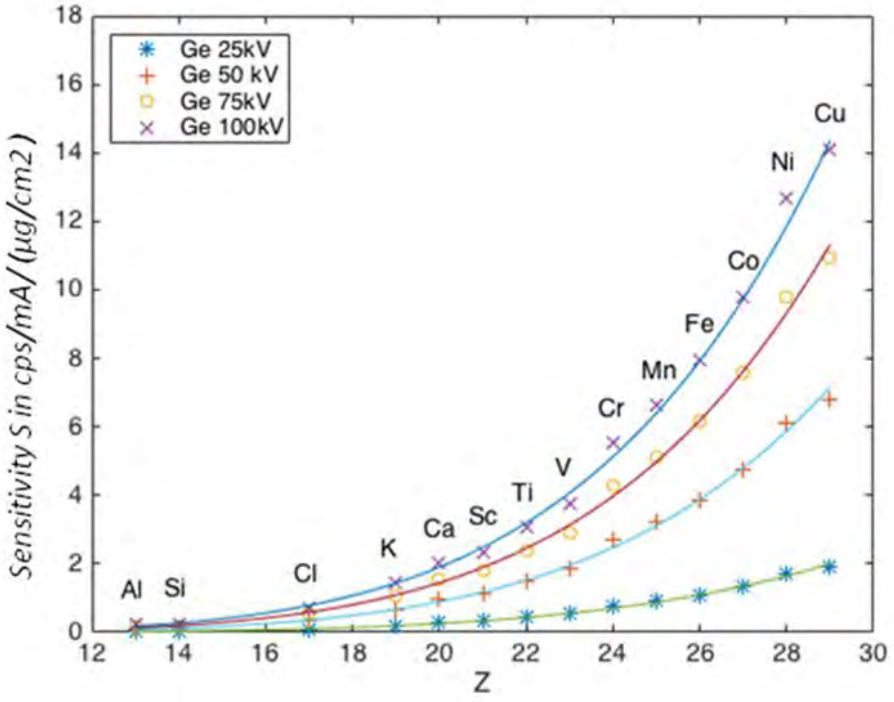

Figure 5.7: Sensitivity S in cps/mA/ (μg/cm^2) for the elements Al to Cu excited with the Ge secondary target at 25, 50, 75 and 100kV.

filter were converted into units of ng/m^3 based on the filter area and the sampled air volume. Blank filters were measured under the same conditions to establish the effect of Teflon membrane. The measured intensities of the filter, loaded with particulate matter were corrected for the blank values. The detection limits for the EDXRF analysis were calculated in accordance with the procedure and guidelines given by the International Union of Pure and Applied Chemistry (IUPAC) [216]. Detection limits were based on the number of counts in the background of the X-ray spectrum

below the Kα or Lα peak and taking into account the variation of the sample and instrumental blank. The method was validated by analyzing the standard reference material 2783 (SRM2783), air particulate on filter media from the National Institute of Standards and Technology (NIST), USA. Some of the standard reference materials are Al, Ba, Ca, Cr, Cu, Fe, K, Mn, Ni, Pb, Sb, Si, Ti, Zn. The result and discussion part of PM and gaseous pollutants will be presented in the next chapter (Chapter 6).

Chapter 6

Results and discussions

This chapter describes the results obtained from the sampling of PM, BC and gaseous pollutants using the experimental set-ups techniques described in Chapter 5. All results are presented alongside the discussion in the following sub-sections.

Daily measurements of particulate matter over a period of one month were carried out in two selected locations of the Museum of Fine Arts of Brussels (MFA), Belgium. The two selected sampling rooms were Magritte museum (that presents an outstanding collection of works of the Belgian Surrealist artist Ren Magritte (1897-1967) and Reserve OB (Storage room for paintings of ancient art) [161]. In the following sections, the impact of the outdoor environment on the museum will be discussed, by comparing concentrations of particulate matter, gaseous pollutants (O_3, NO_2 and SO_2) and black carbon in the indoor and outdoor air.

6.1 Mass concentration of particulate matter

We measured the daily average mass concentration of various particulate matters in the samples PM_1, $PM_{2.5-1}$ and $PM_{10-2.5}$ inside Magritte Museum over a period of two weeks. The daily PM_{10} average mass concentrations inside and outside Magritte

museum is ranged between 2.71 and 5.25 $\mu g/m^3$ with an average concentration of 4.1 $\mu g/m^3$ as indicated in Table 6.1. On the other hand, on Mondays, 13^{th} and 20^{th} April 2015, the average mass concentration of PM (3.8 and 3.9 $\mu g/m^3$ respectively) were lower than the other days of sampling but similar to each other (Fig. 6.1). Because, on Mondays, the museum is usually closed and there are no tourist activities around.

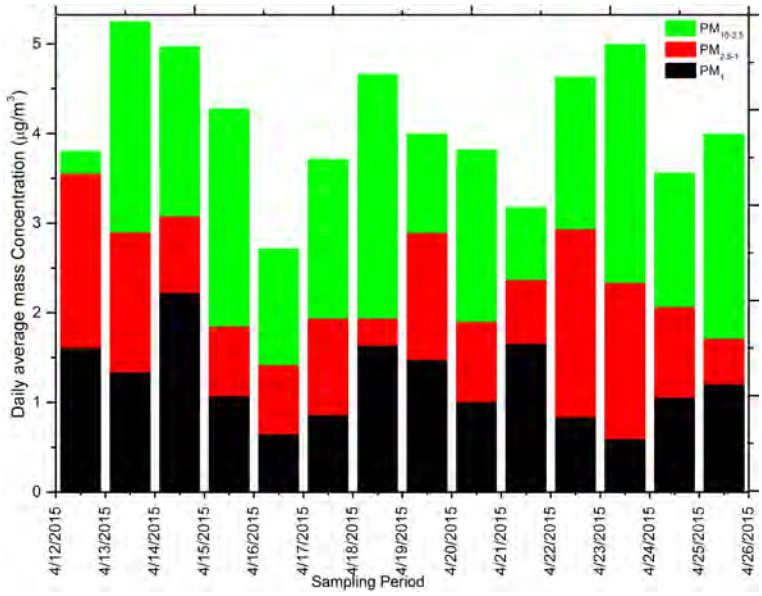

Figure 6.1: Daily average particulate matter mass concentration inside the Magritte Museum.

Furthermore, the average concentrations of the fractions of PM_1, $PM_{2.5-1}$ and $PM_{10-2.5}$ were determined in Reserve OB museum (Fig. 6.2). The mass concentrations of PM_{10} inside and outside Reserve OB museum were in the range of 0.36 to 7.75 and 12.0 to 28.87 $\mu g/m^3$ respectively and their mean values were 2.21 $\mu g/m^3$ inside, 19.37 $\mu g/m^3$ outside the museum (Table 6.1). Comparing inside Magritte with Reserve OB, the average PM_{10} concentrations of particulate matter inside Magritte is greater than that of Reserve OB. This difference is due to the geographical location of Magritte,

which is near to the traffic activities, and the materials inside it. However, dependence of the indoor total PM on the outdoor total PM cannot be entirely eliminated. The difference in pattern of changes between indoor and outdoor PM concentrations evokes the fact that the outdoor environment is not the only factor determining air quality inside the museum. Such aspects as dust re-suspension by walking people or during the cleaning, and opening windows and doors may play a role in increasing the amount of particulate inside the buildings. It is worth to focus on specific PM fractions since the behaviour of particles is strongly dependant on their aerodynamic diameter. Also provenience of certain particle groups is correlated with their size. Smallest particles have higher contributions to the total PM than larger particles. It is even more noticeable for values found inside the museum than outside. This is because small particles behave more like gas molecules and follow virtual hassle air streams through cracks and small openings. As the consequence, they stay suspended in the air for longer periods. Larger particles, however, have certain inertia, making it faster to remove them from the infiltrating air due to impaction and sedimentation [217]. This difference in infiltration leads to a relative enrichment of smaller particles in indoor air. Data collected from other studies in different stations of pollution control in Europe revealed that PM_{10} concentrations were varied based on pollutants sources [218].

It is observed from Table 6.1 that for Magritte museum, the inside concentrations of particle fraction of $PM_{2.5}$ and PM_{10} in order to compare the inside and outside concentrations. Therefore, the inside concentrations of particle fraction of $PM_{2.5}$ and PM_{10} were 2.4 $\mu g/m^3$ and 4.12 $\mu g/m^3$; while, the outside were 16.16 $\mu g/m^3$ and 30.06 $\mu g/m^3$ respectively.

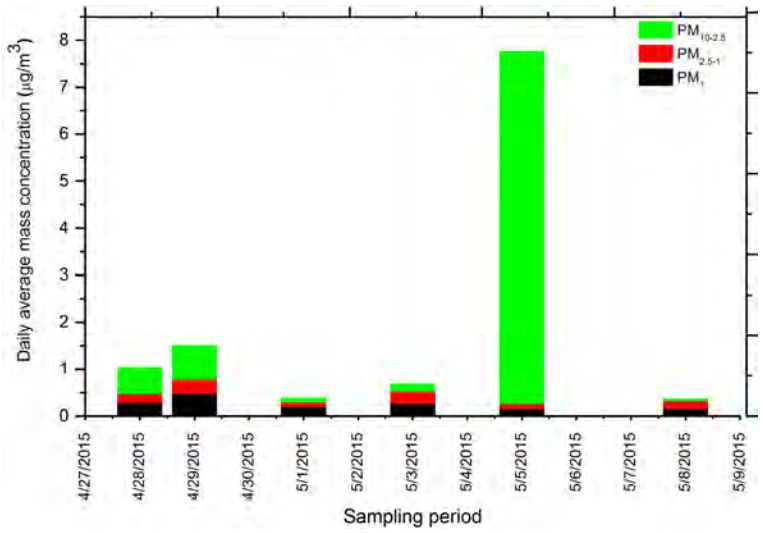

Figure 6.2: Average mass concentrations of Particles PM_1, $PM_{2.5-1}$ and $PM_{10-2.5}$ inside of the Reserve OB Museum .

This clearly indicated that there were higher outside concentrations. There were also daily variations in the amount of the concentrations on some days (14-16 April 2015 -23 April 2015) (Fig. 6.3). Moreover, variation between inside and outside concentrations of PM was observed as shown in Fig. 6.4. The inside average mass of concentrations of $PM_{2.5}$ and PM_{10} were 0.43 and 2.21 $\mu g/m^3$ while that of the outside were 3.48 and 19.37 $\mu g/m^3$ respectively.

At all samples, the average mass concentrations of $PM_{2.5}$ and PM_{10} inside were always lower than that of the outside due to the penetration and deposition losses and absence of indoor sources [219]. In addition, it was also observed that the indoor $PM_{2.5}$ and PM_{10} concentrations were highly reduced by the filtration system [220]. This variability depends on factors such as temperature, wind speed, wind direction, human activity and traffic activities outside of the museums. From Table 6.1, the indoor/outdoor (I/O) ratio of PM in Magritte was 0.14 while that of Reserve OB is 0.11. The indoor/outdoor concentration ratios in both museums were less than 1.

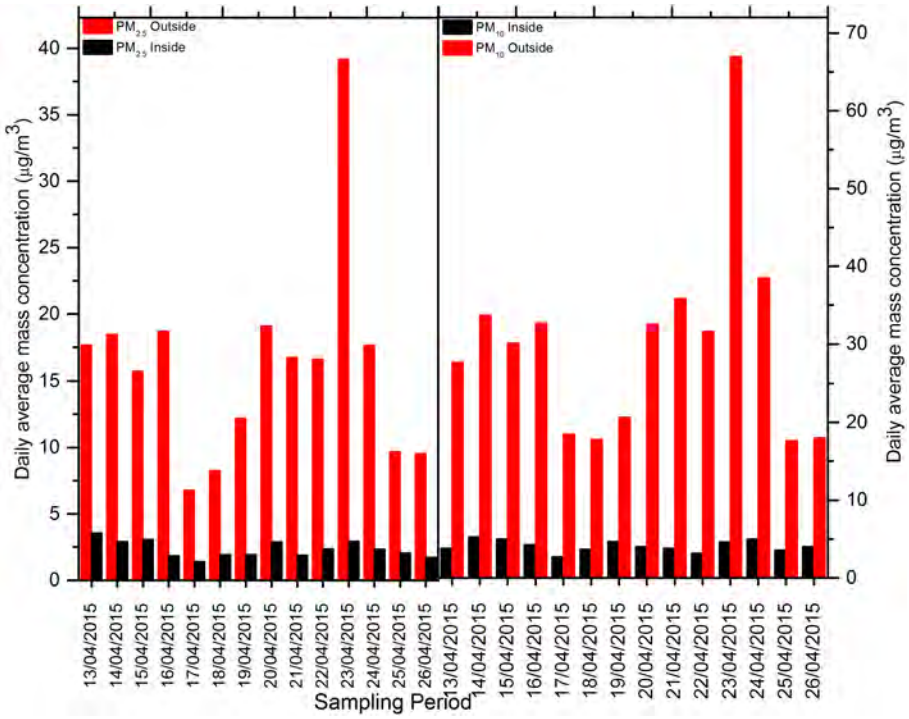

Figure 6.3: Average mass concentrations of $PM_{2.5}$ and PM_{10} of inside and outside Magritte Museum.

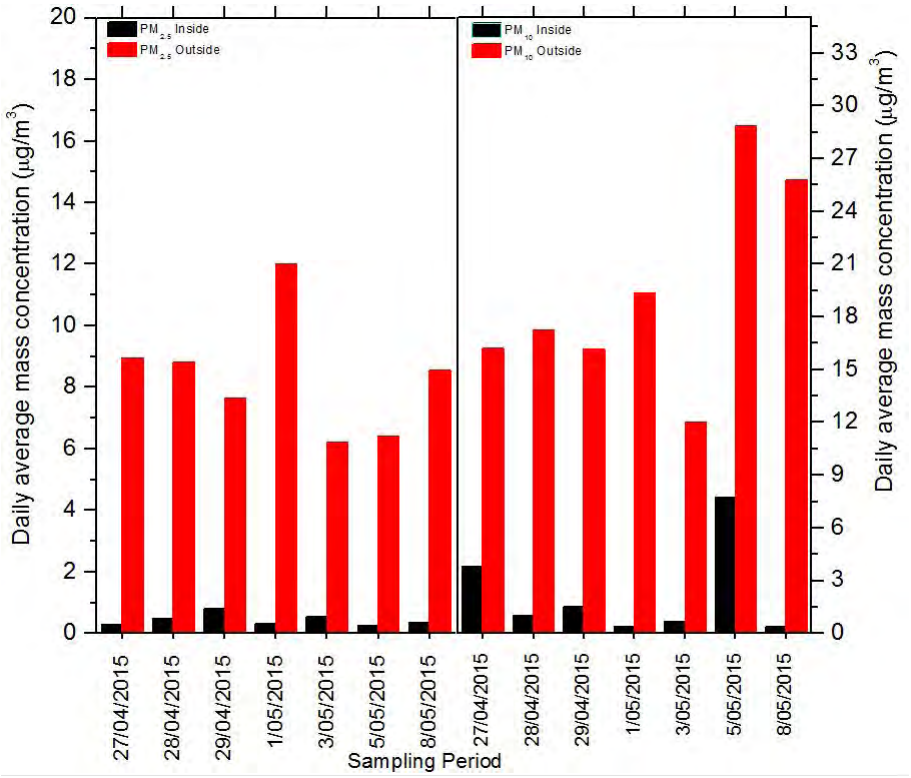

Figure 6.4: Average mass concentrations of $PM_{2.5}$ and PM_{10} of inside and outside Reserve OB Museum..

Location	R_{out} PM_{10} Con. ($\frac{\mu g}{m^3}$)	A_{out} PM_{10} Con. ($\frac{\mu g}{m^3}$)	A_{out} $PM_{2.5}$ Con. ($\frac{\mu g}{m^3}$)	R_{In} PM_{10} Con. ($\frac{\mu g}{m^3}$)	A_{In} PM_{10} Con. ($\frac{\mu g}{m^3}$)	A_{In} $PM_{2.5}$ Con. ($\frac{\mu g}{m^3}$)
Magrrite	17.61-66.72	30.06	16.16	2.71-5.25	4.12	2.4
Reserve OB	12.00-28.87	19.37	3.48	0.36-7.75	2.21	0.43

Table 6.1: The average indoor and outdoor PM_{10} concentration in Magritte and Reserve OB Museums.

High I/O Ratio means high inflow of the outdoor air towards the inside of the museum and low I/O Ratio reflects low inflow. One can see that the I/O Ratios on Reserve OB (I/O=0.11) is the lowest. It underlines the fact that introduction of the outdoor air to the museum is not constant in time and thus it is dependent on other factors such as temperature, wind speed, wind direction and human activities (opening doors and windows, moving-walking which provokes re-suspension of the dust from the surfaces). In addition bringing of the dust on shoes and cloths should be taken into account, together with considering people as potential source of particles, mainly of organic origin (e.g. skin flakes) but also of cloth fibers [221]. Indoor/outdoor ratios points out lower amount of PM concentration inside the museums. This indicates that the sources of particles in the museums were outdoor [222, 223, 224, 225]. Particles detected inside have their sources predominately outside the museums. Mouratidou and Samara [224] explains the indoor sources of PM determined in various museums largely vary depending on ventilation system, outdoor air exchange rate, indoor air recirculation rate, deterioration and erosion procedures and restoration. Furthermore, indoor/outdoor ratio increases when temperature difference increases and when there

is a higher pressure gradient produced between inside and outside result to higher penetration of particulate matter into the museums [223]. Indoor/outdoor ratio also varies in space and time [226]. Table 6.2 and Fig. 6.5 compare our findings with that of other museums. Thus, the average mass concentrations of $PM_{2.5}$ and PM_{10} is lower, was also lower except PM_{10} in one, which is found in Brazil [227].

Museums	$PM_{2.5}$	PM_{10}	References
Rubens room, Platin-Moretus, Antwerp, Belgium	13.4	15.98	[228]
Printing room, Platin-Moretus, Antwerp, Belgium	13.16	15.55	[228]
Archaelogy Ethnology, Megacity Sao Paulo, Brazil	3.5	5.1	[227]
Pinacoteca do Estado de, Megacity Sao paulo, Brazil	5.8	5.4	[227]
Pinacoteca do Estado de, Megacity Sao paulo, Brazil	5.1	3.6	[228]
Capodimonte Museum, Naples, Italy	40	47	[229]
Archaeological museum of Thessaloniki,N. Greece, Greece	40.5	-	[224]
Magritte, MFA, Brussels, Belgium	2.35	4.12	[This study]
Reserve OB, MFA, Brussels, Belgium	0.43	2.21	[This study]

Table 6.2: Comparison of indoor average mass concentration of $PM_{2.5}$ and PM_{10} in Magritte and Reserve OB with other museums.

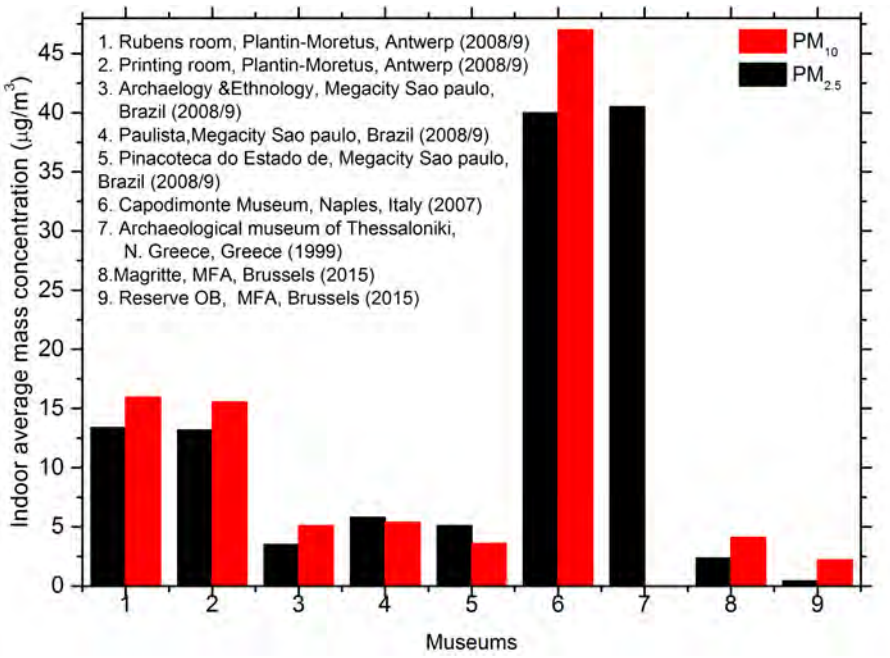

Figure 6.5: Indoor average mass concentration of particulate matter of different museums.

6.2 Particulate matter number concentration

Real time particulate matter number density was measured in the Museum of Fine Arts (Magritte and Reserve OB). The particle number concentrations were classified in three fraction sizes: PM_1, $PM_{2.5-1}$ and $PM_{10-2.5}$, and their relation to temperature and relative humidity were observed as can be seen from Figs. 6.6 and 6.8. It was observed that temperature and relative humidity have direct and indirect relationship with the number concentrations as outlined below respectively. Daily and diurnal variations were investigated in terms of average mass and number concentration patterns for days and hours. It was found that particle number concentrations in all size remained at higher levels during the museums' morning time. This can be seen clearly in Figs. 6.6 and 6.8, which shows the average concentrations during 9:00 A.M.

to 12:00 A.M. of some of the days of the week in the two museums. Many previous studies also showed that diurnal patterns of particle concentrations is caused by traffic activities, population movement of museums' environment, meteorological conditions, visitors and by the strength of air mixing. All of these lead to increasing of sun radiations in the morning time [230, 231, 232, 233]. During the evening and afternoon, the number of concentrations particles were minimum. Investigations of diurnal variation in indoor particle number concentrations showed that high indoor concentrations were normally observed during traffic peak hours. This result is also consistent with findings of Laakso et al. [233] who reported that the mass concentration patterns of outdoor daily variations were significantly affected by the diurnal variations in vehicle emissions, which has a direct relation with the indoor concentration. The result suggests that number concentration of particles are directly correlated with temperature and inversely with relative humidity as shown in Fig. 6.6. The relation between concentrations of PM_1, $PM_{2.5-1}$, $PM_{10-2.5}$, temperature and relative humidity RH are illustrated in Figs. 6.6 and 6.8 at Magritte and Reserve OB respectively. For the majority of the days, PM has a strong positive correlation with temperature. This is because temperature can affect the formation of particles; thus, the high temperature can promote the photochemical reaction between precursors. High temperatures are clearly conducive to intense convection: atmospheric PM is transported quickly and effectively, allowing its accelerated dispersion, and thus decreasing local mass concentrations. Conversely, low temperatures and the temperature inversion layer caused by radiative cooling weaken convection [234]; in these circumstances, atmospheric PM remains suspended under the inversion layer, leading to higher atmospheric PM

concentrations. When the humidity is low because of hygroscopic growth, PM concentration increases [235]. When the humidity is high enough, the particles grow too heavy to stay in the air. Therefore, dry deposition occurs; particles fall to the ground. As a result, particle numbers reduce and PM concentration decreases. Figs. 6.7 and 6.9 shows a good agreement with mass and number concentration of PM using mass filter and lighthouse in the sampling location respectively.

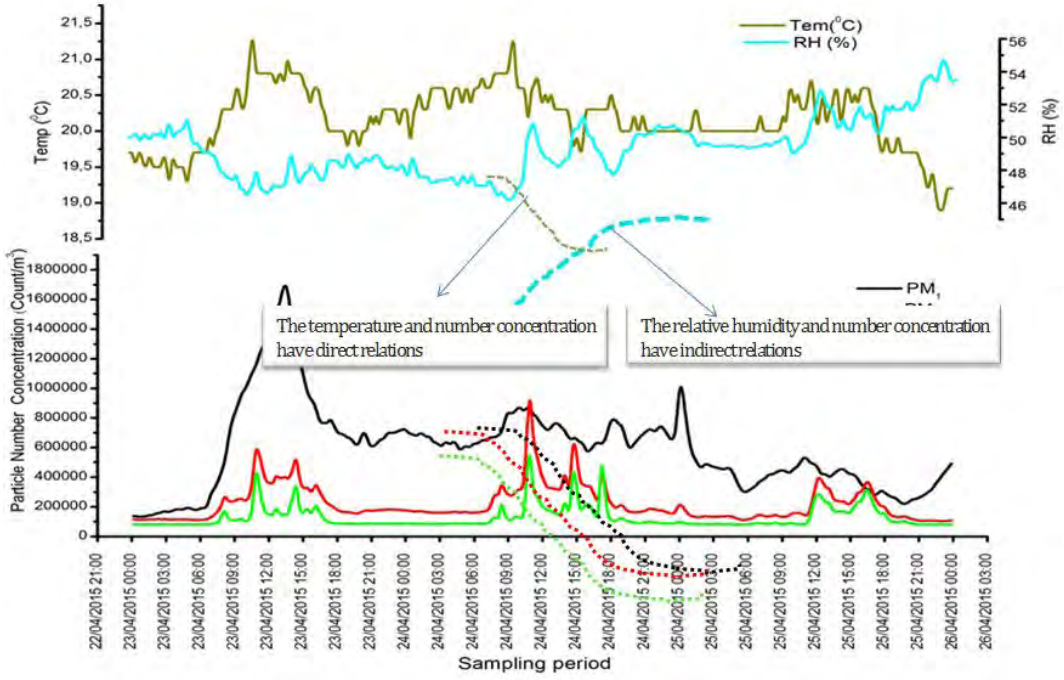

Figure 6.6: Daily time series trend of average PM_1, $PM_{2.5-1}$, $PM_{10-2.5}$, temperature and relative humidity values determined by particle counter over the period from 13 April to 26 April 2015 at Magritte.

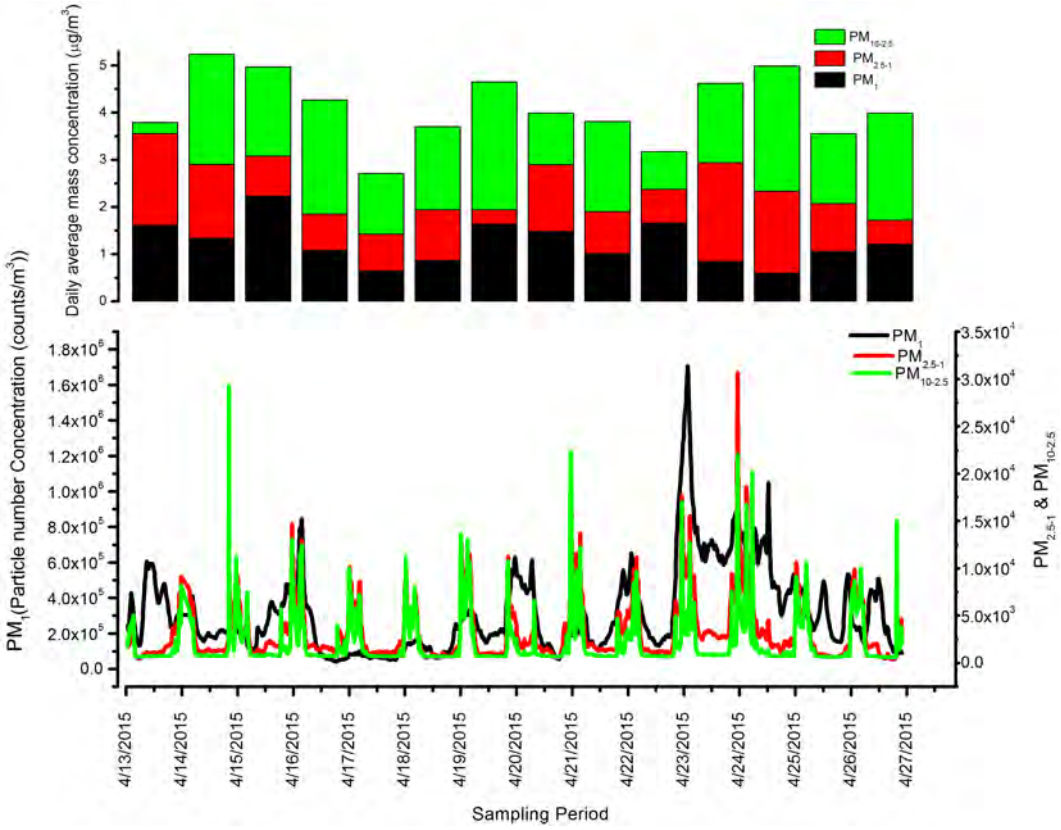

Figure 6.7: Daily average mass and number concentration of particulate matter using mass filter and Lighthouse particle counter instruments inside Magritte museum.

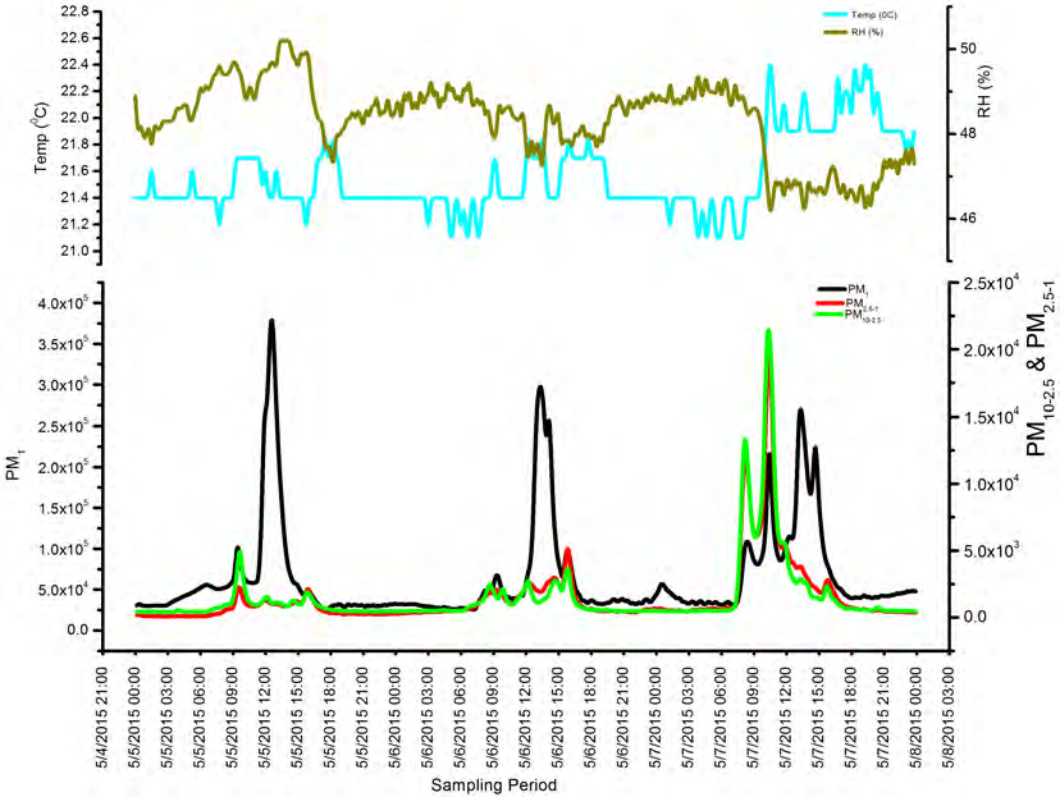

Figure 6.8: Daily time series trend of average of PM_1, $PM_{2.5-1}$, $PM_{10-2.5}$, temperature and relative humidity values determined by the particle counter over the period from 27 April to 11 May 2015 at Reserve OB.

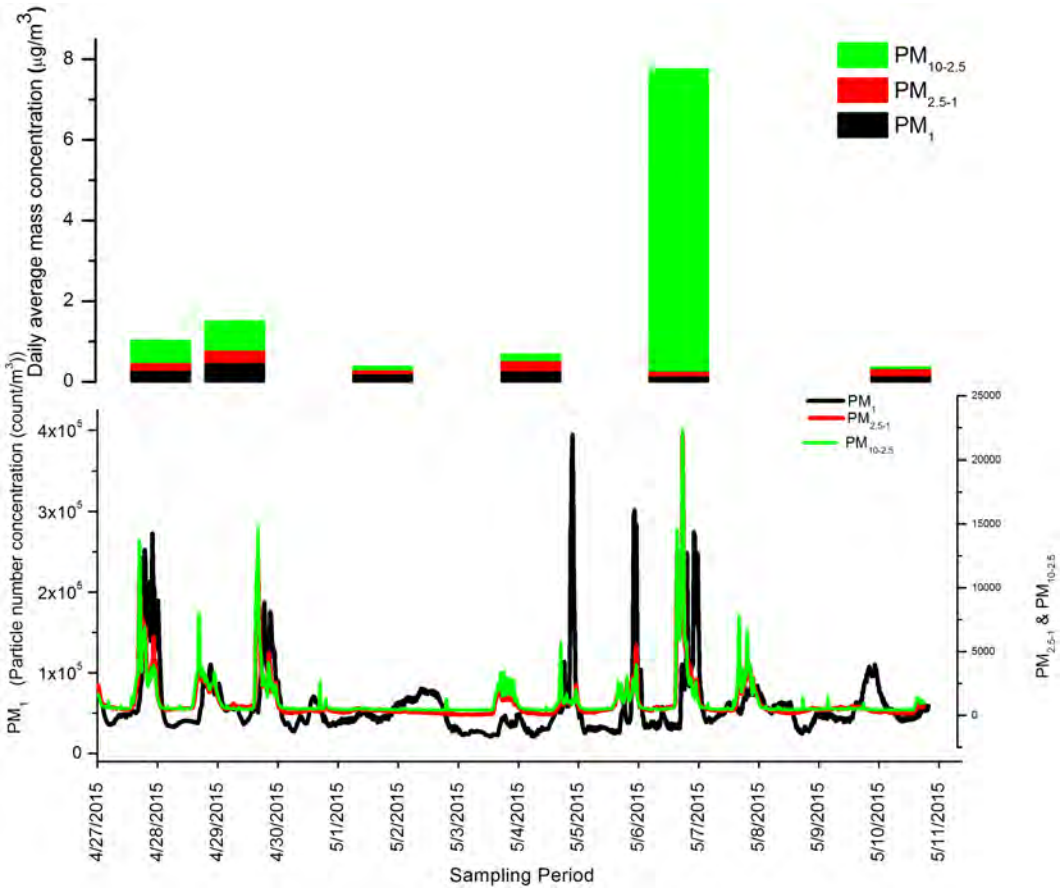

Figure 6.9: Daily average mass and number concentration of particulate matter using mass filter and Lighthouse particle counter instrument inside Reserve OB.

6.3 Gaseous pollutants: NO_2, SO_2 and O_3

Both inside and outside average concentrations of pollutant gaseous such as NO_2, SO_2, and O_3 were measured in Magritte, Magritte Showcase and Reserve OB Museums of Fine Arts. Results of the analysis of investigated gaseous pollutants are summarized in Figs. 6.10-6.12. NO_2 concentrations obtained from all location inside the museums were below the detection limit defined by the United States (US) National Bureau of Standards and the Museum Environment [236]. The outside concentrations of NO_2 were found to be around 23.8 and 12.6 $\mu g/m^3$ in Magritte and Reserve OB respectively. In Magritte's' Showcase, NO_2 concentration, which was inside, was below the detection limit (Table 6.3). Because the showcase is rather a less closed compartment within the gallery that result in a small air exchange. NO_2 is a gas with strong outdoor sources mainly from road traffic and domestic heating for energy generation [236, 237, 238, 239]. These results also showed that NO_2 enters the museums from outdoor air and there were no strong sources inside. In the case of Showcase, the concentration of NO_2 decreases inside because of its closed nature [240]. The indoor concentrations of SO_2 were 0.8, 0.4 and 1.5 $\mu g/m^3$ in Magritte, Reserve OB and Magritte Showcase, respectively. SO_2 was also detected in the outdoors of the Magritte (2.4 $\mu g/m^3$) and Reserve OB (2.7 $\mu g/m^3$). SO_2 was found to be higher in the display case than inside Magritte; this could be due to restricted air circulation that leads to pollutants build up over time. The decreases SO_2 concentration inside the museums was due to the high deposition velocity of SO_2 which leads to quick adsorption on the surface [241].

In addition, the inside concentrations of O_3 were found to be much lower than the outside in all three museums. The lowest value was 1.6 $\mu g/m^3$) in Reserve OB

Location	O_3 ($\frac{\mu g}{m^3}$)	NO_2($\frac{\mu g}{m^3}$)	SO_2($\frac{\mu g}{m^3}$)	O_3(bpp)	SO_2(bpp)	NO_2(bpp)
Magritte	3.1	0.8	<DL	1.56	0.33	<DL
Magritte Show-case	2.1	1.5	<DL	1.04	0.56	<DL
Reserve OB. Inside	1.6	0.4	<DL	0.8	0.17	<DL
Magritte Outside	46.4	2.4	23.8	23.2	0.92	12.70
Reserve OB. Outside	70.9	2.7	12.6	35.45	1.04	6.73

Table 6.3: Indoor and outdoor mean concentrations of NO_2, SO_2 and O_3 in Museum of Fine Art.

(Table 6.3). The highest concentrations of O_3 were found outside of the two museums with an average of 46.4 and 70.9 μg/m^3) in Magritte and Reserve OB respectively as shown in Fig. 6.11. This might be a result of the continuous opening of the windows in the period of very high temperatures during the sampling period. These results can also be explained by the higher reactivity of ozone which also reflects rather its large deposition velocities. Meteorological parameters have an impact on ozone concentrations. Kgabi and Sehloho [242] confirmed that there is a direct relation between ozone and temperature and wind; while, an inverse relation between ozone and relative humidity. The concentration values of all analyzed gases were higher outside the building than in the galleries. It may be argued that part of the gaseous components could have reacted with the art objects, walls, furniture, etc. or with other gases and aerosol particles present in the air and a limited air exchange. In the city main sources of ozone are traffic activities, industrial area and businesses [243]. The most distinct difference between indoor and outdoor concentrations was noticed

in the case of O_3 (Fig. 6.11). This observation applies to all sampling period and is probably due to the higher reactivity of this compound compared to others.

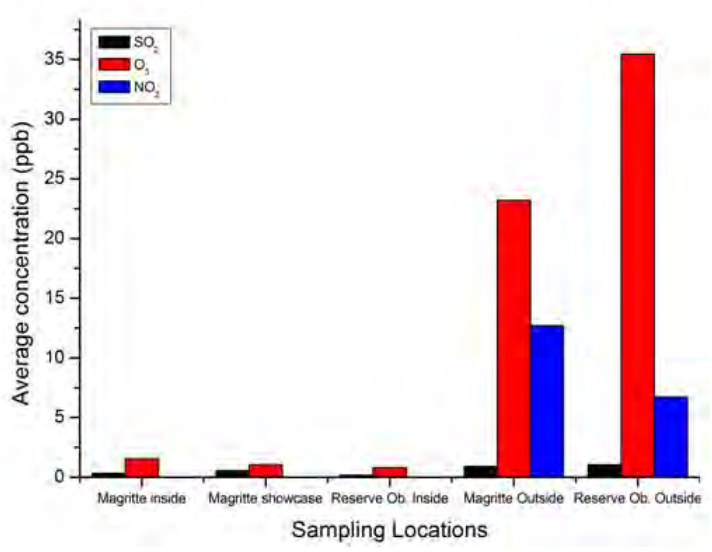

Figure 6.10: Comparison of average Concentration of SO_2, NO_2 and O_3 in Museum of Fine Arts.

In general, the levels of NO_2, SO_2 and O_3 inside the two museums are lower when compared to that of others as indicated in Fig. 6.12.

However, the recommended levels of gaseous pollutants in museums are $SO_2 < 2$ ppb, $NO_2 < 10$ ppb and $O_3 < 5$ ppb [147]. Our findings showed that the level of these gaseous pollutants were below the recommended limits. This may presumably due to centrally heating, ventilation and air conditioning (HVAC) systems used in the museum, which play a significant role in protecting the museums' environment (Magritte and Reserve OB).

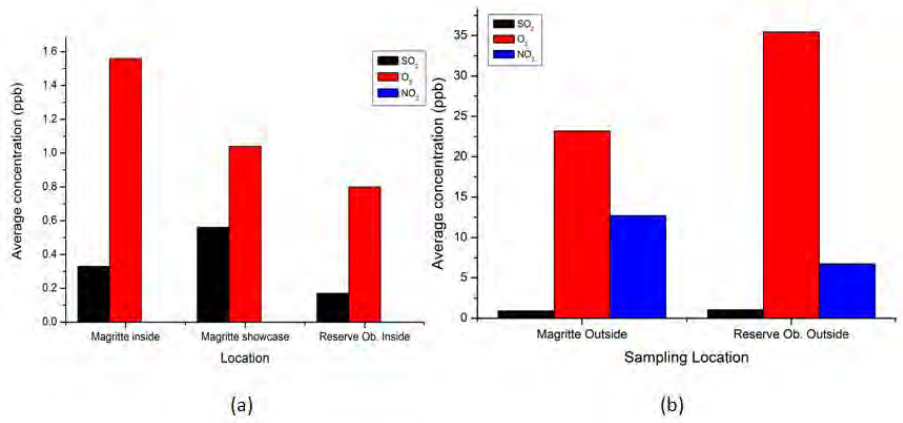

Figure 6.11: Average Concentration of SO_2, NO_2 and O_3 inside (a) and outside (b) Magritte and Reserve OB.

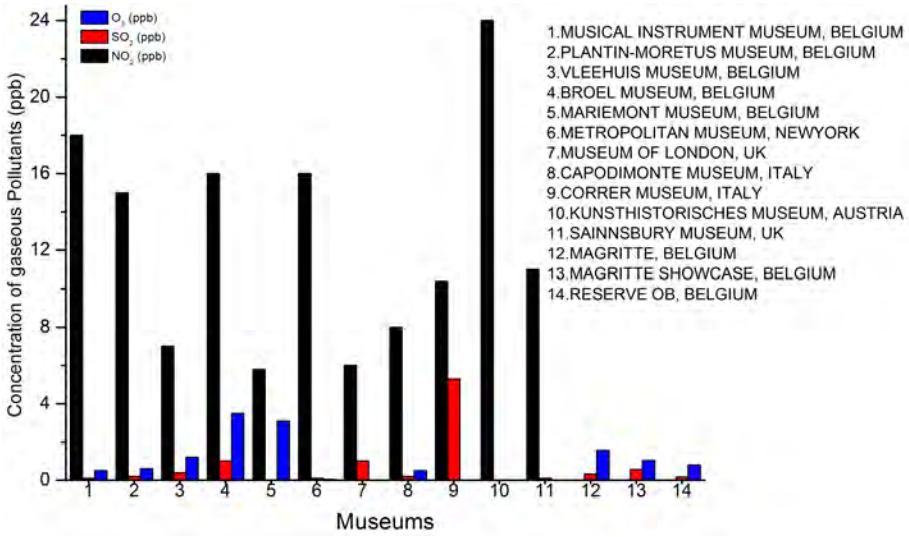

Figure 6.12: Gaseous pollutants in MFAs compared with different museums.

6.4 Black carbon

Black carbon (BC) mass indoor concentrations were measured from 13 April to 11 May 2015 at the two museums of Magritte and Reserve OB. Daily mean BC concentrations are ranged from 89.17 to 288.75 ng/m^3 in Magritte and 14.58 to 60.19 ng/m^3 in Reserve OB with an average of 163.00 and 32.00 ng/m^3 respectively (Fig. 6.13).

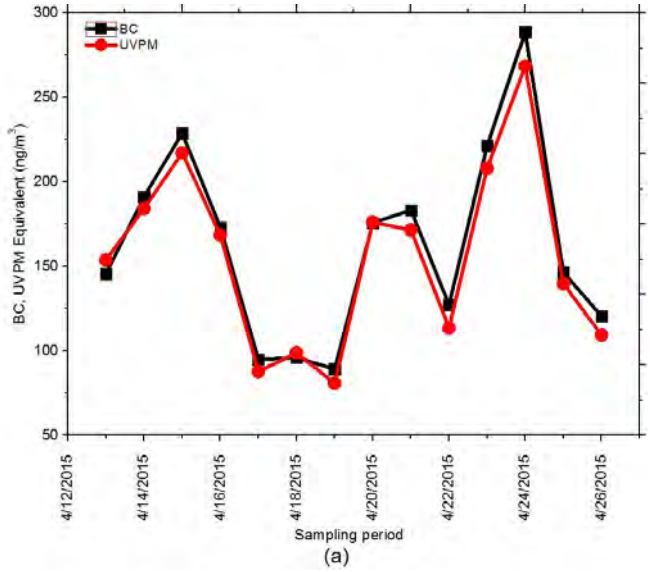

From Figure 6.13a and 6.13b, it is clearly observed that the maximum BC concentrations were recorded during the working days (Tuesday to Friday); the concentration was very high when compared with the off days (on Mondays, the museums were closed). Temporal variation between day and night concentrations is also clearly observed with higher concentration during peak hours and at weekdays when the traffic activity was very high. Comparing the two museums, there is a clear difference of BC concentrations (Magritte has five times that of Reserve OB) (Fig. 6.13). Because Magritte Museum is near to the road and it had higher traffic activities.

Meteorological parameters such as wind speed, wind direction and temperature also

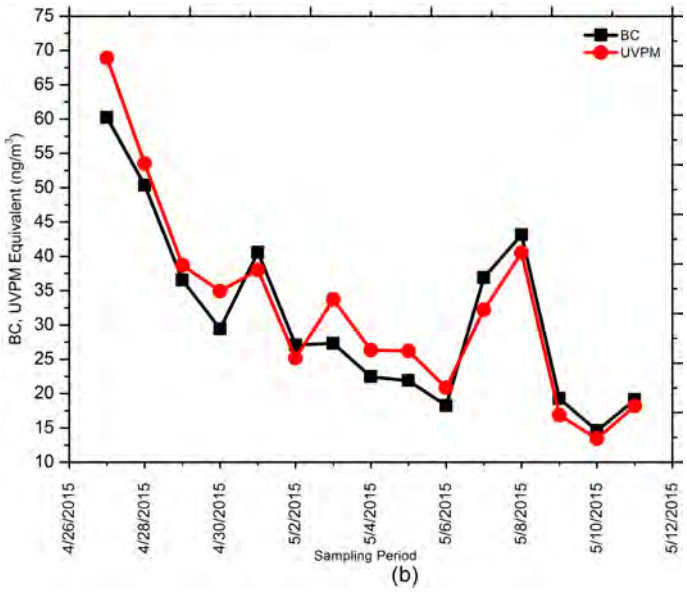

Figure 6.13: Black carbon concentration (ng/m^3) inside Magritte (a) and Reserve OB (b).

an impact on the concentrations of BC. Biomass burning, combustion of fossil fuels and bio-fuels are sources of BC, mainly in urban areas; the sources of BC originate from car exhaust and cooking. BC produced from these sources enter into museums. Moreover, the museum has a shielding effect. It protects from very high outdoor BC concentrations and allows shifting indoor concentration peaks in time for a few hours. On weekend days, the traffic is distributed evenly throughout the day, so the typical peak maxima could not be observed. Therefore, the average indoor concentrations obtained by this study were less than that of the previous studies reported by Krupinska et al. [218] and Ricardo et al. [239]. The UV-absorbing particulate material (UVPM) channel also read the same as the BC channel; this shows the UV absorbing of PM is not much more different from BC but a little bit smaller. It is clearly noticed that BC and PM have direct relation. Fig. 6.14 shows that there is a positive relationship between particulate matter fractional sizes and black carbon.

Black carbon is fine particles with similar size to $PM_{2.5}$. As can be seen from Fig. 6.14, it has the same trend with $PM_{2.5}$. The concentrations of PM_{10}, $PM_{2.5}$, PM_1 and BC showed clear daily peaks (Figure. 6.14a and b). The hourly concentrations of PM (PM_{10}, $PM_{2.5}$, and PM_1) showed significant peak values which decreased towards the night, and increased in day times. This variation suggested that anthropogenic (traffic) activities, particularly during the peak between 9:00 h up to 18:00 h, led to higher concentrations of particulate matter and black carbon, which have the same trend. Meteorological conditions, particularly temperature, affect the concentrations and size of particles, when the particles size decrease movement of the particles increase due to temperature and wind speed (Fig. 6.14a and 6.13b). Fine particles, being favored of the transformations which take place in the atmosphere with the presence of solar radiation reached their peak values during the highest temperature days [244]. From Fig. 6.14b, relative humidity also correlates negatively with black carbon.

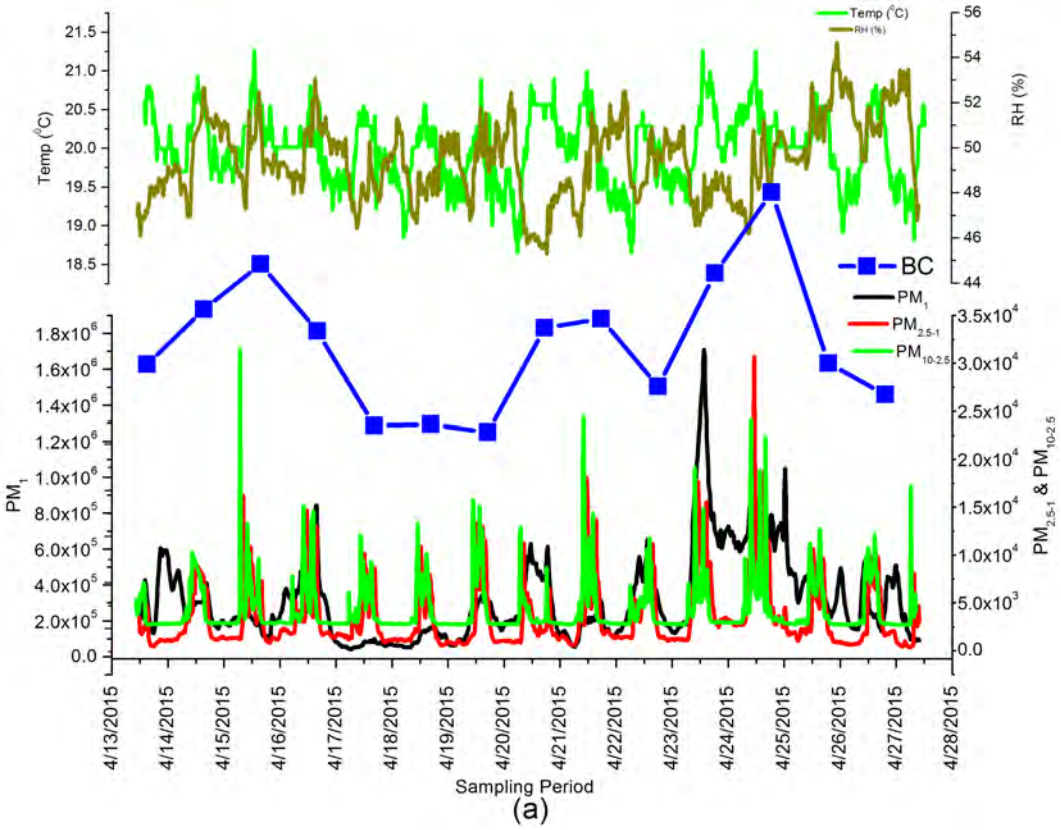
Temp (°C)
RH (%)
BC
PM1
PM2.5-1
PM10-2.5
Sampling Period
(a)

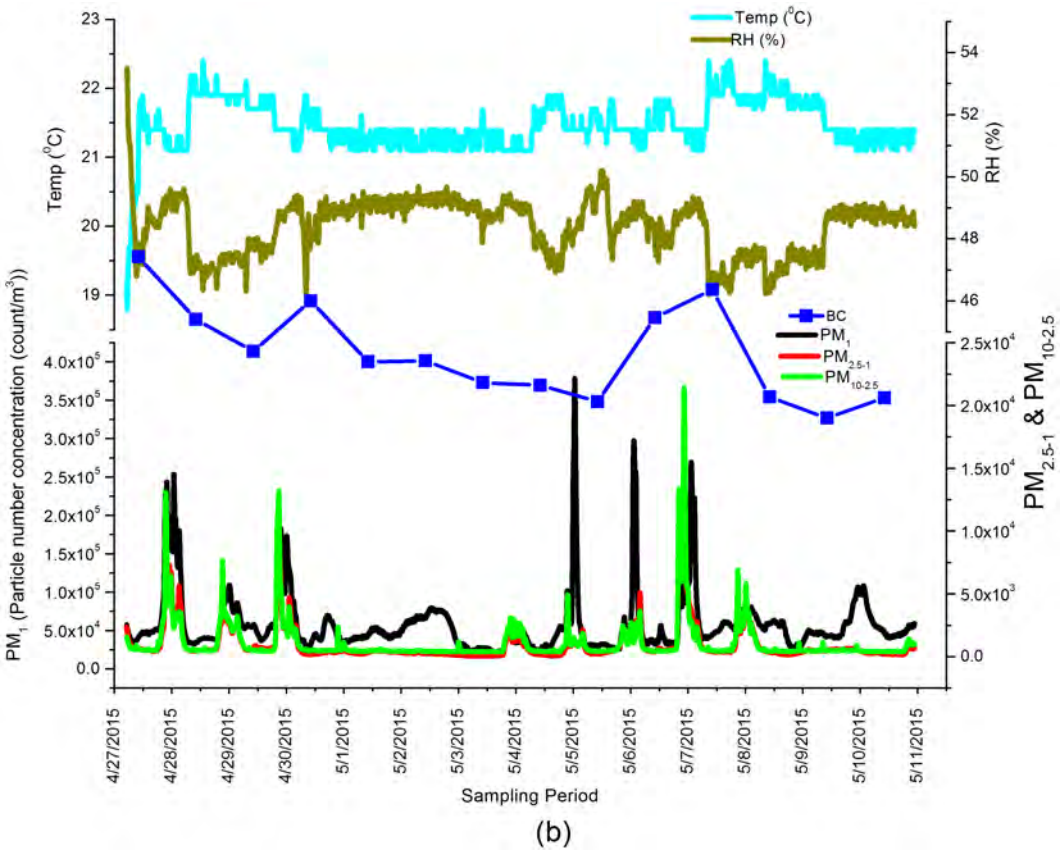

Figure 6.14: Relationship between concentration of black carbon and particulate matter (Magritte (a) and Reserve OR (b).

6.5 Elemental analysis

As shown in Table 6.4, the concentrations of eleven elements viz. Aluminum (Al), Silicon (Si), Phosphorus (P), Sulphur (S), Chlorine (Cl), Potassium (K) , Calcium (Ca), Manganese (Mn), Iron (Fe), Copper (Cu), and Zinc (Zn) were investigated. Table 6.4 gives the elemental concentration based on fractional sizes of the aerosol particles collected from inside and outside Magritte and Reserve OB museums during the entire sampling period. The mean concentrations of the analyzed elements depend on where the sampling took place. Some of these elements are known to have a negative influence on art objects; others are good indicators of certain sources of particulate matter. In PM_1 fraction, the main elements are Aluminum, Silicon, Sulphur and Copper. Only Calcium is the dominant in the $PM_{2.5-1}$ fraction. This division is related to the size of different particulates which are composed of these elements inside Magritte. On a European continental scale, the contribution of brake pad wear to atmospheric copper emissions is estimated to be about 50%. Specifically, in Belgium, the contribution reaches 65% [245]. In Magritte outside, Si, S, Ca and Fe were predominantly present in the $PM_{10-2.5}$ fraction while Fe was mainly detected in the $PM_{2.5-1}$ fraction. This indicates the relative importance of re-suspension of larger particles.

Element	Magritte Conc. (ng/m^3)						Reserve OB. Conc. (ng/m^3)					
	Inside			Outside			Inside			Outside		
	PM_1	$PM_{2.5-1}$	$PM_{10-2.5}$	PM_1	$PM_{2.5-1}$	$PM_{10-2.5}$	PM_1	$PM_{2.5-1}$	$PM_{10-2.5}$	PM_1	$PM_{2.5-1}$	$PM_{10-2.5}$
Al	52.80	0.27	2.42	53.82	6.12	59.35	53.32	9.95	3.63	55.57	8.42	3.99
Si	107.6	0.31	29.10	109.56	0.53	322.89	107.50	15.14	11.20	111.22	13.56	28.52
P	12.77	0.66	1.00	23.58	2.61	15.39	11.83	0.19	0.32	16.12	3.66	5.15
S	130.95	7.84	139.51	1056.30	123.18	540.45	66.18	3.83	37.02	521.57	70.82	332.07
Cl	27.84	0.01	24.22	36.14	0.04	128.72	18.79	7.28	5.30	108.67	396.29	1105.77
K	14.49	9.08	6.92	65.44	35.34	93.36	15.23	0.84	9.26	67.28	13.31	55.68
Ca	38.93	75.90	57.20	44.52	145.10	892.89	38.97	20.28	80.93	193.08	125.62	94.16
Mn	10.69	0.01	0.79	13.06	0.27	14.67	9.44	0.78	0.10	11.19	3.01	0.45
Fe	18.34	31.71	39.30	74.49	92.92	1006.76	18.41	2.00	30.0	171.10	89.36	63.00
Cu	67.80	0.01	0.01	76.80	0.05	2.35	57.80	0.0001	0.0004	167.80	0.002	0.001
Zn	39.01	0.001	1.51	44.77	3.001	23.57	39.06	0.00012	0.000395	44.31	7.91	8.07

Table 6.4: Elemental Concentrations (ng/m^3) inside and outside of Magritte and Reserve OB using Ti, Ge and Mo secondary target.

In the PM_1 fraction, Al, Si, S, Ca, Cu and Zn were the main elements found inside Reserve OB; Ca was predominantly present in $PM_{10-2.5}$ (Fig. 6.15 and Table 6.4). Outside of Reserve OB, S was higher in PM_1 and $PM_{10-2.5}$ while Cl was the main element in $PM_{2.5-1}$ and $PM_{10-2.5}$, predominantly in $PM_{10-2.5}$ (Fig. 6.16) Reserve OB. There was S and Cl inside and outside of Magritte (Fig. 6.15); the source of S in urban air particles could be attributed to secondary reactions on anthropogenic emissions of SO_2 and combustion of fuels containing sulfur and numerous smaller compounds such as sulfur-rich matter like $(NH_4)_2SO_4$ and Na_2SO_4 [166]. Cl an element that occurs mainly as sea salt (NaCl), might be partially caused by bringing the salt on the clothing and shoes of visitors. The presence of Si may be due to the presence

of aluminosilcate. Elements like Al, Si and K (can be released into the atmosphere from wood or plant burning) typically found in samples dominated by the contributions from stone and stone-deterioration. These elements also were found from different anthropogenic outdoors sources like traffic activities and industries near to the museums. The finding of Endjambi, et al. [246] showed that the vicinity of the incinerator and industrial area found in sampling location are sources of particulate matter concentrations. Anthropogenic sources of some of the pollutants are vehicle traffic; Zn and Fe are normally emitted by vehicle exhausts and they also originate from brake wear and tear and the wearing of tyres and added to tyres to facilitate the vulcanization of rubber tire wear particles are the most important source of anthropogenic Zn emission [247, 248]. Iron is present as metal oxide (FeO and Fe_2O_3). Mn can lead to a brown discoloring of the surface layer due to an oxidation process of Mn (II) oxide to manganese dioxide and Oil combustion processes [249]. During sampling all investigated elements' indoor/outdoor ratios (I/O_s) showed lower amount of bulk particles inside of the museum suggesting that the heating, ventilation and air conditioning (HVAC) system are able to play a significant role of total PM [19, 180, 226]. In addition to the elemental analysis, the history of the air masses also had an effect on the concentrations of PM. Figure 6.17 shows a different time scale backward trajectories of air masses arriving at the sampling site during 13 April to 11 May, 2015 when the air masses were calculated once a day at 00:00 local time. As shown in Fig. 6.17, the sources of air masses from Maritime may contain particles as sea salt, which originate from the North Atlantic Ocean and North Sea. On the other hand, there were continental sources from France that arise from industrial and vehicular emissions. The trajectory indicates continental air masses come from central France

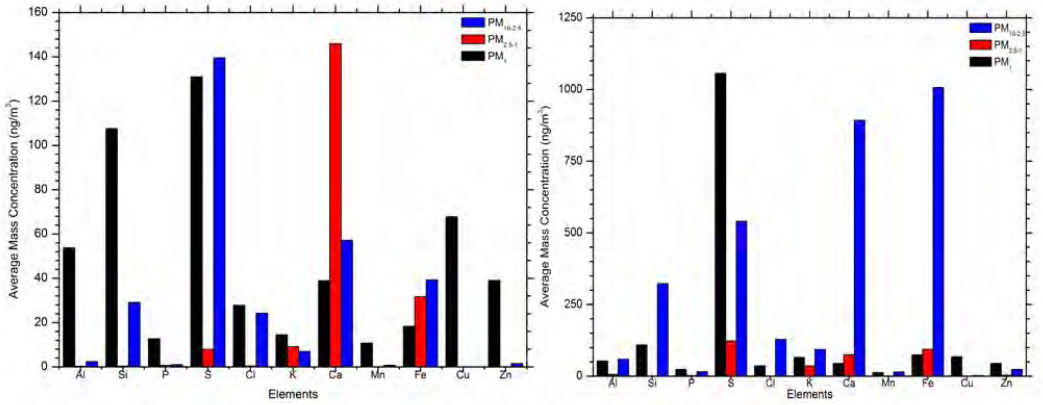

Figure 6.15: Average concentrations of the most remarkable elements inside (a) and outside (b) Magritte using Ti, Ge and Mo a secondary target.

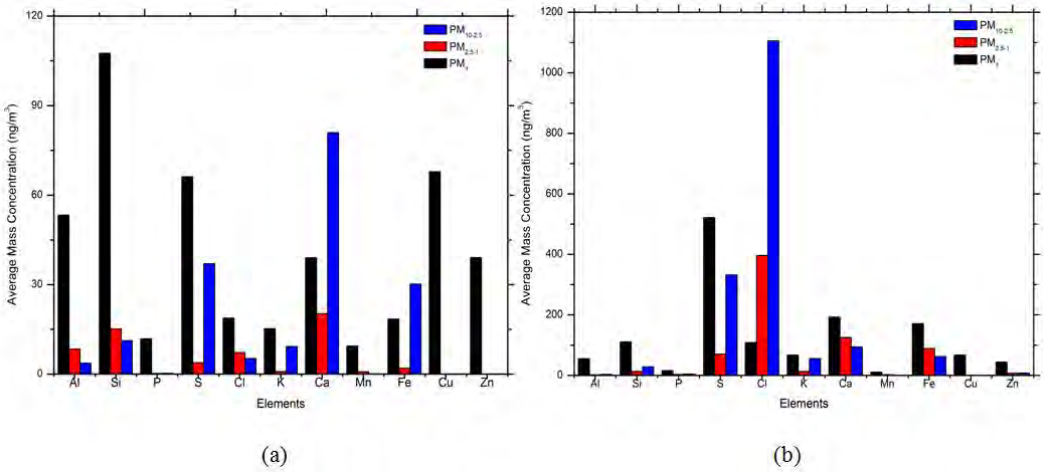

Figure 6.16: Average concentrations of the most remarkable elements inside (a) and outside (b) Reserve OB using Ti, Ge and Mo a secondary target.

and maritime one comes from North Atlantic Ocean; this therefore shows that various pathways of the air masses could cause different pollution results. All the sampling days were dominated by a significant sea salt concentration since their source mainly characterized by maritime. In order to calculate the intrusion of Sahara dust in the sampling (Brussels), the NOAA HYSPLIT Saharan dust dispersion model was applied [177, 178]. The availability of pollutants in Brussels is affected by Sahara dust outbreaks, local emission, mineral dust and construction works [179].

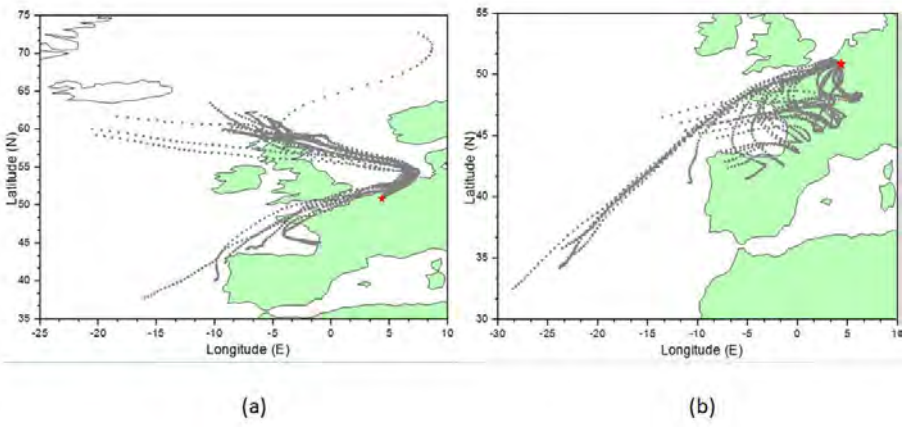

Figure 6.17: Air mass back trajectory analysis from April 13-26, 2015a and April 27-May11, 2015b at the Royal Museums of Fine Arts of Belgium, Brussels.

6.6 Conclusions

A museum, an exhibition space for objects with great cultural and historical value, is ideally considered to be free from internal sources of pollutants. The air pollution comes therefore primarily from outside and is transferred towards inside during the outdoor/indoor air exchange through cracks in walls or other slits in the building, opened windows, doors and ventilation systems. Transport of undesired polluting

compounds can be eased also by tourists. In this study, it was found that the buildings of the Magritte and Reserve OB are a significant protection against particulate matter and gaseous pollutants. The concentration and chemical compositions of particulate matter and gaseous pollutants inside and outside of the two museums were measured. The concentrations of the coarse fraction (PM_{10}) of particulate matter in the museum were much lower compared to the levels found outside, mainly because of their large aerodynamic diameter and the short retention time in the air. However, an accumulation process of fine particles ($PM_{2.5}$) was observed in the case of $(NH_4)_2SO_4$ and Na_2SO_4. The most dangerous particles from the preventive conservation point of view, the S-rich particles, were remarkably present in the fine fraction. The source of S in urban area could be attributed to secondary reactions on anthropogenic emissions of SO_2 and combustion of fuels containing sulfur. The concentrations of gases in the galleries were considered significantly lower than those measured outside the building. In case of sulphur dioxide and ozone, the concentrations measured in the galleries were very low. The differences between their outdoor and indoor concentrations were quite small. A significant increase in indoor concentrations of pollutants was noticed in the day time, when windows and doors were frequently opened to let in some fresh air in addition traffic activities construction activities happening. To improve the preventive conservation, a better insulation of the building should be considered. On the other hand, the inflow of particulate matter due to tourist activity also should be limited, for example through obligatory leaving coats and shoes of visitors in the cloakroom.

Chapter 7

General conclusions and recommendations

7.1 Conclusions

This research constitutes the investigations made at (i) Leeds University in October 2014 and February to April 2015, UK [Part I] and (ii) Magritte and Reserve OB museums, Museums of Fine Arts, Brussles, Belgium [Part II].

Part I

This study seeks to investigates the concentrations of the INPs using impinger at the School of Earth and Environment, University of Leeds, UK in the midst of October 2014 and February to April 2015. The experimental technique where droplets of microliter volume containing ice-nucleating material are cooled down at a controlled rate and their freezing temperatures were recorded. The analysis was performed between 0 to -37^{0}C at which the droplets facilitated heterogeneous freezing temperatures well above the homogenous temperature. Significantly, our investigations reveal that:

(i) The INPs started freezing from a temperature -14^0C down to -25^0C and their concentrations were ranged from $10^{-4}\ cm^{-3}$ to $10^{-1}\ cm^{-3}$. The temperature at which

50% of the droplets froze occurred at -20^0C. Concentrations of the INPs were found to be 10^{-3} cm^{-3}.

(ii) Comparison was made with other studies to identify the type of aerosols that form INPs. The study proves that the type of aerosol species that makes INPs in Leeds was predominantly feldspar. This was confirmed through the global aerosol modeling process (GLOMAP).

(iii) Meteorological condition such as temperature, wind speed and relative humidity, in addition to the trajectory of air masses appear to have an effect on the concentration of INPs. The correlations between wind speed and relative humidity have a direct relation with the concentrations of INPs; while, it has inverse relation with temperature. The strongest correlations ($R^2 = 0.909$) was with relative humidity. This result is in agreement with that reported by Timothy et al. [198]. Higher concentrations were found when the air masses originated from continent is mineral dust.

Part II

The types of particulate matter emitted into the MFAs had fractional sizes PM_1, $PM_{2.5-1}$ and $PM_{10-2.5}$. In addition, NO_2, SO_2 and O_3 gaseous and 11 elements (Al, Si, P, S, Cl, K, Ca, Mn, Fe, Cu and Zn) were identified as pollutants of the MFAs in Brussels, Belgium. PM samples were collected on Teflon membrane filters using Harvard-type Impactor collector. The concentration and chemical composition of airborne particulate matter inside and outside of the two museums was measured. We concluded that:

(i) Indoor/outdoor ratios for PM ranged from 0.14 at Magritte museum and to 0.11 at the Reserve OB. Indoor/outdoor ratio indicates that PM_{10} concentration inside (4.12 and 2.21 $\mu g/m^3$) the museums were lower than outside (30.06 and 19.37 $\mu g/m^3$) of

museums of Magritte and Reserev OB respectively. This shows that the sources of particles in the museums were outside sources and average mass concentration of PM_{10} in this study is smaller than that of the other museums for example Rubens room, Platin-Moretus, Antwerp, Belgium (15.98 $\mu g/m^3$), Printing room, Platin-Moretus, Antwerp, Belgium (15.55 $\mu g/m^3$) and Paulista, Megacity Sao Paulo, Brazil (5.4 $\mu g/m^3$).

(ii) Bulk aerosol samples were analyzed by means of energy-dispersive X-ray fluorescence analysis (EDXRF) with Ti, Ge, and Mo. Secondary targets were used to analyze the solid samples because of the relative simplicity of the technique for filter analysis and high sensitivity. Quantitative X-ray analysis was analyzed by bAxil software package. The analysis result proved that the concentrations of 11 elements namely Al, Si, P, S, Cl, K, Ca, Mn, Fe, Cu and Zn were detected inside and outside the Magritte and Reserve OB. The study confirms that indoor/outdoor ratio (I/O) for all investigated elements were lower inside than outside the museums. The amount of bulk particles concentration inside the museums suggesting that ventilation and air conditioning system plays a significant role to control the total PM concentrations in the museums.

(iii) The measurement of black carbon (BC) was performed using Aethalometry. Black carbon average concentration was 163 ng/m^3 inside Magritte museum greater than in Reserve OB museum (32 ng/m^3). The experiments were performed during the weekdays. A comparison of observations between different days of the week was made on the basis of monitoring performance during the sampling period. In doing so, the variation of the BC concentrations recorded on Friday was higher than other days (it ranges from 60.19 to 288.75 ng/m^3). This may be attributed to more human and traffic activities on Friday.

(iv) Passive diffusion tubes were used for sampling of NO_2, SO_2 and O_3. The results show that the concentration of the gaseous pollutants found in Magritte (NO_2 = <DL, SO_2= 0.8 $\mu g/m^3$ and O_3 = 3.1 $\mu g/m^3$) and Reserve OB (NO_2 = <DL, SO_2 = 0.4 $\mu g/m^3$ and O_3 = 1.6 $\mu g/m^3$) is below the recommended level (NO_2 = 19 $\mu g/m^3$, SO_2 = 5.2 $\mu g/m^3$ and O_3 = 10 $\mu g/m^3$). This implies that meteorological conditions i.e., wind, temperature, relative humidity and outside anthropogenic activities such as movement of vehicles and tourists had major influences on the concentrations of pollutants. The evidence from this study suggests a sound basis for future research on indoor environments should be conducted because the monitoring system and methodology used to analyze the indoor air quality will facilitate the study to identify the nature of pollutants which deteriorate collections and artifacts. Moreover, the results of this study will offer compelling directives to policy makers about what should be done to improve the indoor air quality and will help them in developing long-term strategies.

7.2 Recommendations

This study has gone some way towards enhancing our understanding of INPs to climate change, particulate matter and gaseous pollutants for preserving cultural Heritage. The research has given rise to the following recommendations in need of further investigation:

1. extend the investigation of INPs and identification of INP species in the UK and Ethiopia. INPs from volcanic ash which may have a sporadic impact on clouds as far as thousands of kilometers from the volcano [250] and has been

linked to sporadically high concentrations of INP in the vicinity of volcanoes [251]. Within a volcanic ash influenced air mass, it is thought that ash might compete with other important INP types, such as desert dusts [10]. It may easily verified that Ethiopia has an active volcano in Afar region hence it is important to investigate that region for volcanic ash.

2. input for improving GLOMAP Global Model predictions by inclusion of observed data.

In summary, as stated in the introduction of this study, cultural heritage recognizes that the world has significant cultural diversity together with exceptional ancient architecture, built environment and artifact collections which attract millions of tourists every year to its historical cities and sites, museums and libraries. Our findings would seem to show that results of this research will give direction for preventive strategies and steps can be taken to preserve collections more efficiently. Besides, as implied in the beginning of this study, it is now possible to state that this study highlights potential risks facing a museum and it also points out evaluate potential mitigation measures. Taken together, this experimental approach is necessary for an effective investigation of the dynamics of pollutants inside the museum, with particular attention to their indoor/outdoor exchange or to possible occurrence of indoor concentration gradients. This will certainly help to elaborate more effective strategies for the control of museum air quality as basic preventive action for conservation of artworks. It will extend the research to Ethiopia as the country has many cultural heritage sites like the Rock-Hewn Churches, Lalibela which is a world heritage site.

Supporting publications

1. Whale, T. F., Murray, B. J., O'Sullivan, D., Wilson, T. W., Umo, N. S., Baustian, K. J., Atkinson, J. D., Workneh, D. A. and Morris, G. J. (2015). A technique for quantifying heterogeneous ice nucleation in microlitre supercooled water droplets. Atmos. Meas. Tech., **8**, 2437-2447

2. Workneh, D. A., Ayalew, E. M., De Wael, K., Van Espen, P. and Gholap, A. V. (2017). Effect of gaseous pollutants (NO_2, SO_2 and O_3) on cultural heritage materials: A case of MFAs in Brussels, Belgium. Vol. **-4**, Issue-5, Journal of Scientific and Engineering Research.

3. Workneh, D. A., Ayalew, E. M., De Wael, K. and Gholap, A.V. (2017). Characterizations of particulate matter in Museums: A case of MFAs in Brussels, Belgium. ATMENV-D-17-01016, Journal of Atmospheric Environment.

4. Workneh, D. A., Murray, B. J., Wilson, T. W., Whale, T. F., O'Sullivan, D., Umo, N. S., Gholap, A. V. and Murray, E. J.: Measuring heterogeneous ice nucleating particles in the atmosphere using Biosampler (submitted in Plos-one Journal).

Conference oral and poster presentation

1. 02/2017 (Oral), Measurements of Ice Nucleating Particles Concentrations in the Atmosphere, Ethiopian Physical Society Annual 11^{th} Conference, Dire Dawa University, 3-4 February, 2017.

2. 04/2016 (Poster), Chemical characterization of particulate matter in Museum of Fine Arts, Brussels, Belgium. Chemistry Conference for Young Scientists

(ChemCYS 2016), Blankenberge, Belgium

3. 01/2016 (Poster), The Significance and Measurement of Ice Nucleating Particles (INPs) in the Atmosphere, 96th annual conference of American Meteorological Society (AMS), New Orleans, Louisiana, USA.

4. 06/2015 (Oral), The significance and measurements of atmospheric aerosols, University of Antwerp, Belgium.

5. 06/2015 (Poster), Techniques of Measuring Airborne Particles in Museum Environment, Annual Science Conference, Belgium.

6. 11/2014 (Poster), Measurement of Ice Nucleating Particles in the Atmosphere, Institute for Climate and Atmospheric Science (ICAS) annual science meeting, University of Leeds, UK.

Bibliography

[1] Seinfeld, J. H. and Pandis, S. N. (2006). Atmospheric chemistry and physics: From Air pollution to Climate Change. 2^{nd} ed., Wiley-Inter science, Hoboken, New Jersey, USA.

[2] Hinds, W. C. (1982). Acceleration and Curvilinear Particle Motion. Aerosol Technology. Properties, behavior and measurement of airborne particles. New York, John Wiley & Sons, 104-126.

[3] Baird, C. and Cann, M. (2005). Environmental Chemistry. New York, W.H. Freeman and Company.

[4] Merkus, H. G. (2009). Particle Size Measurements: Fundamentals, Practice and Quality. Dordrecht, Springer.

[5] Baker, M. B. (1997). Cloud Microphysics and Climate. Science, **276**, 1072-1078, doi:10.1126/science.276.5315.1072.

[6] Lohmann, U. (2002). A glaciation indirect aerosol effect caused by soot aerosols. Geophys. Res. Lett., **29**, 1052, doi:10.1029/2001GL014357.

[7] Storelvmo, T., Hoose, C. and Eriksson, P. (2011). Global modeling of mixed-phase clouds: The albedo and lifetime effects of aerosols. J. Geophys. Res., **116**, D05207, doi:10.1029/2010JD014724.

[8] Creamean, J. M., Suski, K. J., Rosenfeld, D., Cazorla, A., DeMott, P. J., Sullivan, R. C., White, A. B., Ralph, F. M., Minnis, P., Comstock, J. M., Tomlinson, J. M., and Prather, K. A. (2013). Dust and Biological Aerosols from the Sahara and Asia Influence Precipitation in the Western U.S. Science, **339**, 1572-1578, doi:10.1126/science.1227279.

[9] Boucher, O., Randall, D., Artaxo, P., Bretherton, C., Feingold, G., Foster, P., Kerminen, V. M., Kondo, Y., Liao, H., Lohmann, U., Rasch, P., Satheesh, S. K., Sherwood, S., Stevens, B. and Boucher, O., Randall, D., Artaxo, P., Bretherton, C., Feingold, G., Foster, P., Kerminen, V. M., Kondo, Y., Liao, H., Lohmann, U., Rasch, P., Satheesh, S. K., Sherwood, S., Stevens, B. and Zhang, X. Y. (2013). Clouds and Aerosols, in Climate Change 2013: The Physical Science Basis. Contribution of Working Group I to the Fifth Assessment Report of the Intergovernmental Panel on Climate Change. Edited by: Stocker, T. F., Qin, D., Plattner, G. K., Tignor, M., Allen, S. K., Boschung, J., Nauels, A., Xia, Y., Bex, V., and Midgley, P. M., Cambridge University Press, Cambridge, United Kingdom and New York, NY, USA.

[10] Murray, B. J., O'Sullivan, D., Atkinson, J. D., and Webb, M. E. (2012). Ice nucleation by particles immersed in supercooled cloud droplets. Chem. Soc. Rev., **41**, 6519-6554, doi:10.1039/c2cs35200a.

[11] WHO (2013). Review of evidence on health aspects of air pollution - REVIHAAP Project.World Health Organization, WHO Regional Office for Europe, Copenhagen.

[12] Fowler, D., Pilegaard, K., Sutton, M., Ambus, P., Raivonen, M., Duyzer, J., Simpson, D., Fagerli, H., Fuzzi, S., Schjoerring, J., Granier, C., Neftel, A., Isaksen, I., Laj, P., Maione, M., Monks, P., Burkhardt, J., Daemmgen, U., Neirynck,

J., Personne, E., Wichink-Kruit, R., Butterbach-Bahl, K., Flechard, C., Tuovinen, J., Coyle, M., Gerosa, G., Loubet, B., Altimir, N., Gruenhage, L., Ammann, C., Cieslik, S., Paoletti, E., Mikkelsen, T., Ro- Poulsen, H., Cellier, P., Cape, J., Horvath, L., Loreto, F., Niinemets, U., Palmer, P., Rinne, J., Misztal, P., Nemitz, E., Nilsson, D., Pryor, S., Gallagher, M., Vesala, T., Skiba, U., Brueggemann, N., Zechmeister-Boltenstern, S., Williams, J., O'Dowd, C., Facchini, M., de Leeuw, G., Flossman, A., Chaumerliac, N., and Erisman, J. (2009). Atmospheric composition change: ecosystems-Atmosphere interactions. Atmos. Environ., **43**, 5193-5267, doi:10.1016/j.atmosenv.2009.07.068.

[13] Camuffo, D., Sturora, G. and Velentino, A. (2000). Showcase: a real effective mean for protecting artworks? Thermochimica Acta, **365**, 65-77.

[14] Charta of Vantaa, (2000). Recommendations for a European approach in preventive conservation. Passed on the Vantaa-meeting, September 21-22.

[15] Camuffo, D., Van Grieken, R., Busse, H. J., Sturaro, G., Valentino, A., Bernardi, A., Blades, N., Shooter, D., Gysels, K., Deutsch, F., Wieser, M., Kim, O. and Ulrych, U. (2001). Environmental Monitoring in Four European Museums. Atmospheric Environment, **35** (Suppl. 1), S127-S140.

[16] Ttreault, J. (2003). Guidelines for Pollutant Concentrations in Museums, CCI Newsletter, No. 31, June.

[17] Vest, M. (2012). Practical Usage of Standards and Guidelines for Indoor Air Quality. Indoor Air Quality in Heritage and Historic Environments, London.

[18] Cecily, M. G. (2006). Monitoring for Gaseous Pollutants in Museum Environments, The Getty Conservation Institute, Los Angeles.

[19] Godoi, R. H. M., Potgieter-Vermaak, S., Godoi, A. F. L., Stranger, M. and Van Grieken, R. (2008). Assessment of Aerosol Particles within the Rubens' House Museum in Antwerp. X-Ray Spectrometry, **37**, 298-303.

[20] Hu, T., Lee, S., Cao, J., Chow, J. C., Watson, J. G., Ho, K., Ho, W., Rong, B. and An, Z. (2009). Characterization of Winter Airborne Particles at Emperor Qin's Terra-cotta Museum, China. Science of the Total Environment, **407**, 5319-5327.

[21] Barbara, J., Finlayson-Pitts, James, N. and Pitts, Jr. (1999). Chemistry of the Upper and Lower Atmosphere: Theory, Experiments and Applications. Academic Press, San Diego, CA, USA.

[22] Andreae, M. O. and Rosenfeld, D. (2008). Aerosol-cloud-precipitation interactions. Part1. The nature and sources of cloud-active aerosols. Earth-Sci. Rev., **89**, 13-41, doi:10.1016/j.earscirev.2008.03.001.

[23] Twomey, S. (1991). Aerosols, clouds and radiation. Atmos. Environ. A-Gen., **25**, 2435-2442, doi:10.1016/0960-1686(91)90159-5.

[24] Albrecht, B. A. (1989). Aerosols cloud microphysics, and fractional cloudiness. Science, **245**, 1227-1230, doi:10.1126/science.245.4923.1227.

[25] Haywood, J. and Boucher, O. (2000). Estimates of the direct and indirect radiative forcing due to tropospheric aerosols: a review. Rev. Geophys., 38, 513-543.

[26] Myhre, G. (2009). Consistency between satellite-derived and modeled estimates of the direct aerosol effect. Science, **325**, 187- 190, doi:10.1126/science.1174461.

[27] Lohmann, U. and Feichter, J. (2005). Global indirect aerosol effects: a review. Atmos. Chem. Phys., **5**, 715-737, http://www.atmos-chem-phys.net/5/715/.

[28] Hansen, J. E., Sato, M. and Ruedy, R. (1997). Radiative forcing and climate response. J. Geophys. Res., **102**, 6831-6864.

[29] Koch, D. and Del Genio, A. D. (2010). Black carbon absorption effects on cloud cover, review and synthesis. Atmos. Chem. Phys., **10**, 7685-7696.

[30] Johnson, B. T. (2003). The Semi-direct Aerosol Effect (Ph.D. thesis). The University of Reading, UK. .

[31] Perlwitz, J., Tegen, I. and Miller, L. R. (2001). Interactive soil dust aerosol model in the GISS GCM: part I: sensitivity of the soil dust cycle to radiative properties of soil dust aerosols. J. Geophys. Res. **106**, 18167e18192. http://dx.doi.org/10.1029/2000JD900668.

[32] Miller, R. L. and Tegen, I. (2004). Feedback upon dust emission by dust radiative forcing through the planetary boundary layer. J. Geophys. Res. **109**, D24209. http://dx.doi.org/10.1029/2004JD004912.

[33] Miller, R. L., Tegen, I. and Perlwitz, J. (2004). Surface radiative forcing by soil dust aerosols and the hydrologic cycle. J. Geophys. Res. **109**, D04203. http://dx.doi.org/10.1029/ 2003JD004085.

[34] Yue, X., Wang, H., Liao, H., and Fan, K. (2010). Simulation of dust aerosol radiative feedback using the GMOD: 2.Dust-climate interactions. J. Geophys. Res. **115**, D04201. http://dx.doi.org/ 10.1029/2009JD012063.

[35] Stanelle, T., Vogel, B., Vogel, H., Baumer, D. and Kottmeier, C. (2010). Feedback between dust particles and atmospheric processes over West Africa during dust episodes in March 2006 and June 2007. Atmos. Chem. Phys., **10**, 10771e10788.

[36] Mallet, M., Tulet, P., Serca, D., Solomon, F., Dubovik, O., Pelon, J., pont, V. and Thouron, O. (2009). Impact of dust aerosols on the radiative budget, surface

heat fluxes, heating rate profiles and convective activity over West Africa during March 2006. Atmos. Chem. Phys., **9**, 7143e7160.

[37] Solomon, F., Elguindi, N. and Malletet, M. (2012). Radiative and climatic effects of dust over West Africa, as simulated by a regional climate model. Clim. Res. **52**, 97e113.

[38] Tesfaye, M., Botai, J., Sivakumar, V. and Mengistu, T. G. (2014). Simulation of biomass burning aerosols mass distributions and their direct and semi-direct effects over South Africa using a regional climate model. Meteorol. Atmos. Phys. **125**, 177e195. http://dx.doi.org/10.1007/ s00703-014-0328-2.

[39] Johnson, B. T., Shine, K. P. and Forster, P. M. (2004). The semidirect aerosol effect: Impact of absorbing aerosols on marine stratocumulus. Q. J. Roy. Meteorol. Soc., **130**, 1407-1422, doi:10.1256/qj.03.61.

[40] Lohmann, U. and Feichter, J. (2001). Can the direct and semi-direct aerosol effect compete with the indirect effect on a global scale? Geophys. Res. Lett., **28**(1), 159-161.

[41] Wallace, J. and Hobbs, P. V. (2006). Atmospheric Science: An Introduction Survey. Elsevier Science and Technology Books.

[42] McFiggans, G., Artaxo, P., Baltensperger, U., Coe, H., Facchini, M. C., Feingold, G., Fuzzi, S., Gysel, M., Laaksonen, A., Lohman, U., Mentel, T. F., Murphy, D. M., O'Dowd, C. D., Snider, J. R. and Weingartner, E. (2006). The effect of physical and chemical aerosol properties on warm cloud droplet activation. Atmos. Chem. Phys. **6**, 2593- 2649.

[43] Köhler, H. (1936). The nucleus in and the growth of hygroscopic droplets. Trans. Faraday Soc., **32**, 1152-1161, doi: 10.1039/TF9363201152.

[44] Raoult, F. M. (1887) General law of the vapor pressure of solvents. Comptes Rendus , **104**, 14303.

[45] Kammermann, and Lukas, P. L. (2010). Aerosol hygroscopicity and CCN properties at remote sites. PhD thesis, ETH.

[46] Andrews and David, G. (2010). An Introduction to Atmospheric Physics. 2^{nd} ed. University of Oxford. Cambridge University Press.

[47] Pruppacher, H. R. and Klett, J. D. (2010). Microphysics of clouds and precipitation. Netherlands, Springer.

[48] Barry, R. G. and Chorley, R. J. (2009). Atmosphere, weather and climate. 8^{th} ed., Routledge.

[49] Mason, B. J. (1962). Clouds, rain and rainmaking, Cambridge University Press.

[50] Rosenfeld, D. and Woodley, W. L. (2000). Deep convective clouds with sustained super-cooled liquid water down to -37.5^{0}C. Nature, **405**, 440-442.

[51] Herbert, R. J., Murray, B. J., Dobbie, S. J. and Koop, T. (2015). Sensitivity of liquid clouds to homogenous freezing parameterizations, Geophys. Res. Lett., **42**, p. 2014GL062729, DOI: 10.1002/2014gl062729.

[52] Choi, Y. S., Lindzen, R. S., Ho, C. H. and Kim, J. (2010). Space observations of cold-cloud phase change. P. Natl. Acad. Sci. USA, **107**, 11211-11216, doi:10.1073/pnas.1006241107.

[53] Murray, B. J., Broadley, S. L., Wilson, T. W., Bull, S. J., Wills, R. H., Christenson, H. K. and Murray, E. J. (2010). Kinetics of the homogeneous freezing of water. Phys. Chem. Chem. Phys., **12**, pp. 10380-10387, DOI: 10.1039/c003297b.

[54] Hoose, C. and Möhler, O. (2012). Heterogeneous ice nucleation on atmospheric aerosols: a review of results from laboratory experiments. Atmos. Chem. Phys., **12**, 9817-9854, doi: 10.5194/acp-12-9817.

[55] Rogers, D. C., DeMott, P. J., Sonia, M., Chen, K. Y. A. (1998). Measurements of ice nucleating aerosols during SUCCESS. Geophysical Research Letters, Vol. **25**, NO. 9, pages 1383-1386.

[56] DeMott, P. J., Prenni, A. J., Liu, X., Kreidenweis, S. M., Petters, M. D., Twohy, C. H., Richardson, M. S., Eidhammer, T. and Rogers, D. C. (2010). Predicting global atmospheric ice nuclei distributions and their impacts on climate. P. Natl. Acad. Sci. USA, **107**, 11217- 11222, doi:10.1073/pnas.0910818107.

[57] Carslaw, K. S., Boucher, O., Spracklen, D. V., Mann, G. W., Rae, J. G. L., Woodward, S. and Kulmala, M. (2010). A review of natural aerosol interactions and feed backs within the earth system. Atmos. Chem. Phys., **10**, 1701-1737.

[58] Andreae, M. O. (2007). Aerosols before pollution. Science, **315**, 50-51, i:10.1126/science.1136529.

[59] Mangan, T. P., Atkinson , J. D., Neuberg, J. W., O'Sullivan , D., Wilson, T. W., Whale, T.F., Neve, L., Umo, N. S., Malkin, T. L. and Murray, B. J. (2017). Heterogeneous Ice Nucleation by Soufriere Hills Volcanic Ash Immersed in Water Droplets. PLoS ONE, **12** (1), e0169720. doi:10.1371/journal.

[60] Korolev, A. (2007). Limitations of the Wegener-Bergeron-Findeisen Mechanism in the Evolution of Mixed-Phase Clouds. J. Atmos. Sci., **64**, 3372-3375, doi:10.1175/JAS4035.1.

[61] Lau, K. M. and Wu, H. T. (2003). Warm rain processes over tropical oceans and climate implications. Geophys. Res. Lett., **30**, 2290, doi:10.1029/2003GL018567.

[62] Zeng, X., Tao, W. K., Zhang, M., Hou, A. Y., Xie, S., Lang, S., Li, X., Starr, D. O., Li, X. and Simpson, J. (2009). An Indirect Effect of Ice Nuclei on Atmospheric Radiation. J. Atmos. Sci., **66**, 41-61, doi:10.1175/2008JAS2778.1.

[63] Hartmann, D. L., Ockert-Bell, M. E. and Michelsen, M. L. (1992). The effect of cloud type on Earth's energy balance: Global analysis. J. Clim., **5**, 1281-1304.

[64] Chen, T., Rossow, W. B. and Zhang, Y. (2000). Radiative Effects of Cloud-Type Variations. J. Clim., **13**, 264-286.

[65] Mitchell, D. L. and Finnegan, W. (2009). Modification of cirrus clouds to reduce global warming. Environ. Res. Lett., **4**, 45102, doi:10.1088/1748-9326/4/4/045102.

[66] Lynch, D. K., Sassen, K., Starr, D. C. and Stephens, G. (2002). Cirrus. Oxford University Press, New York, NY, USA.

[67] Jensen, E. J. and Toon, O. B. (1997). The potential impact of soot particles from aircraft exhaust on cirrus clouds. Geophys. Res. Lett., **24**, 249-252, doi:10.1029/96GL03235.

[68] DeMott, P. J., Rogers, D. C., Kreidenweis, S. M., Chen, Y., Twohy, C. H., Baumgardner, D., Heymsfield, A. J. and Chan, K. R. (1998). The role of heterogeneous freezing nucleation in upper tropospheric clouds: Inferences from SUCCESS. Geophys. Res. Lett., **25**, 1387- 1390, doi:10.1029/97GL03779.

[69] Kärcher, B. and Lohmann, U. (2003). A parameterization of cirrus cloud formation: Heterogeneous freezing. J. Geophys. Res., **108**, 4402, doi:10.1029/2002JD003220.

[70] Cziczo, D. J., Murphy, D. M., Hudson, P. K. and Thomson, D. S. (2004). Single particle measurementsof the chemical composition of cirrus ice residue during CRYSTAL-FACE. J. Geophys. Res., **109**, D04201, doi:10.1029/2003JD004032.

[71] Barahona, D. and Nenes, A. (2009). Parameterizing the competition between homogeneous and heterogeneous freezing in ice cloud formation - polydisperse ice nuclei. Atmos. Chem. Phys., **9**, 369-381, doi:10.5194/acp-9-369.

[72] Lohmann, U. (2002). A glaciation indirect aerosol effect caused by soot aerosols. Geophys. Res. Lett., **29**, 1052, doi:10.1029/2001GL014357.

[73] Storelvmo, T., Hoose, C. and Eriksson, P. (2011). Global modeling of mixed-phase clouds: The albedo and lifetime effects of aerosols. J. Geophys. Res., **116**, D05207, doi:10.1029/2010JD014724.

[74] Prospero, J. M., Ginoux, P., Torres, O., Nicholson, S. E. and Gill, T. E. (2002). Environmental characterization of global sources of atmospheric soil dust identified with the NIMBUS 7 Total Ozone Mapping Spectrometer (TOMS) absorbing aerosol product. Rev. Geophys., **40**, p. 1002, DOI: 10.1029/2000rg000095.

[75] Atkinson, J. D., Murray, B. J., Woodhouse, M. T., Whale, T. F., Baustian, K. J., Carslaw, S. Dobbie, K. S., O'Sullivan, D. and Malkin, T. L. (2013). The importance of feldspar for ice nucleation by mineral dust in mixed-phase clouds. Nature, **498**, pp. 355-358, DOI: 10.1038/nature12278.

[76] O'Sullivan, D., Murray, B. J., Ross, J. F., Whale, T. F., Price, H. C., Atkinson, J. D., Umo, N. S. and Webb, M. E. (2015). The relevance of nanoscale biological fragments for ice nucleation in clouds. Scientific Reports, **5**, DOI: 10.1038/srep08082.

[77] DeMott, P. J. (1990). An Exploratory-Study of Ice Nucleation by Soot Aerosols. J. App. Meteorol., **29**, pp. 1072-1079.

[78] Steinke, I., Möhler, O., Kiselev, A., Niemand, M., Saathoff, H., Schnaiter, M., Skrotzki, J., Hoose, C. and Leisner, T. (2010). Ice nucleation properties of fine ash

particles from the Eyjafjallajkull eruption in April 2010. Atmos. Chem. Phys., **11**, pp. 12945-12958, DOI: 10.5194/acp-11-12945-2011.

[79] Rogers, R. R. and Yau. M. K. (1989). A short course in cloud physics. International series in natural philosophy, Butterworth Heinemann, Burlington, MA.

[80] Vali, G. (1999). Ice nucleation theory. A tutorial [Online]. Available: http://www- as.uwyo.edu/ vali/nuclth.pdf.

[81] Murray, B. J., Broadley, S. L., Wilson, T. W., Atkinson, J. D. and Wills, R. H. (2011). Heterogeneous freezing of water droplets containing kaolinite particles. Atmospheric Chemistry and Physics, **11**, 4191-4207.

[82] Vali, G. (1985). Nucleation terminology. Journal of Aerosol Science, **16**, 575-576.

[83] Fornea, A. P., Brooks, S. D., Dooley, J. B. and Saha, A. (2009). Heterogeneous freezing of ice on atmospheric aerosols containing ash, soot and soil. Journal of Geophysical Research: Atmospheres, **114**, D13201.

[84] Hoffmann, N., Duft, D., Kiselev, A. and Leisner, T. (2013). Contact freezing efficiency of mineral dust aerosols studied in an electrodynamic balance: Quantitative size and temperature dependence for illite particles. Faraday Discussions, **165**, 383-390.

[85] Pratt, K. A., DeMott, P. J., French, J. R., Wang, Z., Westphal, D. L., Heymsfield, A. J., Twohy, C. H., Prenni, A. J. and Prather, K. A. (2009). In situ detection of biological particles in cloud ice-crystals. Nature Geoscience, **2**, 398- 401.

[86] Knopf, D. A., Alpert, P. A., Wang, B. and Aller, J. Y. (2010). Stimulation of ice nucleation by marine diatoms. Nature Geoscience, **4**, 88-90.

[87] Tobo, Y., Prenni, A. J., DeMott, P. J., Hu man, J. A., McCluskey, C. S., Tian, G., Christopher Pohlker, C., Poschl, U. and. Kreidenweis, S. M. (2013). Biological aerosol particles as a key determinant of ice nuclei populations in a forest ecosystem. Journal of Geophysical Research: Atmospheres, **118**, 10,100-10,110.

[88] Poschl, U., Martin, S. T., Sinha, B., Chen, Q., Gunthe, S. S., Hu-man, J. A., Borrmann, S., Farmer, D. K., Garland, R. M., Helas, G., Jimenez, J. L., King, S. M., Manzi, A., Mikhailov, E., Pauliquevis, T., Petters, M. D., Prenni, A. J., Roldin, P., Rose, D., Schneider, J., Su, H., Zorn, S. R., Artaxo, P. and Andreae, M. O. (2010). Rainforest aerosols as biogenic nuclei of clouds and precipitation in the Amazon. Science (New York, N.Y.), **329** (5998):1513-6.

[89] Möhler, O., Field, P. R., Connolly, P., Benz, S., Saathoff, H., Schnaiter, M., Wagner, R., Cotton, R., Kramer, M., Mangold, A. and Heymsfield, J. A. (2006). Efficiency of the deposition mode ice nucleation on mineral dust particles. Atmos. Chem. Phys., **6**, 3007-3021, 10.5194/acp-6-3007-2006.

[90] Connolly, P. J., Möhler, O., Field, P. R., Saathoff, H., Burgess, R., Choularton, T. and Gallagher, M. (2009). Studies of heterogeneous freezing by three different desert dust samples. Atmos. Chem. Phys., **9**, 2805-2824, 10.5194/acp-9-2805-2009.

[91] Rogers, D. C. (1993). Measurements of natural ice nuclei with a continuous flow diffusion chamber. Atmos. Res., **29**, 209-228.

[92] Rogers, D. C. (1988). Development of a continuous flow thermal gradient diffusion chamber for ice nucleation studies. Atmos. Res., **22**, 149-181, doi:10.1016/0169-8095(88)90005-1.

[93] Saito, A., Murakami, M. and Tanaka, T. (2011). Automated Continuous-Flow Thermal-Diffusion-Chamber Type Ice Nucleus Counter. SOLA, Vol.**7**, 029032, doi:10.2151/sola.2011-008.

[94] Rogers, D. C., DeMott, P. J., Kreidenweis, S. M. and Chen, Y. (2001). A continuous-flow diffusion chamber for airborne measurements of ice nuclei. J. Atmos. Ocean. Technol., **18**, 725-741.

[95] DeMott, P. J., Cziczo, D. J., Prenni, A. J., Murphy, D. M., Kreidenweis, S. M., Thomson, D. S., Borys, R. and Rogers, D. C. (2003). Measurements of the concentration and composition of nuclei for cirrus formation. P. Natl. Acad. Sci. USA, **100**, 14655-14660, doi:10.1073/pnas.2532677100.

[96] Garcia, E., Hill, T. C. J., Prenni, A. J., DeMott, P. J., Franc, G. D. and Kreidenweis, S. M. (2012): Biogenic ice nuclei in boundary layer air over two U.S. High Plains agricultural regions. J. Geophys. Res., **117**, D18209, doi:10.1029/2012JD018343.

[97] Whale, T. F., Murray, B. J., O'Sullivan, D., Wilson, T. W., Umo, N. S., Baustian, K. J., Atkinson, J. D., Workneh, D. A. and Morris, G. J. (2015). A technique for quantifying heterogeneous ice nucleation in microlitre supercooled water droplets. Atmos. Meas. Tech., **8**, 2437-2447.

[98] Wright, T. P. and Petters, M. D. (2013). The role of time in heterogeneous freezing nucleation. Journal of Geophysical Research: Atmospheres, **118**, 3731-3743.

[99] Gibbs, J. (1948). The collected works. Vol. 1. Thermodynamics, Yale University Press.

[100] Mullin, J. W. (2001). Crystallization. Butterworth-Heinemann.

[101] Murphy, D. M. and Koop, T. (2005). Review of the vapour pressures of ice and supercooled water for atmospheric applications. Quarterly Journal of the Royal Meteorological Society, **131**, 1539-1565.

[102] Riechers, B., Wittbracht, F., Hutten, A. and Koop, T. (2013). The homogeneous ice nucleation rate of water droplets produced in a microfluidic device and the role of temperature uncertainty. Physical Chemistry Chemical Physics, **15**, 5873-5887.

[103] Vali, G. and Stansbury, E. (1966). Time-dependent characteristics of heterogeneous nucleation of ice. Canadian Journal of Physics, **44** (2), 477-502.

[104] Vali, G. (2008). Repeatability and randomness in heterogeneous freezing nucleation. Atmos. Chem. Phys., **8**, 5017-5031.

[105] Vali, G. (1994). Freezing rate due to heterogeneous nucleation. Journal of the Atmospheric Sciences, **51**, 2683-2683.

[106] Broadley, S. L., Murray, B. J., Herbert, R. J., Atkinson, J. D., Dobbie, S., Malkin, T. L., Condliffe, E. and Neve, L. (2012). Immersion mode heterogeneous ice nucleation by an illite rich powder representative of atmospheric mineral dust. Atmos. Chem. Phys., **12**, 287-307.

[107] Marcolli, C., Gedamke, S., Peter, T. and Zobrist, B. (2007). Efficiency of immersion mode ice nucleation on surrogates of mineral dust. Atmospheric Chemistry and Physics, **7**, 5081-5091.

[108] Niedermeier, D., Shaw, R. A., Hartmann, S., Wex, H., Clauss, T., Voigtlnder, J. and Stratmann, F. (2011). Heterogeneous ice nucleation: Exploring the transition from stochastic to singular freezing behavior. Atmos. Chem. Phys., **11**, 8767-8775.

[109] Herbert, R. J., Murray, B. J., Whale, T. F., Dobbie, S. J. and Atkinson, J. D. (2014). Representing time-dependent freezing behaviour in immersion mode ice nucleation. Atmos. Chem. Phys. Discuss., **14**, 1399-1442.

[110] Kireeva, E. D., Popovicheva, O. B., Persiantseva, N. M., Khokhlova, T. D. and Shonija, N. K. (2009). Effect of black carbon particles on the efficiency of water droplet freezing. Colloid Journal, **71**, 353-359.

[111] Wright, T. P., Petters, M. D., Hader, J. D., Morton, T. and Holder, A. L. (2013). Minimal cooling rate dependence of ice nuclei activity in the immersion mode. Journal of Geophysical Research: Atmospheres, **118**, 10,535-10,543.

[112] Ervens, B. and Feingold, G. (2013). Sensitivities of immersion freezing: Reconciling classical nucleation theory and deterministic expressions. Geophysical Research Letters, **40**, 3320-3324.

[113] Vali, G. (1971). Quantitative evaluation of experimental results the heterogeneous freezing nucleation of supercooled liquids. Journal of the Atmospheric Sciences, **28**, 402-409.

[114] BioSampler Operating Instructions. SKC Inc. 863 Valley View Road Eighty our, PA 15330 USA. www.skcinc.com/catalog/pdf/instructions/37084.pdf. [Accessed Oct.24, 2014.]

[115] Lüond, F., Stetzer, O., Welti, A. and Lohmann, U. (2010). Experimental study on the ice nucleation ability of size-selected kaolinite particles in the immersion mode. Journal of Geophysical Research: Atmospheres, **115**, D14201.

[116] O'sullivan, D., Murray, B. J., Malkin, T. L., Whale, T. F., Umo, N. S., Atkinson, J. D., Price, H. C., Baustian, K. J., Browse, J. and Webb, M. E. (2014). Ice nucleation by fertile soil dusts: Relative importance of mineral and biogenic components. Atmos. Chem. Phys., **14**, 1853-1867.

[117] Umo, N. S., Murray, B. J., Baeza-Romero, M. T., Jones, J. M., Lea-Langton, A. R., Malkin, T. L., O'Sullivan, D., Plane, J. M. C. and Williams, A. (2014). Ice nucleation by combustion ash particles at conditions relevant to mixed-phase

clouds. Atmos. Chem. Phys. Discuss., **14**, pp. 28845-28883, DOI: 10.5194/acpd-14-28845-2014.

[118] Hiranuma, N., Augustin-Bauditz, S., Bingemer, H., Budke, C., Curtius,J., Danielczok, A., Diehl, K., Dreischmeier, K., Ebert, M., Frank, F., Hoffmann, N., Kandler, K., Kiselev, A., Koop, T., Leisner, T., Möhler, O., Nillius, B., Peckhaus, A., Rose, D., Weinbruch,S., Wex, H., Boose, Y., DeMott, P. J., Hader, J. D., Hill, T. C. J., Kanji, Z. A., Kulkarni, G., Levin, E. J. T., McCluskey, C. S., Murakami, M., Murray, B. J., Niedermeier, D., Petters, M. D., O'Sullivan, D., Saito, A., Schill, G. P., Tajiri, T., Tolbert, M. A., Welti, A., Whale, T. F., Wright, T. P. and Yamashita, K. (2015). A comprehensive laboratory study on the immersion freezing behavior of illite NX particles: a comparison of 17 ice nucleation measurement techniques. Atmos. Chem. Phys., **15**, 2489-2518, doi:10.5194/acp-15-2489.

[119] Riechers, B., Wittbracht, F., Hütten, A. and Koop, T. (2013). The homogeneous ice nucleation rate of water droplets produced in a microfluidic device and the role of temperature uncertainty. Phys.Chem. Chem. Phys., **15**, 5873-5887, doi:10.1039/C3CP42437E.

[120] Berezinski, N. A., Stepanov, G. V. and Khorguani, V. G. (1988). Ice-forming activity of atmospheric aerosol particles of different sizes. Lecture Notes in Physics, eds PE Wagner and G Vali (Springer, Heidelberg), **309**, p. 709.

[121] Mathews, S., Richardson, DeMott, P. J., Kreidenweis, S. M., Daniel, J., Cziczo, Edward, J., Dunlea, Jimenez, J. L., Thomson, D. S., Ashbaugh, L. L. Borys, R. D., Westphal, D. L., Casuccio, G. S. and Traci, L., Lersch, T. L. (2007). Measurements of heterogeneous ice nuclei in the Western United States in spring time and their relation to aerosol characteristics. J. Geophys Res-Atmos., **112**, D02209 doi: 10.1029/2006JD007500.

[122] Draxler, R. R., and Hess, G. D. (1998). An Overview of the HYSPLIT-4: Modelling System for Trajectories, Dispersion and Deposition. Aust. Met. Mag., **47**, 295-308.

[123] DeMott, P. J., Hill, T. C. J., McCluskey, C. S., Prather, K. A., Collins, D. B., Sullivan, R. C., Ruppel, M. J., Mason, R. H., Irish, V. E., Lee, T., Hwang, C. Y., Rhee, T. S., Snider, J. R., McMeeking, G. R., Dhaniyala, S., Lewis, E. R., Wentzell, J., Abbatt, J. P. D., Lee, C., Sultana, C. M., Ault, A. P., Axson, J. I., Martinez, M. D., Venero, I., Figueroa, G. S., Stokes, M. D., Deane, G. B., Mayol-Bracero, O. L., Grassian, V. H., Bertram, T. H., Bertram, A. K., Moffett, B. F. and Franc, G. D. (2016). Sea spray aerosol as a unique source of ice nucleating particles. P. Natl. Acad. Sci. USA, **113**, 5797-5803.

[124] Szyrmer, W. and Zawadzki, I. (1997). Biogenic and anthropogenic sources of ice-forming nuclei: a review. B. Am. Meteorol. Soc., **78**, 209-228.

[125] Möhler, O., DeMott, P. J., Vali, G. and Levin, Z. (2007). Microbiology and atmospheric processes: the role of biological particles in cloud physics. Biogeosciences, **4**, 1059-1071, doi:10.5194/bg-4-1059.

[126] Garcia, E., Hill, T. C. J., Prenni, A. J., DeMott, P. J., Franc, G. D. and Kreidenweis, S. M. (2012): Biogenic ice nuclei in boundary layer air over two U.S. High Plains agricultural regions. J. Geophys. Res., **117**, D18209, doi:10.1029/2012JD018343.

[127] Hiranuma, N., Möhler, O., Yamashita, K., Tajiri, T., Saito, A., Kiselev, A., Hoffmann, N., Hoose, C., Jantsch, E., Koop, T. and Murakami, M. (2015). Ice nucleation by cellulose and its potential contribution to ice formation in clouds. Nat. Geosci., **8**, 273-277, doi:10.1038/ngeo2374.

[128] Hoose, C. and Möhler, O. (2012). Heterogeneous ice nucleation on atmospheric aerosols: a review of results from laboratory experiments. Atmos. Chem. Phys., **12**, 9817-9854, doi:10.5194/acp-12-9817.

[129] Schnell, R. C. (1975). Ice nuclei produced by laboratory cultured marine phytoplankton. Geophys. Res. Lett., **2**, 500-502, doi:10.1029/GL002i011p00500.

[130] Schnell, R. C. and Vali, G. (1975). Freezing nuclei in marine waters. Tellus, **27**, 321-323, doi:10.1111/j.2153-3490.1975.tb01682.x.

[131] Jayaweera, K. and Flanagan, P. (1982). Investigations on biogenic ice nuclei in the Arctic atmosphere. Geophys. Res. Lett., **9**, 94-97, doi:10.1029/GL009i001p00094.

[132] Parker, L. V, Sullivan, C. W., Forest, T. W. and Ackley, S. F. (1985). Ice nucleation activity of antarctic marine microorganisms. Antarct. J. USA, **20**, 126-127.

[133] Alpert, P. A., Aller, J. Y. and Knopf, D. A. (2011). Ice nucleation from aqueous NaCl droplets with and without marine diatoms. mos. Chem. Phys., **11**, 5539-5555, doi:10.5194/acp-11-5539-2011.

[134] Knopf, D. A., Alpert, P. A., Wang, B. and Aller, J. Y. (2011). Stimulation of ice nucleation by marine diatoms. Nat. Geosci., **4**, 88-90, doi:10.1038/ngeo1037.

[135] Wilson, T. W., Ladino, L. A., Alpert, P. A., Breckels, M. N., Brooks, I. M., Browse, J., Burrows, S. M., Carslaw, K. S., Huffman, J. A., Judd, C., Kilthau, W. P., Mason, R. H., McFiggans, G., Miller, L. A., Najera, J., Polishchuk, E., Rae, S., Schiller, C. L., Si, M., Vergara Temprado, J., Whale, T. F., Wong, J. P. S., Wurl, O., Yakobi-Hancock, J. D., Abbatt, J. P. D., Aller, J. Y., Bertram, A. K., Knopf, D. A. and Murray, B. J. (2015). A marine biogenic source of atmospheric ice nucleating particles. Nature. Vol. **525**, doi:10.1038/nature, 14986.

[136] Prather, K. A., Bertram, T. H., Grassian, V. H., Deane, G. B., Stokes, M. D., DeMott, P. J., Aluwihare, L. I., Palenik, B. P., Azam, F., Seinfeld, J. H., Moffet, R. C., Molina, M. J., Cappa, C. D., Geiger, F. M., Roberts, G. C., Russell, L. M., Ault, A. P., Baltrusaitis, J., Collins, D. B., Corrigan, C. E., Cuadra-Rodriguez, L. A., Ebben, C. J., Forestieri, S. D., Guasco, T. L., Hersey, S. P., Kim, M. J., Lambert, W. F., Modini, R. L., Mui, W., Pedler, B. E., Ruppel, M. J., Ryder, O. S., Schoepp, N. G., Sullivan, R. C. and Zhao, D. (2013). Bringing the ocean into the laboratory to probe the chemical complexity of sea spray aerosol. P. Natl. Acad. Sci. USA, **110**, 7550-7555, doi:10.1073/pnas.1300262110.

[137] Burrows, S. M., Hoose, C., Pöschl, U. and Lawrence, M. G. (2013). Ice nuclei in marine air: biogenic particles or dust? Atmos. Chem. Phys., **13**, 245-267, doi:10.5194/acp-13-245.

[138] Meyers, M. P., DeMott P. J. and Cotton, W. R. (1992). New Primary Ice-Nucleation Parameterizations in an Explicit Cloud Model. J. App. Meteorol., **31**, pp. 708-721.

[139] Fletcher, N. H. (1962). The physics of rainclouds. Cambridge University Press.

[140] Hogan, A. W. (1979). Meteorological transport of particulate material to the South Polar Plateau. J. Appl. Meteor., **18**, 741-749.

[141] Timothy, P., Wright, John, D., Hader, Gavin, McMeeking, R. and Petters, M. D. (2014). High Relative Humidity as a Trigger for Widespread Release of Ice Nuclei. Aerosol Science and Technology, **48**, i-v.

[142] Kumai, M. (1962). Snow crystals and the identification of nuclei in the northern United States of America. J. Meteorol., **18**, 139-150.

[143] Georgii, H. W. and Kleinjung, J. (1967). Relations between the chemical composition of aerosols and the concentration of natural ice nuclei. J. Rech Atmos., **1**,145-156.

[144] Isono, K., Komabayasi, M. and Ono, A. (1959). Volcanoes as a Source of Atmospheric Ice Nuclei. Nature, **183**, 317-318, Doi 10.1038/183317a0.

[145] Thomson, G. (1965). Air pollution-A review for conservation chemists. Stud. Conserv., **10**, 147-167.

[146] Baer, N. S. and Banks, P. N. (1985). Indoor air pollution: Effects on cultural and historical materials. Int. J.Mus. Mgmt. Cur., **4**, 9-20.

[147] Brimblecombe, P. (1990). The composition of museum atmospheres. Atmos. Environ., **24**, 1-8.

[148] Nazaroff, W. W., Salmon, L. G. and Cass, G. R. (1990). Concentration and fate of airborne particles in museums. Environ. Sci. Technol., **24**, 66-77.

[149] Brimblecombe, P., Blades, N., Camuffo, D., Sturaro, G., Valentino, A., Gysels, K., van Grieken, R., Busse, H. J., Kim, O. and Ulrych, U. (1999). The indoor environment of a modern museum building, the Sainsbury Centre for Visual Arts, Norwich, UK. Indoor Air, **9**, 146-164.

[150] Oddy, W. A. (1994). Chemistry in the conservation of archaeological materials. Sci. Total Environ., **143**, 121-126.

[151] De Bock, L. A., Van Grieken, R. E., Camuffo, D. and Grime, G. W. (1996). Microanalysis of museum aerosols to elucidate the soiling of paintings: Case of the Correr Museum, Venice, Italy. Environ. Sci. Technol., **30**, 3341-3350.

[152] Ligocki, M. P., Liu, H. I. H., Cass, G. R. and John, W. (1990). Measurements of particle deposition rates inside Southern California Museums. Aerosol Sci. Technol., **13**, 85-101.

[153] Gysels, K., Deutsch, F. and Grieken, R. V. (2002). Characterisation of particulate matter in the Royal Museum of Fine Arts, Antwerp, Belgium. Atmos. Environ., **36**, 4103-4113.

[154] Camuffo, D., Brimblecombe, P., Van Grieken, R., Busse, H. J., Sturaro, G., Valentino, A., Bernardi, A., Blades, N., Shooter, D., de Bock, L., Gysels, K., Wiser, M. and Kim, O. (1999). Indoor air quality at the Correr Museum, Venice, Italy. Sci. Total Environ., **236**, 135-152.

[155] Worobiec, A., Samek, L., Karaszkiewicz, P., Kontozova-Deutsch, V., Stefaniak, E. A., van Meel, K., Krata, A., Bencs, L. and Van Grieken, R. (2008). Seasonal study of atmospheric conditions influenced by the intensive tourist flow in the Royal Museum of Wawel Castle in Cracow, Poland. Microchem. J., **90**, 99-106.

[156] Grosjean, D., Salmon, L. G. and Cass, G. R. (1992). Fading of organic artists' colorants by atmospheric nitric acid: Reaction products and mechanisms. Environ. Sci. Technol., **26**, 952-959.

[157] Thomson, G. (1978). The Museum Environment. Conservation in the Arts, Archaeology and Architecture. London.

[158] Hinds, W. C. (1982). Aerosol Technology. Properties, Behavior and Measurement of Airborne Particles. New York, John Wiley & Sons.

[159] United Kingdom Department of Environment, Food and Rural Affairs, Expert Panel on Air Quality Standards. Airborne particles: what is the appropriate measurement on which to base a standard? A discussion document; (2004).

[160] Kulmala, M., Vehkamki, H., Petj, T., Dal Maso, M., Lauri, A., Kerminen, V. M., Birmili, W. and McMurry, P. H. (2004). Formation and growth rates of ultrafine atmospheric particles: a review of observations. Journal of Aerosol Science, **35**, 143-176.

[161] Napari, I., Noppel, M., Vehkamki, H. and Kulmala, M. (2002). Parameterization of ternary nucleation rates for $H_2SO_4 - NH_3 - H_2O$ vapors. Journal of Geophysical Research, **107** (D19), 4381, doi:10.1029/2002JD002132.

[162] Vehkamki, H., Kulmala, M., Napari, I., Lehtinen, K. E. J., Timmreck, C. Noppel, M. and Laaksonen, A. (2002). An improved parameterization for sulfuric acid/water nucleation rates for tropospheric and stratospheric conditions. Journal of Geophysical Research, **107** (D22), 4622, doi:10.1029/2002JD002184.

[163] Korhonen, H., Lehtinen, K. E. J. and Kulmala, M. (2004). Aerosol dynamic model UHMA: Model development and validation. Atmospheric Chemistry and Physics, **4**, 757-771.

[164] Wilson, W. E. and Suh, H. H. (1997). Fine particles and coarse particles: concentration relationships relevant to epidemiologic studies. Journal of the Air & Waste Management Association, **47**, 1238-1249.

[165] Tetreault, J. (2003). Key Airborne Pollutants. Airborne pollutants in museums, galleries, and archives. Risk assessment, control strategies, and preservation management TTREAULT. J. Ottawa, Canadian Conservation Institute, 7-19.

[166] Lloyd, H. and Brimblecombe, P. (2003). Focussing on Dust. Views, **39**, 49-52.

[167] Lloyd, H., Bendix, C., Brimblecombe, P. and Thickett, D. (2007). Dust in Historic Libraries. Museum Microclimates. Copenhagen, The National Museum of Denmark, 135-144.

[168] Nazaroff, W. W. and Cass, G. R. (1991). Protecting Museum Collections from Soiling Due to the Deposition of Airborne Particles. Atmospheric Environment Part A-General Topics, **25** (5-6), 841-852. ISSN 0960-1686.

[169] Brimble, P. and Grossi, C. M. (2005). Aesthetic Thresholds and Blackening of Stone Buildings. Science of the Total Environment, **349** (1-3), 175-189.

[170] Lithgow, K. and Brimble, P. (2003). Dust: the Visitors' Point of View. Views, **39**, 47-49.

[171] Ioanid, G. E., Parpauta, D. and Vlad, A. M. (2005). The Electrostatic Behaviour of Materials Used in Restoration-Conservation Process. Journal of Optoelectronics and Advanced Materials, **7** (3), 1643-1649.

[172] Wei, W., Joosten, I., Keim, K., Douna, H., Mekking, W., Reuss, M. and Wagemakers, J. (2007). Experience with Dust Measurements in Three Dutch Museums. Zeitschrift fr Kunsttechnologie und Konservierung, **21** (2), 261-269.

[173] Szostak-kotowa, J. (2004). Biodeterioration of Textiles. International Biodeterioration & Biodegradation, **53** (3), 165-170.

[174] Prajapati, C. L. (2003). Accumulation of Solid Particles on Documents, a Threat for Preservation of Documentary Heritage-The Example of the National Archives of India. Restaurator-International Journal for the Preservation of Library and Archival Material, **24** (1), 46-54.

[175] Ballard, M. (2002). World Trade Center Dust. Its Potential to Interact with Artifacts & Works Of Art, Health & Safety Committee.

[176] Garg, K. L., Jain, K. K. and Mishra, A. K. (1995). Role of Fungi in the Deterioration of Wall Paintings. Science of the Total Environment, **167**, 255-271.

[177] Appelbaum, B. (1991). Guide to Environmental Protection of Collections. Madison, Connecticut, Sound view Press.

[178] Lloyd, H. (2004). Economics of Dust. 6^{th} European Commission Conference on Sustaining Europe's Cultural Heritage: from Research to Policy Queen Elizabeth II Conference Centre. London, UK.

[179] Caneva, G., Nugari, M. P. and Salvadori, O. E. (2008). Plant Biology for Cultural Heritage, Biodeterioration and Conservation. Getty Conservation Institute.

[180] Van Grieken, R., Gysels, K., Hoornaert, S., Joos, P., Osan, J., Szaloki, I. and Worobiec, A. (2000). Characterisation of Individual Aerosol Particles for Atmospheric and Cultural Heritage Studies. Water Air and Soil Pollution, **123** (1-4), 215-228.

[181] Yoon, Y. H. and Brimblecombe, P. (2001). The Distribution of Soiling by Coarse Particulate Matter in the Museum Environment. Indoor Air, **11** (4), 232-240.

[182] Geerinckx, S. (2003). Measurement of $PM_{2.5}$ in Flanders: the ionic composition of particulate dust, Healthcare and Chemicals. Katholieke Hogeschool Kempen, Geel, 2003.

[183] Swan, A. (1981). Conservation of photographic print collections. Library Trends, **30**, 267-296.

[184] Spedding, D. J. and Rowlands, R. P. (1971). Sorption of sulphur dioxide by indoor surface (leather), J. Appl. Chem. Biotech., **21**, 68-70.

[185] Pavlogeorgatos, G. (2003). Environmental parameters in museums. Building and Environment, 38 (12), 1457-1462.

[186] Shahani, C. J. and Wilson, W. K. (1987). The preservation of libraries and archives. Am. Sci., **75**, 240-251.

[187] Langwell, W. H. (1976). Measurement of the effect of air pollution on paper documents. J. Soc. Arch., **5**, 372-373.

[188] Hudson, F. L. and Milner, W. D. (1961). Atmospheric sulphur and the durability of paper. J. Soc. Arch., **2**, 166-167.

[189] Zeronian, S. H. (1970). Reaction of cellulose fabrics to air contaminated with sulphur dioxide. Text. Res. J., **40**, 695-698.

[190] Zeronian, S. H., Alger, K. W. and Omaye, S. T. (1973). Effects of sulphur dioxide on the chemical and physical properties of Nylon. **66**, Text. Res. J., **43**, 228-237.

[191] Pope, D., Gibbens, H. R. and Moss, R. L. (1986). The tarnishing of silver at naturally occurring H_2S and SO_2 levels. Corros. Sci., **8**, 883-887.

[192] Whitmore, P. M. (1987). Concentration Dependence of Ozone Fading of Alizarin Crimson/Paper: Memorandum to the Environmental Quality Laboratory. California Institute of Technology, Pasadena, CA.

[193] Whitmore, P. M. and Cass, G. R. (1998). The ozone fading of traditional Japanese colorants. Studies in Conservation, **33**, 29-40.

[194] Giles, G. H. (1965). Fading of colouring matters. J. Appl. Chem., **15**, 541-550.

[195] Salmon, L. G., Cass, G. R., Bruckman, K. and Haber, J. (2000). Ozone exposure inside museums in the historic central district of Krakow, Poland. Atmos. Environ., **34** (22), 3823-3832.

[196] Shahani, C. J. and Wilson, W. K. (1987). The Preservation of Libraries and Archives. 240-251.

[197] Newton, R. G. (1945). Mechanism of exposure cracking of rubber with a review of the influence of ozone. J. Rubber Res., **14**, 27-39.

[198] Morris, M. A., Young, M. A. and Molvig, T. A. W. (1964). The effects of air pollution on cotton. Text. Res. J., **34**, 563-564.

[199] Camuffo, D. (1998). Microclimate for Cultural Heritage. Elsevier, Amsterdam, 235-292.

[200] Worobiec, A., Samek, L., Karaszkiewicz, P., Kontozova-Deutsch, V., Stefaniak, E. A., Van Meel, K., Krata, A., Bencs, L. and Van Grieken, R. (2008). A seasonal study of atmospheric conditions influenced by the intensive tourist flow in the Royal Museum of Wawel Castle in Cracow, Poland. Microchem. J., **90** (2) 99-106.

[201] The collection-Royal Museums of Fine Arts of Belgium: http://www.fine-arts-museum.be/en/the-collection. Accessed Sept. 27, 2015.

[202] Hinds, W. C. (1982). Filtration. Aerosol Technology. Properties, behavior and measurement of airborne particles. New York, John Wiley & Sons, 164-186.

[203] Chow, J. (1995). Measurement methods to determine compliance with ambient air quality standards for suspended particles. J. Air Waste Manage Assoc., **45**, 32082.

[204] Sarnat. J. A., Demokritou, P. and Koutrakis, P. (2003). Measurement of fine, coarse and ultrafine particles. Ann Ist Super Sanitá, **39** (3), 351-355.

[205] Lighthouse HANDHELD 3016/5016. (2005). Airborne Particle Counter Operating Manual, USA.

[206] Edwards, J. D., Ogren, J. A., Weiss, R. E. and Charlson, R. J. (1983). Particulate air pollutants: a comparison of British 'Smoke' with optical absorption coefficient and elemental carbon concentration. Atmospheric Environment, **17**, 2337-2341.

[207] Methods for measurement of air pollution-part 11: determination of a Black Smoke index in ambient air (ISO9835:1993).

[208] Hansen, A. D. A. (2005). The Aethalometer Book. Magee Scientific Company, Berkeley, California, USA.

[209] Radiello's Manual (2006). V. **01**, Salvatore Maugeri Foundation IRCCS, Environmental Research Center, via Switzerland, **16**, 35127 Padova, Italy. F1-F2 , (G1-G2).

[210] Eva, M. and Van Grienken, R. (2013). X-ray fluorescence spectroscopy and related techniques: An introduction. Momentum Press, LLC, New work.

[211] Kaufman, L. and Camp, D.C. (1975). Polarised radiation for x-ray fluorescence analysis. Adv. X-ray Anal. **18**, 247-258.

[212] Standzenieks, P. and Selin, E. (1979). Background reduction of x-ray fluorescence spectra in a secondary target energy dispersive spectrometer. Nucl. Instrum. Methods **165**, 63-65.

[213] Brouwer, P. (2003). Theory of XRF. Getting Acquainted with the Principles. Almelo, PANalytical.

[214] Spolnik, Z., Belikov, K., Van Meel, K., Adriaenssens, E., De Roeck, F. and Van Grieken, R. (2005). Optimization of measurement conditions of an energy dispersive X-ray fluorescence spectrometer with high-energy polarized beam excitation for analysis of aerosol filters. Applied Spectroscopy, **59**, 1465-1469.

[215] Van Espen, P., Janssens, K. and Nobels, J. (2015). bAxil, software, user's Manual, version.

[216] Currie, L. A. (1995). International Union of Pure and Applied Chemistry (IUPAC). Vol. **67**, No. 10, pp. 1699-1723.

[217] Yiantsios, S. G. and Karabelas, A. J. (1998). The effect of gravity on the deposition of micron-sized particles on smooth surfaces. Int. J. Multiphase Flow, **24** (2), 283-293.

[218] Krupinska, B., Van Grienken, R. and De Wael, K. (2013). Air quality monitoring in a museum for preventive conservation: Results of a three year study in Plantin-moretus Museum in Antwerp, Belgium. Microchemical Journal, **110**, 350-360.

[219] Wallace, L. (1996). Indoor Particles: a review. J. Air & Waste Manage. Assosc., **46**, 98-126.

[220] Walker, A. (2014). Natural Ventilation. National Renewable Energy Laboratory, US Department of Energy.

[221] Yoon, Y. H. and Brimblecombe, P. (2000). Clothing as a source of fibres within museums. J. Cult. Herit., **1** (4), 445-454.

[222] Mihalis, L., Katsivela, E., Kopanakis, I., Raisi, L. and Panagiaris, G. (2015). Indoor/outdoor particulate matter concentrations and microbial load in cultural heritage collections. Heritage Science, **3**, 35, DOI 10.1186/s40494-015-0063-0.

[223] Camuffo, D. (2014). Microclimate for cultural heritage. Conservation, restrotation and maintenance of indoor and outdoor monuments. Amsterdam:Elservier Science.

[224] Mouratidou, T. and Samara, C. (2004). $PM_{2.5}$ and associated ionic component concentrations inside the archaeological museums of Thessaloniki, N. Greece. Atmopspheric Environment, **38**, 4593-4598.

[225] Thatcher, T. L. and Layton, D. W. (1995). Deposition, resuspension and penetration particles within a residence. Atmo.Envir., **29**, 1487-1497.

[226] Gysels, K., Deutsch, F. and Van Grieken, R. (2004). Characterization of particulate matter in the Royal Museum of Fine Arts, Antwerp, Belgium. Atmospheric Environment, **36**, 4103-4113.

[227] Andrea, C., Ericka, P. and Adalgiza, F. (2014). Particulate matter in door environment of Museum megacity of Sao Paulo, Brazil. Quim. Nova, Vol., **37**, No. 9, 1427-1435.

[228] Krupinska, B., Worobiec, A., Gatto Rotondo, G., Novakovic, V., Kontozova, V., Ro, C., Van Grieken, R. and De Wael, K. (2012). Assessment of the air quality (NO_2, SO_2, O_3 and particulate matter) in the Plantin-Moretus Museum/Print Room in Antwerp, Belgium, in different seasons of the year. Microchem. J., **102** (1) 49-53.

[229] Chianese, E., Riccio, A., Trifuoggi, M., Iovino, P., Capasso, S. and Barone, G. (2012). Measurements for indoor air quality assessment at the Capodimonte Museum in Naples (Italy). Int. J. Environ. Res., **6** (2):509-518.

[230] Li, H., Hu, T., Jia, W., Cao, J., Liu, S., Huang, R., Ma, T. and Xi, N. (2015). Evaluation of Policy Influence on Long-Term Indoor Air Quality in Emperor Qin's Terra-Cotta Museum, China. Atmosphere, **6**, 474-489; doi:10.3390/atmos6040474.

[231] Aalto, P., Hmeri, K., Paatero, P., Kulmala, M., Bellander, T., Berglind, N., Bouso, L., Castao-Vinyals, G., Sunyer, J., Cattani, G., Marconi, A., Cyrys, J., Klot, S., Peters, A., Zetzsche, K., Lanki, T., Pekkanen, J., Nyberg, F., Sjövall. B. and Forastiere, F. (2005). Aerosol Particle Number Concentration Measurements in Five European Cities Using TSI-3022 Condensation Particle Counter over a Three-Year Period during Health Effects of Air Pollution on Susceptible Subpopulations, Journal of the Air & Waste Management Association. **55** (8), 1064-1076, DOI:10.1080/10473289.10464702.

[232] Xiu, G., Xin, W., Wang, L., Chen, Y., Xu, F. and Wu, L. (2014). Characterization of Particulate Matter, Ions and OC/EC in Museums, in Shangaie, China.

Aerosol and Air Quality Research, Taiwan Association for Aerosol Research, x, 1-11, xxx. oi:14.4209/aagr.07.0147.

[233] Laakso, L., Hussein, T., Aarnio, P., Komppula, M., Hiltunen, V., Viisanen, Y. and Kulmala, M. (2003). Diurnal and annual characteristics of particle mass and number concentrations in urban, rural and Arctic environments in Finland. Atmospheric Environment, **37**, 2629-2641.

[234] Mu, C.Y., Tu, Y.Q. and Feng, Y. (2011). Effect analysis of meteorological factors on the inhalable particle matter concentration of atmosphere in Hami. Meteorol. Environ. Sci., **34**, 75-79.

[235] Liu, P. F., Zhao, C. S., Gbel, T., Hallbauer, E., Nowak, A., Ran, L., Xu, W. Y., Deng, Z. Z., Ma, N. and Mildenberger, K. (2011). Hygroscopic properties of aerosol particles at high relative humidity and their diurnal variations in the north china plain. Atmos. Chem. Phys. **11**, 3479-3794.

[236] Thomson, G. (1986). The museum environment. 2^{nd} ed. London: Butterworths.

[237] Kontozova-Deutsch, V., Cardell, C., Urosevic, M., Ruiz-Agudo, E., Deutsch, F. and Van Grieken, R. (2011). Characterization of indoor and outdoor atmospheric pollutants impacting architectural monuments: the case of San Jeronimo Monastery (Granada, Spain). Environ Earth Sci., **63**, 1433-1445 DOI 10.1007/s12665-010-0657-5.

[238] Kontozova, V., Spolnik, Z., Worobiec, A., Godoi, R., Van Grieken, R., Deutsch, F. and Bencs, L. (2005). Assessment of air pollutant levels in some European museums and churches, in: R. Van Grieken, K. Janssens (Eds.). (2005). Cultural Heritage Conservation and Environmental Impact Assessment by Non-Destructive Testing and Micro-Analysis, A. A. Balkema Publishers, Leiden, pp. 245-263.

[239] Ricardo, H. M., Godoi, H. B., Carneiro, S. L., Paralovo, V. P., Campos, H. E., Van Grieken, R., Ana, F. L., Godoi and Tania, M. T. (2013). Indoor air quality of a museum in a subtropical climate: The Oscar Niemeyer museumin Curitiba, Brazil. Science of the Total Environment, 452-453: 314-320.

[240] Brimblecombe, P., Raychaudhuri, M. and Bowden, D. (2001). Surface reactions of deposited NO_2 in the museums environment. Abstract of the 4^{th} meeting of the Indoor Air Pollution Working Group. National Museums of Denmark, Compenhagen, Nov.8^{th}-9^{th}.

[241] Grontoft, T. and Raychaudhuri, M. R. (2004). Compilation of tables of surface deposition velocities for O_3, NO_2 and SO_2 to the range of indoor surfaces. Atmos Environ., **38**, 533-544.

[242] Kgabi, N. A. and Sehloho, R. M. (2012). Tropospheric Ozone Concentrations and Meteorological Parameters, Global Journal of Science Frontier Research (B), **12**, Issue 6, Version 1.0, 11 - 21.

[243] Kgabi, N. A. and Sehloho, R. M. (2012). Seasonal Variations of Ground Level Ozone Concentrations, Global Journal of Science Frontier Research (B), **12** Issue 5, Version 1.0, 21- 29.

[244] Vassilakos, C., Pateraki, S., Veros, D., Maggos, T., Michopoulos, J., Saraga, D. and Helmis, C. G.(2007). Temporal determination of heavy metals in $PM_{2.5}$ aerosols in a suburban site of Athens, Greece. J Atmos Chem.; **57**:1-17.

[245] Hulskotte, J. H. J., Schaap, M. and Visschedij, A. J. H. (2006). Brake wear from vehicles as an important source of diffuse copper pollution. 10^{th} Int. Specified conference on diffuse pollution and sustainable basin management Sept. 18-22. Istanbul Turkey.

[246] Endjambi, K. W., Hamatui, N., Onjefu, S. A., Kgabi, N. and Maposa, I. (2016). Particulate Matter Concentrations in the Vicinity of an Incinerator, Journal of Geoscience and Environment Protection, 4, 88-100.

[247] Yi, C., Davis, K. J., Bakwin, P. S. and Berger, B. W. (2001). Long-term observations of the dynamics of the continental planetary boundary layer. J Atmos. Sci., **58**, 1288-99.

[248] Hilde, M., L. M., Mazurek, M. A., Cass, G. R. and Simoneit, B. R. T. (1991). Quantitative characterization of urban sources of organic aerosol by high-resolution gas chromatography. Environmental Sci. Technology, **25**, 1311-25.

[249] Schreiner, M. (1991). Glass of the past: the degradation and deterioration of medieval glass artifacts. Mikrochim Acta, **2**, 255-64.

[250] Bingemer, H., Klein, H., Ebert, M., Haunold, W., Bundke, U., Herrmann, T., Kandler, K., Müuller-Ebert, D., Weinbruch, S., Judt, A., Wéeber, A., Nillius, B., Ardon-Dryer, K., Levin, Z. and Curtius, J.(2012). Atmospheric ice nuclei in the Eyjafjallajökull volcanic ash plume. Atmospheric Chemistry and Physics, **12**, 857-867.

[251] Hobbs, P. V., Fullerton, C. M., Bluhm, G. C. (1971). Ice Nucleus Storms in Hawaii. Nature-Physical Science, **230**, 90-91.

Appendix

Appendix A: Determination of air trajectories

Air trajectories can either be forward, moving away, from the station or backwards; where the air flow is into the station. Different models for air trajectories can be used depending on the availability of input data. Each model requires gridded fields of meteorological variables at regular temporal intervals. The time interval between fields should be constant for each defined grid; the fine grid regional data may be available at three hour intervals while the coarser grid global model fields may be available only every six hours. The Hybrid Single - Particle Lagrangian Integrated Trajectory (HYSPLIT) is used for two primary applications of trajectories or concentrations. The model structure consists of a modular library with main programs for each application. It has two independent operational options; it can be installed in a personal computer and run or done on the over the web-based http://ready.arl.noaa.gov/. The HYSPLIT model can run interactively on the Web through the READY system on NOAA's site. The PC based version of HYSPLIT has also been used. The details of trajectory model procedure and configuration are given Hysplit4 user guide found in $http://www.arl.noaa/documents/reports/hysplit-user-guide.pdf$. The model will be configured to run the example case discussed in more detail below. The quick start menu tab can be used to run any simulation in one-step. The last configuration will be used for the simulation. The quick start menu brings up a global map with the current source location shown as a blue dot. A right-click of the mouse button

will write that source location to the control file, click Yes to exit the window, which will close the map, run the model simulation, create the output file, and display the graphics. A left-click of the mouse button will set a new source location. A left-click-hold-drag-release will define a new zoomed domain and the map will be redrawn. An exit from the window's menu bar will close the map without updating the control file or running the model. For more detailed simulation configurations, follow the steps below. To run the model is to use the GUI menu to create the model's input CONTROL file. For the purposes of this demonstration appropriate meteorological files are provided. If for some reason the menu system is not available, perhaps because Tcl/Tk was not installed, the Control file can be created manually.

Step 1 - start the GUI menu system using working hysplit4.tcl or the desktop shortcut to Hysplit4. A widget will appear with the HYSPLIT graphic and three button options: Menu, Help and Exit.Click on Menu tab.

Step 2 - The four main menus of the Hysplit4 GUI will appear: Meteorology, Trajectory, Concentration, and Advanced. An additional small widget underneath the main menu gives the current Hysplit4 version information. Do not delete this widget as it will terminate the GUI. It provides the reference frame for the model's standard output and messages. Click on the Trajectory tab.

Step 3 - Five options appear under this item: Setup Run, Run Model, Display, Utilities, and Special Runs. Normally these are run in sequence, however any item can be selected and run if the appropriate input files were created during a previous simulation. Click on the Setup tab.

Step 4 - Setup Run is used to enter the basic model simulation parameters: the starting time of the calculation; starting location in terms of latitude, longitude, and height; the run-time or duration of the trajectory calculation; and the names and locations of all required files. When modifications to this menu are complete, click on save. However for this example, you will use the Retrieve option for predefined configurations, so do nothing here and go on to Step 5.

Step 5 - The example calculation is configured by clicking on Retrieve and then entering the text: sample traj, which is the name of the example simulation control file that was created for this demonstration. Then click on OK. After the data entry widget is closed, click on Save and the setup menu will close.

Step 6 - Click on Run Model, which first copies the setup configuration (default traj) saved in the previous step, to the model's input CONTROL file. The model calculation is then started. A series of messages will appear on standard output text window showing the progress of the calculation. When the simulation is completed, the trajectory end-points output file is ready to be converted for graphical display. Under some operating systems, the standard output widget will not show any output until the end of the calculation and the Trajectory menu items will be locked until the calculation completes. After completion click on Exit to close the window.

Step 7 - Selecting Display will run a special program that converts the text file of trajectory end-point positions into a high quality Postscript file (trajplot.ps) suitable for printing. The conversion widget provides options for the frequency of the labels on the trajectory, a variable zoom factor, and color or black and white graphics options. If the Postscript viewer (Ghostscript) has been installed and associated with the .ps file suffix, then it will be invoked by the GUI. If the viewer does not automatically open, it may be necessary to manually edit.guicode hysplit 4.tcl to change the directory location associated with the program gsview 32.exe. After clicking on Execute Display, the following graphic will appear in the Ghostview window:

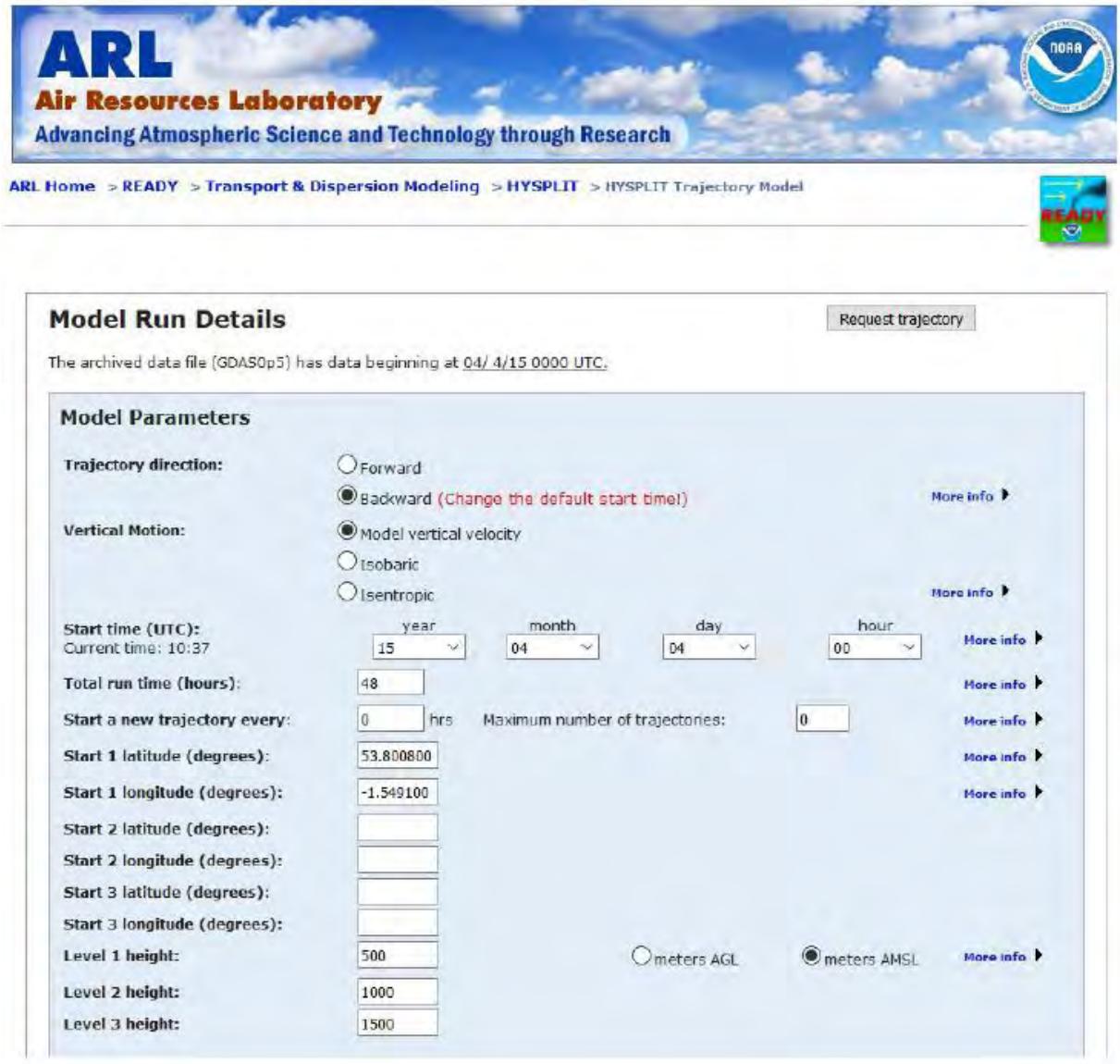

Figure 7.1: Sample for model run details of HYSPLIT.

Appendix B: Calculation of INP concentrations using GLOMAP model

Assuming that the active sites from which ice nucleation can occur under the singular description are randomly distributed in the aerosol population, the probability of one particle having a certain number of active sites (k) can be represented by the Poisson distribution of Eq.(B1)

$$f(k,\lambda) = \frac{e^{-\lambda}\lambda^{k}}{k!} \tag{B1}$$

where, f is the probability of having k active sites in a particle and λ represents the expected value of active sites per particle at a certain temperature (T). We can calculate the probability of a particle immersed in a super-cooled water droplet to freeze it (P) as the sum of the probabilities of having 1 or more active sites in Eq. B2:

$$P = \sum_{k=1}^{\infty} f(k,\lambda) \tag{B2}$$

As the sum from k = 0 to k =∞ of Eq. B1 has to be equal to 1, we can also represent this sum as Eq. B3:

$$P = \sum_{k=1}^{\infty} f(k,\lambda) - f(0,\lambda) = 1 - e^{-\lambda} \tag{B3}$$

If we have a distribution of particles of the same size and same density of active sites, this probability P will be the same for all of them and so the fraction of super-cooled water droplets that will freeze known as fraction frozen (ff), will therefore be

$$ff = 1 - e^{-\lambda} \tag{B4}$$

We can then calculate the INP concentration as

$$[INP] = ff.[N] \tag{B5}$$

where [N] represents the concentration of a certain type of aerosol. For the case in which we have a density of active sites distributed across the surface area of a particle

depending on temperature n_s(T), we can calculate for a particle of radius r as

$$\lambda(r,T) = 4\pi r^2.n_s(T) \tag{B6}$$

Hence,

$$ff(r,T) = 1 - e^{-n_s(T).4r^2} \tag{B7}$$

In GLOMAP mode, the size distribution of aerosols is represented in log-normal modes, and their probability density function (PDF) is given by

$$PDF(r) = \frac{1}{r.ln(\sigma).\sqrt{2\pi}}.e\frac{-(ln(r) - ln(r_m))^2}{2.ln(\sigma)^2}, \tag{B8}$$

where r_m is the mean radius of the mode and σ the standard deviation of the mode. The INP concentration is therefore the integral across all the possible values of r for every mode, and it will change for every temperature:

$$[INP]_{mode}(T) = \int_0^\infty (1 - e^{-4\pi r^2.n_s(T)}).N.\frac{1}{r.ln(\sigma).\sqrt{2\pi}}.e\frac{-(ln(r) - ln(r_m))^2}{2.ln(\sigma)^2}dr. \tag{B9}$$

In our case, we consider that the soluble modes can activate into water droplets, so the total INP concentration is the sum of the concentrations for every soluble mode. In the special case of having a value of λ small ($\lambda < 0.1$), we can approximate the value of the fraction frozen (ff) using a first-order Taylor series centered in 0:

$$ff \approx ff_{\lambda=0} + \frac{\partial ff}{\partial \lambda} \mid_{\lambda=0} .\lambda + \cdots \tag{B10}$$

$$ff_\lambda = 1 - e^0 = 0 \tag{B11}$$

$$\frac{\partial ff}{\partial \lambda} \mid_{\lambda=0} = [-e^{-\lambda.(-1)}]_{\lambda=0}.\lambda = 1.\lambda \tag{B12}$$

$$ff \approx \lambda \tag{B13}$$

In other words, if the number of active sites is small compared with the number of particles, we can approximate the number of particles having one or more active sites, to the number of active sites. And the INP concentration can be calculated as follows:

$$[INP](T) \approx \lambda(T).[N] \tag{B14}$$

Appendix C- Pictures taken during the concentrations of measuring ice nucleating particles

Figure 7.2: D.A. Workneh during INPs sampling.

Figure 7.3: D.A. Workneh During droplet freezing experiment.